AN APPROACH FOR MULTI-HAZARD SUSCEPTIBILITY ASSESSMENT FOR LANDSLIDES, EARTHQUAKES AND FLOODS

HEYELAN, DEPREM VE TAŞKIN TEHLİKELERİNİN ÇOKLU DUYARLILIK DEĞERLENDİRMESİ İÇİN BİR YAKLAŞIM

GİZEM KARAKAŞ

PROF. DR SULTAN KOCAMAN GÖKÇEOĞLU

Supervisor

Submitted to

Graduate School of Science and Engineering of Hacettepe University

As a Partial Fulfillment to Requirements

For the Award of Degree of Doctor of Philosophy

in Geomatics Engineering

2024

To my family, Veysel Emre Karakaş and Doruk Ege Karakaş

For their endless support and love

ABSTRACT

AN APPROACH FOR MULTI-HAZARD SUSCEPTIBILITY ASSESSMENT FOR LANDSLIDES, EARTHQUAKES AND FLOODS

Gizem KARAKAŞ

Doctor of Philosophy, Department of Geomatics Engineering

Supervisor: Prof. Dr. Sultan KOCAMAN GÖKÇEOĞLU

May 2024, 130 pages

Production of precise and up-to-date susceptibility maps at regional level is essential for mitigating disasters, selecting new sites for settlements and construction, and planning in areas prone to various natural hazards. This thesis introduced a novel approach to multi-hazard susceptibility assessment (MHSA) for evaluating landslide, flood, and earthquake risks, combining expert opinion with supervised machine learning (ML) techniques. The methodology was tested in five basins within Elazig and three basins in Adiyaman Provinces, Türkiye. The susceptibility maps were produced at basin scale since various environmental characteristics affecting the hazard conditioning factors are relatively coherent within them. Regarding landslide susceptibility mapping (LSM), the random forest (RF) ensemble machine learning algorithm, was utilized. For flood susceptibility mapping (FSM), a modified analytical hierarchical process (m-AHP) method was employed using factor scores provided by experts for each site. Seismic hazard

assessment relied on ground motion parameters, specifically Arias intensity values, as they are considered to be effective especially for landslides. These individual assessments were then synthesized using a Mamdani fuzzy inference system (FIS), incorporating expert-defined membership functions. The thesis findings indicated high overall accuracies (over 90%) can be achieved with the random forest model for the LSM. The Mamdani fuzzy algorithm is recommended for the MHSA, as it can be adapted to different regions with its intuitive membership functions. While the thesis provided a robust framework for multi-hazard susceptibility assessment at the regional scale, fine-tuning of the algorithms in different geographical areas may require further expert input.

Keywords: Multi-hazard assessment, landslide, flood, earthquake, machine learning, fuzzy inference.

ÖZET

HEYELAN, DEPREM VE TAŞKIN TEHLİKELERİNİN ÇOKLU DUYARLILIK DEĞERLENDİRMESİ İÇİN BİR YAKLAŞIM

Gizem KARAKAŞ

Doktora, Geomatik Mühendisliği Bölümü

Tez Danışmanı: Prof. Dr. Sultan KOCAMAN GÖKÇEOĞLU

Mayıs 2024, 130 sayfa

Bölgesel düzeyde doğru ve güncel duyarlılık haritalarının üretilmesi, çeşitli doğal tehlikelere duyarlı bölgelerde afetlerin etkilerini hafifletme, yerleşim alanları ve altyapı inşaatı için yeni yerlerin seçilmesi ve planlama amaçlı olarak oldukça önemlidir. Bu tez, heyelan, sel ve deprem risklerini değerlendirmek için uzman görüşü ile denetimli makine öğrenimi (MÖ) tekniklerini birleştiren çoklu tehlike duyarlılık değerlendirmesine (ÇTDD) yeni bir yaklaşım getirmiştir. Metodoloji, Türkiye'nin Elazığ ilindeki beş ve Adıyaman ilindeki üç havzada test edilmiştir. Tehlike koşullandırma faktörlerini etkileyen çeşitli çevresel özellikler havzalar içinde nispeten tutarlı olduğundan, duyarlılık haritaları havza ölçeğinde üretilmiştir. Heyelan duyarlılık haritalamasında (HDH), rastgele orman (RO) topluluk makine öğrenimi algoritması kullanılmıştır. Taşkın duyarlılık haritalaması (TDH) için, her bölge için uzmanlar tarafından sağlanan faktör puanları kullanılarak modifiye edilmiş analitik hiyerarşik süreç (m-AHP) yöntemi uygulanmıştır. Deprem tehlike değerlendirmesi, özellikle heyelanlar için etkili olduğu düşünülen yer hareketi parametrelerine, özellikle de Arias yoğunluk değerlerine

dayanmıştır. Bu bireysel değerlendirmeler daha sonra uzman tanımlı üyelik fonksiyonlarını içeren bir Mamdani bulanık çıkarım sistemi kullanılarak sentezlenmiştir. Tez bulguları, LSM için rastgele orman modeli ile yüksek genel doğruluklara (%90'ın üzerinde) ulaşılabileceğini göstermiştir. Mamdani bulanık algoritması, sezgisel üyelik fonksiyonları ile farklı bölgelere uyarlanabildiği için ÇTDD için önerilmektedir. Tez, bölgesel ölçekte çoklu tehlike duyarlılık değerlendirmesi için sağlam bir çerçeve sağlamış olsa da, farklı coğrafi alanlarda algoritmaların ince ayarının yapılması daha fazla uzman girdisi gerektirebilir.

Anahtar Kelimeler: Çoklu tehlike değerlendirmesi, heyelan, taşkın, deprem, makine öğrenimi, bulanık mantık.

ACKNOWLEDGMENTS

In the completion of this PhD thesis, I feel deep satisfaction and appreciate the learning opportunities I have gained regarding the thesis subject. I would like to thank many people who have been with me throughout this academic journey and supported me continously.

First and foremost, I would like to thank Prof. Dr. Sultan Kocaman Gökçeoğlu for supervising my thesis. I am always grateful for her valuable guidance, expertise and constant support throughout my studies. I have learned a lot from her guidance not only in my academic but also in my personal life. It will always be an honor for me to be her student.

I am very thankful to my PhD thesis committee members Prof. Dr. Ali Özgün Ok and Prof. Dr. Bekir Taner San for their valuable comments and suggestions on the progress of my thesis, and also Prof. Dr. Hakan Ahmet Nefeslioğlu and Assoc. Prof. Dr. Nurgül Gültekin for taking their valuable time and contributions to my thesis as jury members.

I would especially like to thank Prof. Dr. Candan Gökçeoğlu, who always helped and guided my work by sharing his expertise and ideas. I am grateful for his contributions to my thesis and his valuable time.

I would also like to thank my dear friends and colleagues Recep Can, İlyas Yalçın, Mehmet Büyükdemircioğlu, Beste Tavus, Sinem Çetinkaya, Erdinç Örsan Ünal and Nazlı Tunar Özcan for their help and motivation and for the great pleasure of working together in our project and field studies.

I owe gratitude to my mother, father and sister, who have always been with me throughout my life and who have always been supportive and understanding. I would also like to thank my parents in law for supporting me during this process.

Finally, I would like to express my heartfelt thanks to my beloved husband, Veysel Emre KARAKAŞ, who has been by my side throughout my graduate studies, never withholding his patience and support, and motivating me with his understanding, help, and encouragement. And finally to my dear son Doruk Ege KARAKAŞ, who has shown great understanding and maturity for his age, for bringing joy to my life.

CONTENTS

LIST OF FIGURES

LIST OF TABLES

SYMBOLS AND ABBREVIATIONS

Symbols

A_s	Specific catchment area
β	Slope gradient
R_i	Percentage of variance
r	Correlation coefficient
X_a, Y_a	Features related to landslides
$\bar{X}$, $\bar{Y}$	the mean of values the variables
g	Acceleration of gravity
t	time
t_d	Total recording length

Abbreviations

AFAD	The Disaster and Emergency Management Presidency of Turkey
AHP	Analytical Hierarchy Process
ANFIS	Adaptive Neuro-Fuzzy Inference System
ANN	Artificial Neural Network
ANP	Analytical Network Process
AUC	Area Under Curve
CNN	Convolutional Neural Network
DEM	Digital Elevation Model
DEMATEL	Decision-making Trial and Evalution Laboratory
DSHA	Deterministic Seismic Hazard Assessment
DSM	Digital Surface Model

DT	Decision Tree
EAFZ	East Anatolian Fault Zone
EOPs	Exterior Orientation Parameters
FIS	Fuzzy Inference System
FR	Frequency Ratio
FSM	Flood Susceptibility Map
GBM	Gradient Boosting Machine
GDM	Genaral Directorate of Mapping
GIS	Geographic Information System
GNSS	Global Navigation Satellite System
GWO	Grey Wolf Optimizer
ICESat	Ice, Cloud, and land Elevation Satellite
IDW	Inverse Distance Weighted
IGR	Information Gain Ratio
INS	Inertial Navigation System
IOPs	Interior Orientation Parameters
LiDAR	Light Detection and Ranging
LR	Logistic Regression
LSM	Landslide Susceptibility Map
LULC	Land Use Land Cover
m-AHP	modified Analytical Hierarchical Process
MCDM	Multi-Criteria Decision-Making
MHS	Multi-Hazard Susceptibility
MHSA	Multi-Hazard Susceptibility Assessment
ML	Machine Learning
MLP	Multi-Layer Perceptron

MTA	Mineral Research and Exploration
NDVI	Normalized Difference Vegetation İndex
NF	Neuro-Fuzzy
OA	Overall Accuracy
PGA	Peak Ground Accelaration
PSHA	Probabilistic Seismic Hazard Assessment
ROC	Receiver Operating Characteristic
RF	Random Forest
SAR	Synthetic-Aperture Radar
SDGs	Sustainable Development Goals
SPI	Stream Power Index
SVM	Support Vector Machine
SWARA	Stepwise Weight Assessment Ratio Analysis
TOL	Tolerance
TPI	Topographic Position Index
TWI	Topographic Wetness Index
UN	United Nations
VIF	Variance Inflaction Factor
WLC	Weighted Linear Combination

1. INTRODUCTION

This chapter provides the motivation of the thesis and discusses the problems addressed here, including natural hazards, their occurrences, and effects. The thesis objectives and outline are also covered in the following sub-headings.

1.1. Problem Statement/Motivation

Natural hazards are technology and human-induced events that occur at unpredictable times and have a negative impact on life on Earth, potentially causing injuries or death, as well as damages to properties, socioeconomic assets, environment, and historical and cultural heritage [1]. There are several types of natural hazards seen on a global scale. These include earthquakes, volcanoes, landslides, avalanches, tsunamis, wildfires, debris flows, and floods. Among them, earthquakes, landslides and floods affect people and the natural environment more than the others, inducing quite destructive and economic losses worldwide.

Landslides refer to the movement of a slope, either natural or man-made, in a downhill and outward direction due to the combined effects of gravity, slope angle, water, and other external pressures [2]. Floods can be defined as water bodies overflowing their regular bounds or water accumulations in areas that are typically flooded [3]. An earthquake is an event in which the energy generated as a result of the fracture of the earth's crust due to tectonic or volcanic activities spreading in the form of seismic waves and strongly shakes the earth and the environments they are observed [4].

The frequencies and intensity of natural hazards have significantly increased in Türkiye and worldwide in recent years. Factors such as climate change, rapid urbanization and environmental factors have caused many complex processes that impacted the frequency

and impacts of natural hazards and caused rises. The Disaster and Emergency Management Presidency of Turkey (AFAD) published that between 1950 and 2022, roughly 368,477 natural hazards, such as earthquakes, landslides, rockfalls, sinkholes, floods, and avalanches, occurred in Türkiye [5-6], As a global effort, a total of 17 Sustainable Development Goals (SDGs), also known as Agenda 2030, were defined at the Sustainable Development Summit in 2015 by the United Nations (UN). Within the framework of these objectives, natural hazards were also mentioned several times. The SDGs aim to increase catastrophe resilience and decrease vulnerability, among others, to achieve equality and ending poverty. Particularly, items 1.5, 2.4, 11.5, 11.b and 13.1 of these targets emphasize the importance of developing the capacity to withstand climate-related hazards, natural disasters, and other economic, social, and environmental shocks and disasters [7].

The majority of studies in the literature concentrate on a single hazard type. However, it is possible that an area is impacted by many natural hazards, which can interact with one another and potentially lead to cascading catastrophes. Precise prediction of disaster-related hazards is necessary in these areas to effectively manage the adverse consequences. Therefore, it is essential to evaluate multiple hazards in a region at the same time also by analyzing the interactions between them. The importance of multi-hazard assessments was proven on 24 January 2020 Elazig Earthquake (Mw 6.8) and the 6 February 2023 Kahramanmaras Earthquakes (Mw 7.7 and Mw 7.6) occurred in Türkiye. The term multi-hazard has been adopted in the UN Environment Program [8], which aims to identify and manage areas prone to natural hazards for a safer world in the 21st century and to reduce disaster sourced risks.

Different datasets and methods have been used to produce single susceptibility maps in the literature. While there have been numerous production of susceptibility maps for single natural hazards, there is still no agreement on the appropriate methodology for combining them. Thus, this matter remains as an essential research topic that has yet to be further explored in the international literature on natural hazards. Thus, this thesis focused on a novel multi-hazard susceptibility assessment (MHSA) method at the regional scale and applied it, based on the Mamdani fuzzy inference system (FIS), in two

areas prone to earthquake, landslide, and flooding. Special attention was also paid to the production of accurate single hazard maps, suitable input features used for this purpose, and the spatial sampling strategies especially for the data-driven machine learning (ML) methods. The objectives and contributions are detailed in the following.

1.2. Thesis Objectives

The literature analysis has shown that further research and novel methods are needed for the production of accurate multi-hazard susceptibility (MHS) maps. Most MHSA studies have focused on simple spatial analysis, such as overlay or sum of the individual maps. This thesis focused on the production of a more advanced methodology with stochastic input based on expert opinion. In addition, although a mass body of literature exists on the production of landslide susceptibility maps (LSMs) and a number of flood susceptibility maps (FSMs), the selection of suitable input features (or conditioning factors) is still an open question. Thus, considering the selection methods for the production of the univariate and multi-hazard susceptibility maps based on data availability, suitability to the target region and prediction performances, this thesis aimed to develop a novel approach for multi-hazard susceptibility map production. The following main objectives can be listed as a summary:

- Development of an advanced decision-making approach for MHSA based on stochastic inputs and expert opinion,
- Joint analysis of geohazards triggering each other such as earthquakes and landslides, which are caused by geomorphological features, and a climate-related hazard, i.e. flooding, together for the MHSA;
- Investigating joint use of the ML and expert-based methods for the MHSA;
- Evaluating the results in two different regions delineated based on basin boundaries.

In order to fullfill the thesis objectives, two different sites, one in Elazig Province and the other one in Adiyaman Province of Türkiye, were selected and the methods and their parameters, such as input features and the sampling strategies, were evaluated from an accuracy perspective.

1.3. Contributions

The study outcomes indicated that assessing multi-hazards together for a region allows for a more accurate understanding of complex natural processes and their impacts on each other. Considering multiple natural hazards together encourages disaster risk management from a more holistic perspective than traditional methods that focus on single hazards. This expands the scope of risk assessment processes, allowing a comprehensive investigation of all possible hazards. Thus, the main contributions of this thesis can be listed as following:

- An important contribution to this thesis study is the utilization of the Mamdani FIS for the MHSA. The study used Mamdani FIS, the first of its kind in the literature, by creating specific rules for each hazard, and this approach significantly increased the usability and level of detail of the resulting maps.

- The developed methods were adapted to different environmental characteristics and risk conditions allows for featuring customized solutions that are sensitive to regional characteristics. This enables the development of strategies for disaster risk management and planning for different regions that take into account local conditions.

- Various types of spatial datasets with diverse resolutions and data sources were evaluated and their usability for achieving high performance was assessed.

- The preparation of landslide inventories using pre- and post-earthquake orthophotos and surface models contributed greatly to the production of reliable

and up-to-date databases for landslide risk management and susceptibility assessments in Türkiye. High prediction performances for the production of high resolution LSMs could be achived, which proves their usability for urban and rural planning purposes.

- Different sampling strategies for the LSMs were evaluated with the popular ML methods such as random forest and multi-layer perceptron, and it was found that class imbalance between landslide and non-landslide classes must be accounted. However, the spatial selection of the samples were found to be less important when high amount of training and test data are available.

1.4. Thesis Outline

This thesis is presented under seven chapters as briefly explained below:

Chapter 1 describes the problem statement/motivation and objectives of the thesis, and highlights the contributions of the study.

Chapter 2 presents a literature review on the methods used to produce the univariate (such as landslides, floods and earthquakes) and multi-hazard susceptibility maps, and the input features derived when producing these maps.

Chapter 3 provides the general and geological characteristics of the study sites, flood and earthquake events, landslide inventories and the geospatial datasets used in the thesis study.

Chapter 4 explains in detail the proposed methodological workflow, data pre-processing, and production of the univariate and multi-hazard susceptibility maps.

Chapter 5 gives detailed quantitative and qualitative results of the method applied to two different fields.

Chapter 6 discusses the results of the thesis on input features, univariate and multi-hazard susceptibility maps from various aspects.

Chapter 7 concludes the thesis and provides recommendations for future research.

2. BACKGROUND ON HAZARD SUSCEPTIBILITY MAPPING

In this chapter, a comprehensive review of previous research on natural hazards was presented. First, studies focusing on the selection of conditioning factors for the production of univariate susceptibility maps were evaluated. In the literature, most susceptibility assessment studies have predominantly considered only a single type of natural hazard. Therefore, susceptibility assessment studies related to landslides, floods, and earthquakes were presented in different sub-sections. Additionally, studies evaluating the multi-hazard susceptibility were discussed in the scope of this work.

2.1. Conditioning Factors

Besides data quality, resolution and the applied model, the selection and analysis of conditioning factors are extremely important in producing landslide and flood susceptibility maps with high accuracy. The extent, type and importance of these factors, which are mostly topographical, environmental, geological, hydrological, climatic, vary according to the geological structure of the study area, regional environmental characteristics, data availability and the requirements of the model to be used for susceptibility modeling. Different conditioning factors were utilized in the literature and there is no standard approach for their selection. In addition, many studies carried out analyses on factor importance and their prediction abilities to determine the most effective factors.

Carrara et al. [9] compared five different statistical and physically-based models for the production of debris-flow susceptibility map. Rainfall, morphology and soil properties were found to be the main predictors for shallow landslides. Xie et al. [10] selected seventeen conditioning factors associated with landslide occurrence based on the previous studies conducted in the study area. Elevation, lithology, settlement density and distance from fault were found to be the most important features in the study.

Yang et al. [11] categorized the conditioning factors as topographic, geological, hydrological, geophysical and land use/land cover. Elevation, peak ground accelaration (PGA) and slope were observed as the most important factors in their study. Lewandowski et al. [12] emphasized that the most important and critical step in any prediction model is the selection of the appropriate conditioning factors to obtain high accuracy. The features were determined based on literature review, expert opinion and preliminary analyses with statistical methods. Pearson correlation was the most widely used statistical method and was found suitable for the factor selection.

Meena et al. [13] investigated the importance of factors in predicting landslide occurrences with statistical and ML methods. The feature importance results obtained with the statistical model indicated that distance to drainage, topographic position index (TPI), rainfall, lithology and land cover were the most important features. From the ML model, distance to road, rainfall, lithology and elevation were found to be the most important factors. In the study, susceptibility maps were reproduced by removing the least important conditioning factors. As a result, it was found that the removal of these factors did not affect the accuracy. It was also emphasized that the a factor might hold greater significance in one model while being less influential in another.

Bernat Gazibara et al. [14] emphasized that the input layers were selected by an expert according to the study area conditions, scale, purpose, and data availability. Six conditioning factors (slope gradient, lithology, proximity to geological contact, land use, terrain dissection and proximity to drainage network) were selected and implemented in total. According to the results of the study, it was observed that the slope gradient was the most important effect on the production of the susceptibility map.

Wang et al. [15] employed thirteen conditioning factors including elevation, slope, aspect, plan curvature, profile curvature, topographic wetness index (TWI), engineering rock group, normalized difference vegetation index (NDVI), land cover, distance to faults, distance to rivers, mean annual rainfall and distance to roads for the LSM production. In the study, importance of these conditioning factors for different algorithms was also analyzed. It was observed that the factor importance obtained from different algorithms

was inconsistent. Elevation, slope and rainfall parameters were found to be more important in three algorithms. Bravo-López et al. [16] emphasized the importance of selecting relevant conditioning factors to minimize dimensionality and produce a LSM with suitable quality. The research also highlighted the importance of selecting features to enhance the accuracy of the resulting LSMs and decrease the computational time required to produce them.

In this thesis study, parameters, which have been used the most frequently in the literature between 2017-2023, and the study area characteristics were considered in selecting conditioning factors for landslide and flood susceptibility assessments. Studies published between 2017-2023 and having at least fifteen citations were analyzed and the most frequently used conditioning parameters were determined. Graphical representations of conditioning factors used in the production of landslide and flood susceptibility maps obtained from the literature analysis are shown in Figures 2.1(a) and 2.1(b). The topographical features (slope, aspect, altitude, curvature, TWI, stream power index - SPI), lithology, distance to river, distance to fault and land use land cover (LULC) were found to be among the most commonly used factors for the LSM. For flood susceptibility, again topography, lithology, hydrology and LULC have been used frequently.

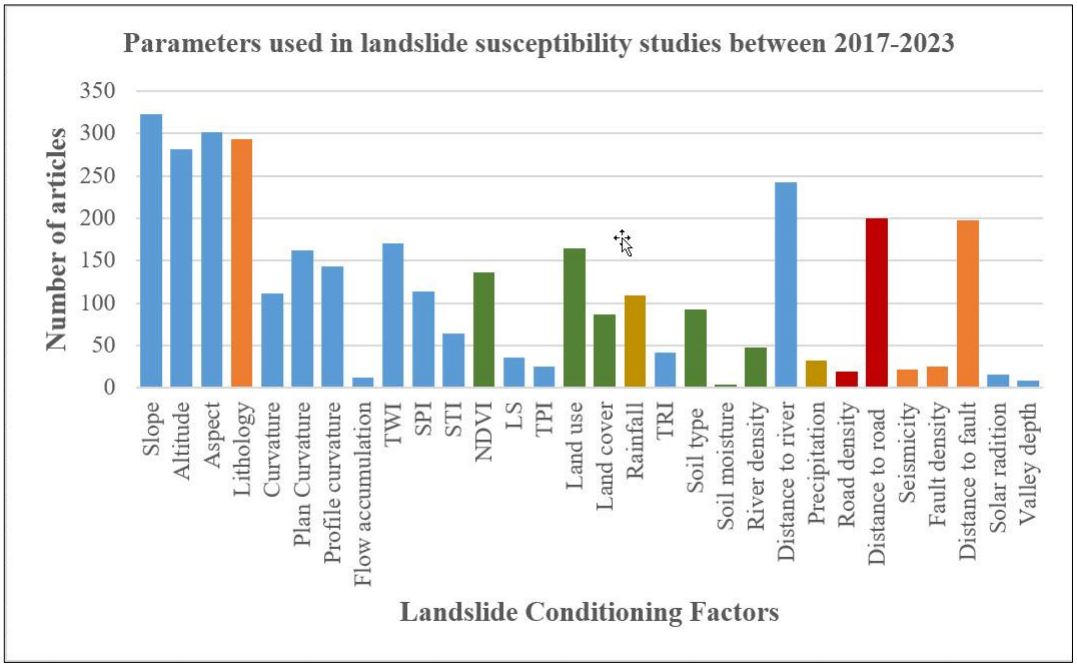

(a)

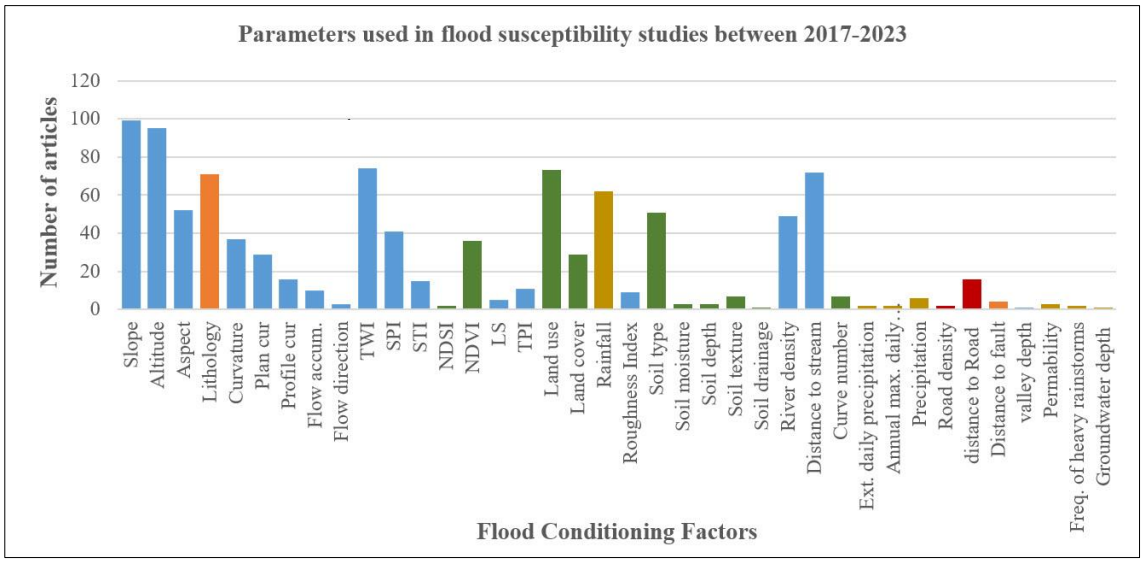

(b)

Figure 2.1. The conditioning parameters used for (a) landslide (b) flood susceptibility assessment studies between 2017 and 2023.

2.2. Landslide Susceptibility Map Production Methods

In recent years, the number of natural hazards occurred in Türkiye and in the world has been increasing. For this reason, it becomes important to automatically identify areas susceptible to natural hazards. LSM production is one of the popular research subject in the literature and it aims to spatially identify potential landslide-prone areas. According to Reichenbach et al. [17], a great deal of literature has been published on landslide susceptibility since the mid-1970s. A statistical assessment on the landslide literature by Gokceoglu and Sezer [18] emphasized that there was a sharp increase between 1945 and 2008 and this rise was expected to continue.

Different methods and data sources were used to identify landslide-prone areas. These methods can be categorized as qualitative (knowledge-driven and inventory based) and quantitative (data-driven and physically-based) [19-20]. Overviews of the techniques applicable to the evaluation of landslide susceptibility are provided by Soeters and [21-24] as illustrated in Figure 2.2.

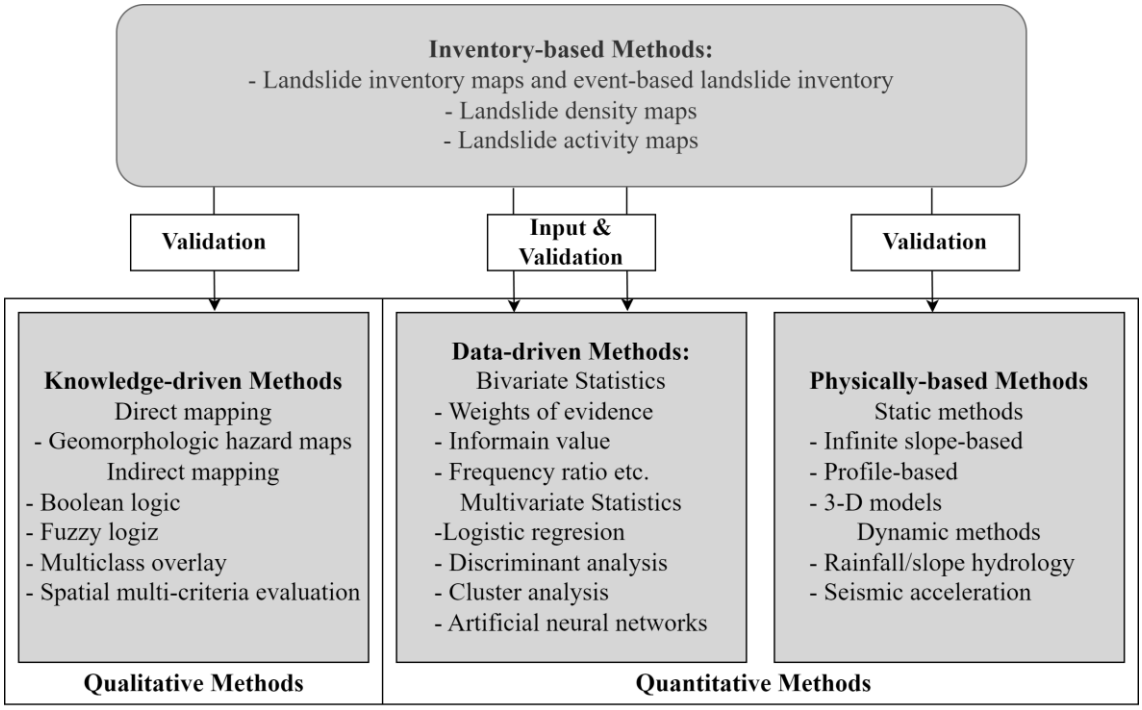

Figure 2.2. Overviews of the methods for landslide susceptibility assessment ([20]).

All methods require inventories, which can also be utilized to validate the final maps [20]. In knowledge-driven approaches, LSMs can be prepared either on-site using expert information or generated in the office as derivative maps from geomorphological maps. Direct and indirect applications of knowledge-driven approaches are possible. It can be used directly as it is the expert's field interpretation based on the observed events and geological environment. By merging many factor maps that are considered to be significant in the landslide occurrence, it can also be applied indirectly in a Geographic Information Sytem (GIS) environment [20]. In knowledge-driven methods, experts identify and weight landslides and relevant factors.

Physically based methods have been used based on modeling of slope failure processes. These methods have been applied in large areas where landslide types are simple and geomorphological/ geological conditions are rather homogeneous. These models are typically employed to investigate landslides with a depth of less than a few meters, as they rely on the infinite slope model. In physically based models for shallow landslides,

various triggers are included. These include the transient groundwater reactivity of slopes to rainfall and the effect of earthquake excitation [20].

In data-based (or data-driven) LSM production methods, the combinations of factors that are more closely associated with the spatial distribution of past landslides are statistically evaluated [25]. Quantitative estimates are made for areas that are not affected by existing landslides with similar geological, topographic, land cover and hydrological conditions. The output of a LSM is given in the sense of probability. These methods are called "data-driven" because data from past landslide occurences are used to obtain information about factor maps and the relative importance of their classes [20]. There are two main data-driven methods widely used in the literature: bivariate and multivariate statistical analysis. In bivariate statistical methods, each factor and landslide distribution are first combined. The weight value is calculated for each parameter class, taking into account the landslide intensity. Some statistical methods are used to calculate the weight value.

The frequency ratio (e.g [26-28]), fuzzy logic (e.g., [29-31]), weight of evidence (e.g., [32-34]), information value (e.g., [35-36]), Dempster-Shafer method (e.g., [37-39]) are among the frequently used bivariate methods. It is a preferred learning tool for determining which factors or combinations of factors play significant roles [20]. Bivariate statistical methods ignore how different variables are dependent on one another and plays an important role in getting to know the dataset before using multivariate statistical methods.

Multivariate statistical models explore the relationship between dependent (landslide occurrence) and a set of independent variables (landslide conditioning factors). Methods such as logistic regression (LR) (e.g.[40-41]), artificial neural network (ANN) (e.g.[42]), support vector machine (SVM) (e.g.[43]) and RF (e.g.[44]) have been among the most frequently used methods. These techniques have become regionally accepted for assessing landslide susceptibility.

These methods were also mentioned in bibliometric studies on landslide susceptibility researches. One of the recent reviews on bibliometric analysis concerns the evaluation of the period 1999-2021 for landslide susceptibility by Liu et al. [45]. In the bibliometric study conducted by Lima et al. [46], data-driven methods used for LSM were investigated. Reichenbach et al. [17] emphasized that only five methods were used for LSM in studies conducted before 1995. Liu et al. [45] stated that the trends on LSM methods have changed from traditional methods such as expert-based, statistical to supervised ML methods in recent years. Today, with the availability of inventory and geospatial datasets, novel ML methods, and their importance in computational power, the use of data-driven methods in landslide susceptibility studies has been increasing. Data-driven algorithms such as LR, ANN, SVM, neuro-fuzzy (NF), decision tree (DT), gradient boosting machine (GBM) and RF have been frequently used in LSM production [47-54].

In the production of LSMs, as mentioned above, different data sources have also been utilized. The data can be obtained by techniques such as photogrammetry and remote sensing. Satellite and aerial images, synthetic-aperture radar (SAR), light detection and ranging (LiDAR) are among these data sources as well [55-60]. Data obtained from different sources (landslide inventory, surface model, etc.) are crucial for the input parameters and accuracy assessment of the LSM to be produced. In addition, these data can be obtained from the existing geodatabase.

The methods used for the production of LSMs can also be classified as expert-based ([61], [29], [62-64]), statistical and probabilistic analysis ([65-67]) and supervised ML ([68], [48], [50], [51], [46], [45]) in the literature. The quality of the dataset used in the study, the suitability of the methods, the proper selection of conditioning factors, and the availability of inventory affect the accuracy of the results. Comparison of different methods is frequently used in the literature.

In a study by Pourghasemi et al. [29], both analytical hierarchy process (AHP) and fuzzy logic methods were used. Accuracy obtained from both methods was evaluated with receiver operating characteristic (ROC) curve and frequency ratio validation. The fuzzy

logic model showed better prediction accuracy than the AHP method. Pradhan [54] evaluated the three different approaches (DT, SVM and adaptive neuro-fuzzy inference system (ANFIS)). In the study, five models were produced using different landslide conditioning parameters in each model. The reason was to evaluate the effect and importance of different parameters on the performance of the methods. According to the results of the study, the DT method provided slightly better estimation performance than the ANFIS and SVM methods.

Can et al. [69] used the XGBoost method, which is one of the ML algorithms used in the production of more accurate and up-to-date LSMs in recent years. It was observed that high classification accuracy can be achieved with this method in large regions.

In a study conducted by Karakas et al. [70], the LSM was produced by comparing the RF and the multi-layer perceptron (MLP) methods. In the study, accuracy assessment and validation were conducted in three different approaches. Numerous landslides were triggered after the 24 January 2020 Elazig earthquake (Mw 6.8). The landslide inventory was produced using the pre- and post-earthquake aerial photogrammetric datasets by Karakas et al. [71]. The model training of both methods was carried out using the inventory obtained from pre-earthquake photogrammetric datasets. Accuracy assessment was made with the inventory obtained from the post-earthquake photogrammetric datasets. In addition, the model transferability was evaluated since model training was carried out only in a part of the study area. In the results, the RF method yielded higher classification accuracy than the MLP method. However, for some lithological units that were not used in model training, the MLP method showed better prediction performance.

The earthquakes in Kahramanmaras were notable for the fact that multi-hazards interacted and afflicted the same area. This was especially observed in Tut and Adiyaman regions. Karakas et al. [72] evaluated the MHS (landslide, flood and earthquake) of Tut and its surroundings in their study. The LSM was produced with RF algorithm, and a high level of accuracy was obtained with an F1 score of 0.93 for landslide pixels. In another study conducted by Karakas et al. [73], the landslide susceptibility prediction accuracy was analyzed with the event-based landslide inventory after the Kahramanmaras

earthquakes. A LSM of the region, which was significantly affected by the Kahramanmaras earthquakes and covers an area of 38,500 km^2, was produced using the pre-earthquake inventory and the RF algorithm. The susceptibility map produced was evaluated with the inventory of 2611 co-seismic landslides that were triggered during the earthquake and and not seen by the model. As a result of this evaluation, the statistics showed that the OA was 76%. The evaluation of co-seismic landslides using an independent validation set revealed the importance of considering previously unnoticed elements, such as uncommon lithological units.

Merghadi et al. [74] implemented different methods in a comparative overview of ML algorithm performances. The RF provided more robust results in the production of LSMs compared to other algorithms tested. Wang et al. [75] compared two models (RF and extreme gradient boosting decision trees) optimized with Bayesian algorithm in their study. According to the results, it was seen that the RF yielded a higher predictive ability than the extreme gradient boosting decision trees. In another study [76], the RF and the ANN methods were compared and the performances of both methods were found to be acceptable. But, the RF outperformed the ANN in accuracy.

Most studies in the literature utilized the RF method for the production of LSMs in recent years, since it produces accurate predictions. For this reason, the RF method was preferred for the production of LSM in this thesis study.

The accuracy assessment methods of the LSMs can be either qualitative, involving expert inspection, or quantitative, based on multiple measures such as recall, precision, F-1 score, Kappa index, ROC curve, area under curve (AUC) value, overall accuracy (OA), etc. Alternatively, a combination of both approaches may be employed at the same time. In a bibliometric analysis study conducted by Lima et al. [46], this issue was mentioned under the title of performance evaluation. According to the study outcomes, nearly half of the publications in the literature used the AUC for accuracy assessment.

2.3. Flood Susceptibility Map Production Methods

Studies on flood susceptibility assessment are less common in the literature than those on the landslides since they are heavily based on expert opinion and often lack accurate flood inventories. However, flood susceptibility assessment studies are becoming more and more popular, much like the landslide susceptibility assessment. Although various methods have been employed in susceptibility analysis, in practice, a few of them have been preferred more often than the others. Nevertheless, while there is no consensus among scientists in this field regarding the superiority of commonly used methods, the prevalent approaches in evaluating flood susceptibility in the literature include multi-criteria decision-making (MCDM) methods, physically based hydrological models, statistical methods, and various soft computing methods [77]. These approaches vary in their reliance on expert opinion and ease of application.

Flood susceptibility assessment studies have mostly been carried out with the MCDM methods. Decision-making involves selecting from various options, while MCDM allows for the evaluation of multiple criteria and the assignment of values to alternatives in complex scenarios such as disasters. The MCDM methods enable the selection of the best choice from multiple criteria simultaneously [78]. The MCDM methods, due to their straightforward structure, have been extensively utilized in flood susceptibility analysis. Examples of MCDM methods used in this context include the AHP (e.g., [79-82]), analytical network process (ANP) (e.g., [83-84]), weighted linear combination (WLC) (e.g., [85-87]) and decision-making trial and evaluation laboratory (DEMATEL) (e.g., [88]). However, it is important to note that the MCDM methods heavily rely on expert opinion and may yield subjective results. At the same time, the strength of these methods lies in their ability to consider potential effects that may not have emerged until the time of analysis [77].

Due to the difficulty of accessing flood inventory data, expert-based methods such as AHP ([79-81]) and fuzzy inference system ([90-92]) have been used more frequently. It was also preferred in data-driven approaches such as decision tree ([93-94]), LR ([95-97]), RF ([98-99]), SVM ([82]), bivariate and multivariate statistics ([93], [95]). In addition to these methods, some studies used hybrid techniques ([93], [100], [101], [90]).

On the other hand, data-driven methods require high quality and representative inventories, which are often not available. In addition, satellite-based flood data compilation methods may either fail at the slopes or not provide timely data. Therefore, expert-based methods are still preferred for this purpose. As an example, Sozer et al. [102] used an expert-based method, a modified AHP (m-AHP), for urban areas in Ankara, Türkiye. This method has the capability to correct expert errors to some extent (Yanar et al., [103]) and was found successful for producing FSMs.

The FSMs have often been analyzed by visual evaluation in expert-based methods. In data-driven methods, metrics such as the ROC curve, AUC value were also used (e.g., see [98], [99]), [82]).

2.4. Seismic Hazard Mapping Methods

Seismic hazard maps have been produced using various methods to assess earthquake risk in a region and evaluate the seismic resilience of structures. Historical seismicity analysis, seismotectonic studies, ground motion prediction equations, probabilistic seismic hazard assessment (PSHA) and deterministic seismic hazard assessment (DSHA) are among these methods. In historical seismicity analysis, past earthquake records in a region are investigated and the magnitudes, depths and frequencies of earthquakes occurring in this region are analyzed. These data help to understand the general seismic activity in a region. Seismotectonic studies are used to research regional geology and tectonic features to identify active fault lines, seismic potential zones, and other tectonic characteristics. These data have been used to understand where seismic activity ground motion prediction equations are used to predict the motion that an earthquake will create at the surface. These calculations are generally based on the magnitude, depth, and source-to-ground distance of the seismic activity.

In particular, probabilistic and deterministic seismic hazard assessments have been widely used based on its geological and seismological structure of a region. The DSHA

focuses on evaluating the worst-case scenario that a specific earthquake would create at a specific location. It estimates the worst-case ground motion at a particular location, usually using a given earthquake magnitude and location [104]. Within the DSHA process, seismic hazard is assessed through numerical techniques that do not rely on probability and incorporate inherent uncertainties. This method considers only the highest magnitudes of earthquakes and the most direct path between the source and the site, without taking into consideration the recurrence periods of earthquakes. PSHA is a method that evaluates the earthquake hazard in a region through probability distributions. In this method, seismic hazard maps are created based on the probability of occurrence in a region within a certain period of time, using different earthquake parameters and probability distributions. All potential earthquake scenarios that may affect the region are taken into account.

In 1968, Cornell [105] published the first-ever study on seismic hazard assessment, introducing a model for a probabilistic approach to evaluate seismic hazard. In the study, he formulated a quantitative method to establish the necessary correlations among ground motion parameters such as PGA, peak ground velocity, and the average return time specific to a particular region.

The PGA has been commonly utilized in the probabilistic evaluation of seismic hazards for site selection and engineering structure design. In 1999, Erdik et al. [106] conducted a probabilistic assessment of seismic hazard in Turkiye and its neighboring regions. They generated a map of PGA based on distinct return periods. Alpyürür and Lav [104] appraised seismic hazard in the southwestern region of Turkiye and developed a novel database for seismic susceptibility.

In another study conducted by Ince and Yilmazoglu [107], aimed to use the probabilistic seismic hazard method to ascertain the seismic risk in Mugla province and the surrounding area. In 2022, Gupta and Satyam [108] conducted an extensive probabilistic seismic hazard assessment focusing on Arias intensity (AI) and the PGA. The research offered new perspectives on the assessment of seismic hazards.

2.5. Multi-hazard Susceptibility Map Production Methods

The MHSA is a research discipline that aims to comprehensively determine susceptibility to various types of natural hazards and includes scientific, technical and social dimensions in this context. Rather than focusing on a single disaster type, this assessment offers a more holistic approach by considering the simultaneous impacts of different hazard types and their potential to create combined risk. This literature review on the MHSA aimed to explore and discuss the fundamental concepts, methodologies, and application examples in the field.

A limited number of publications in the literature were dedicated to the MHSA. Most of them followed a stepwise approach, integrating univariate susceptibility maps through either weighted overlay analysis or the AHP. Mukhopadhyay et al. [109] used the MCDA method in generating the multi-hazard (coastal erosion, sea-level rise, storm surge, coastal flood, tsunami, and earthquake) susceptibility map and the weights were defined by experts that were essential for achieving high accuracy. Skilodimou et al. [80] proposed the AHP supported by a GIS to assess hazards from landslides, floods, and earthquakes in the drainage basin of Peneus (Pinios) River in Western Peloponnesus, Greece. The researchers combined these assessments into a multi-hazard map to determine the suitability for urban development in the region. An uncertainty analysis was conducted on the variables used in the study by adjusting the weighting coefficients to evaluate the reliability of the model predictions. The study identified high hazard zones mainly in the western and north-eastern parts of the study area. The comparison between the spatial arrangement of urban areas and the road network with the suitability map demonstrated that roughly half of both are situated in areas susceptible to natural hazards.

Askha et al. [110] presented a multi-hazard risk assessment framework using geospatial and socioeconomic data in Dharan, Nepal, considering landslides, floods, and earthquakes. By employing statistical methods and the AHP, the study combined a Social Vulnerability Index (SoVI) with a multi-hazard map to create a total risk map. The results showed high-risk areas along the Seuti River in eastern Dharan and the left bank of the Sardu River in southwestern Dharan, while central Dharan and the western hills were classified as low-risk areas. Yanar et al. [103] created a MHSA model for a specific area

in Ankara by employing fuzzy logic to integrate a FSM and a Landslide Susceptibility Map (LSM). Khatakho et al. [111] utilized AHP and GIS to assess floods, landslides, earthquakes, and urban fire hazards in Kathmandu Valley, Nepal and integrating them once more through the application of AHP. Based on collective observations, it was determined that densely populated areas, historical settlements, and the central valley exhibit a high to very high level of multi-hazard risk.

Rehman et al. [112] utilized field surveys and remote sensing data to develop inventories of geo-hazards and calculated the subjective and objective weights of causative factors using geospatial techniques such as the AHP and Frequency Ratio (FR) within a GIS environment. The results showed that the southern and northwestern parts of the region are the most suitable areas for future sustainable development and economic activities, while the eastern and western regions, including Muzaffarabad City, exhibit high to very high susceptibility.

Moreover, recent research studies conducted in China ([113]), in Iran ([114-117]), and in Saudi Arabia ([118]), diverse ML approaches were utilized for the MHSA. Pourghasemi et al. [119] developed a MHS model in Iran, employing a novel ensemble model called stepwise weight assessment ratio analysis (SWARA). They utilized the adaptive neuro-fuzzy inference system (ANFIS) and grey wolf optimizer (GWO) for the assessments of landslide-, flood-, and earthquake-prone areas. In their study, a PGA map was produced based on PSHA. The accuracies of the FSM and the LSM were evaluated using the ROC curves.

Ullah et al. [120] proposed a MHSA framework using Convolutional Neural Networks (CNN) to predict and mitigate the risk of flash floods, debris flows, and landslides. The proposed CNN method has good performance in predicting the probability of hazards. The susceptibility maps of the three hazards, generated using CNN, were integrated to produce a multi-hazard susceptibility map. This map reveals that 62.43% of the research region exhibited vulnerability to hazards.

3. STUDY SITES AND GEOSPATIAL DATASETS

The methodology proposed in the thesis was applied to two different study areas with different characteristics in terms of destructive earthquake and flood events and their secondary hazards; the data availability, land cover and topography. In this chapter, the earthquake and flood events, study areas and characteristics, and the geospatial datasets used in the thesis are explained.

3.1. Elazig Study Site

In this section, the geographical and geological characteristics of the Elazig study site, the January 24, 2020 Elazig earthquake event, and various previous flood events in the region were explained. The site was selected because it is susceptible to multi-hazards, namely landslides, floods and earthquakes.

3.1.1. Location and geological characteristics for Elazig study site

The Elazig study site is located in the southeastern part of Türkiye and consists of the Elazig Province and surrounding basins (Figure 3.1). In the study site covering approximately 5,150 km², the altitude values obtained from EUDEM v1.1 of the Copernicus Land Monitoring Service [121] vary between 524 m and 2592 m. The mean annual temperature recorded in Elazig Province was 13.2°C, while the average annual precipitation amounts to 420.2 mm [122]. The environmental conditions were represented using LULC classes derived from a global land cover map released by the ESA [123]. The Elazig study site predominantly consists of 69% grassland. Subsequently, it encompasses 9% bare/sparse vegetation, 8% cropland, 6% permanent water bodies, 5% tree cover, 2% built-up area, and 1% shrubland (Figure 3.2).

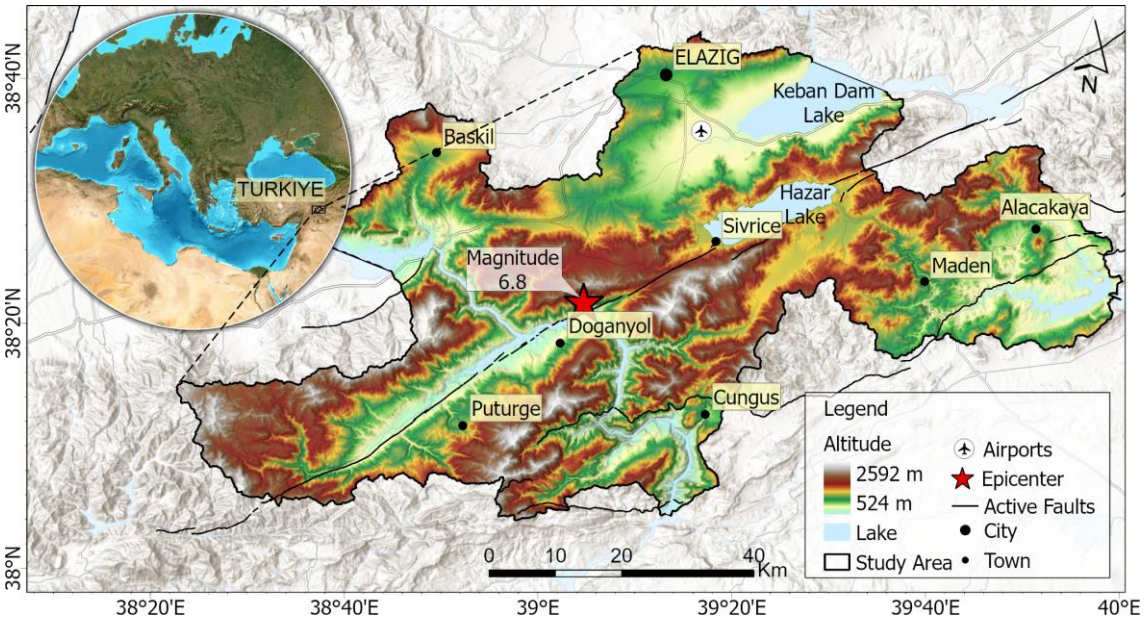

Figure 3.1. The Elazig study site with EUDEM v1.1 data, the epicenter of Elazig earthquake and fault lines

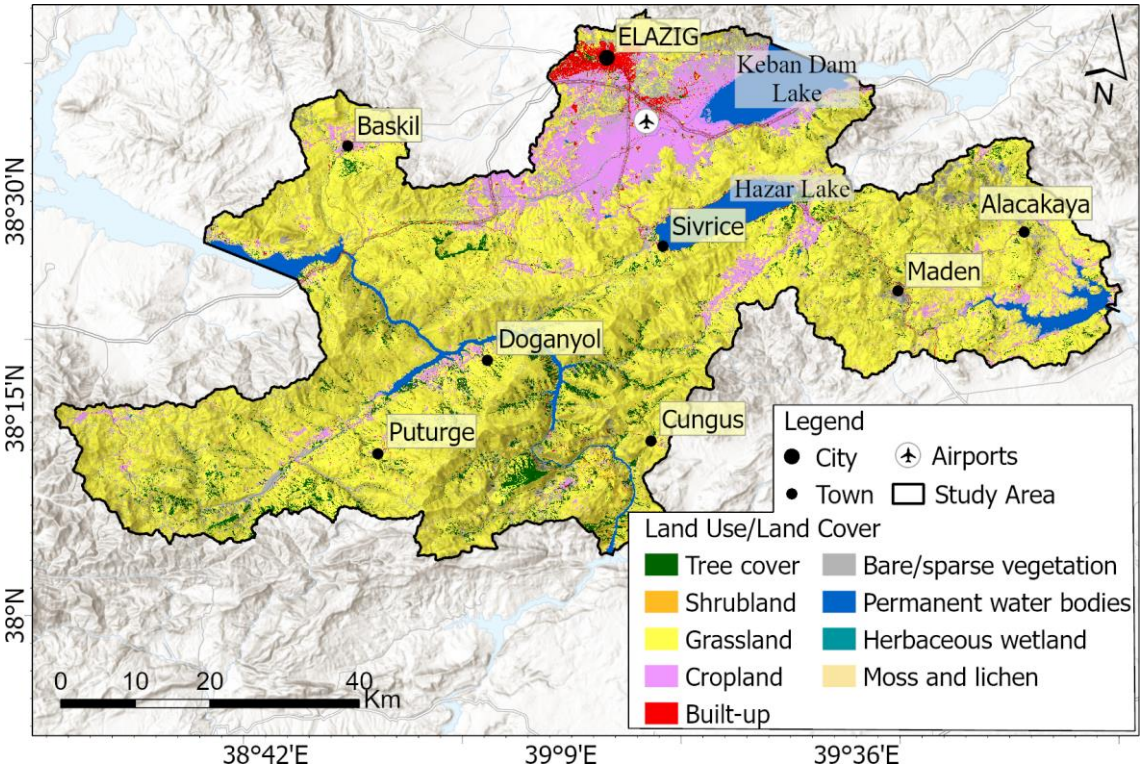

Figure 3.2. LULC map for the Elazig site derived from the ESA WorldCover 2021 dataset [123].

Since the study site is situated along the East Anatolian Fault Zone (EAFZ), it is exposed to significant seismic activities and ongoing tectonic changes. This also results in a young and rugged terrain. The geological formations in the region also exhibit limited shear strength. These conditions make the region prone to landslides [124]. Avci and Sunkar [125] explored the correlation between lithological units and the proximity to fault lines concerning landslides in Elazig and its adjacent northern province. Their findings revealed that the majority of landslides in the area were induced by seismic activity. Moreover, the area has a long-standing history of experiencing frequent and catastrophic earthquakes [126-127].

The EAFZ exhibits the characteristics of strike-slip movement triggered by the continent-to-continent collision of the Arabian-African and Eurasian Plates. The interaction between the four main tectonic plates of Arabia, Eurasia, India, and Africa with the relatively smaller tectonic block of Anatolia generates high activity in the region [127]. Due to the active tectonism in the study site, geological formations exhibit diversity. The youngest and oldest units are of Quaternary and Precambrian ages, respectively. The geological map for the Elazig study site is provided in the Figure 3.3. A total of 339 geological units in the area were combined based on similar characteristics to obtain 19 units. The unit of gneiss, schist is the most commonly observed within these geological units. This is followed by units volcanites and sedimentary rocks, clastics and carbonates, terrigenous clastics, neritic limestone and undifferentiated alluvial, respectively (Table 3.1).

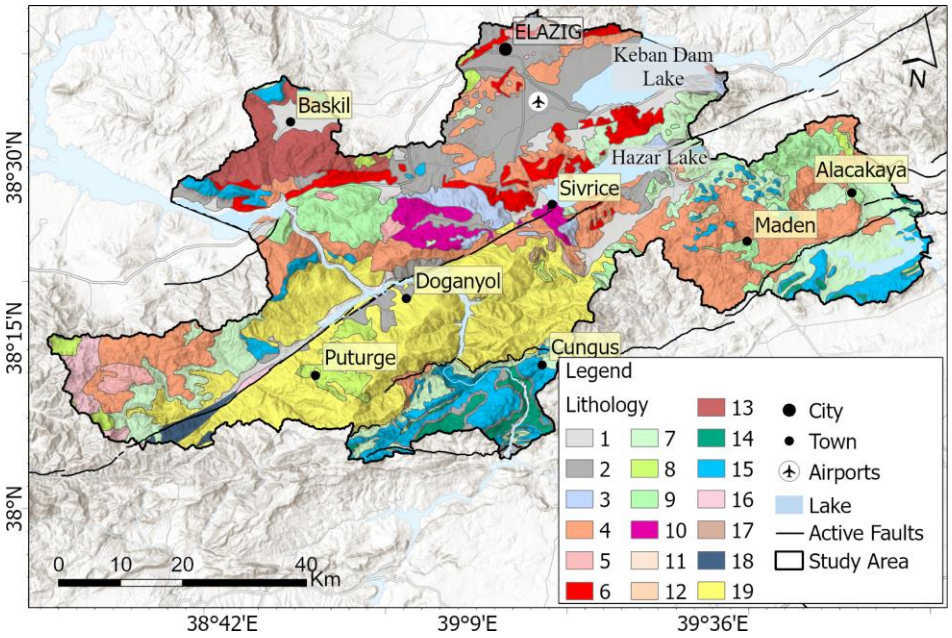

Figure 3.3. Geological map in the Elazig study site ([128-132]).

Table 3.1. Areas of the geological units in the Elazig study site

Unit ID	Lithological Units	A_i (km²)
1	Undifferentiated Alluvial	208.00
2	Terrigenous clastics	543.89
3	Sheeted dyke complex	89.49
4	Volcanites and sedimentary rocks	916.53
5	Granitoids	50.80
6	Basalt	192.21
7	Clastics and carbonates	637.22
8	Marble	121.89
9	Undifferentiated basic and ultrabasic rocks	273.40
10	Gabbro	93.34
11	Serpentinite	1.44
12	Ophiolitic melange	1.05
13	Diorite, tonalite, monzonite, gabbro etc.	180.78

14	Pelagic limestone, clastics, radiolarite, chert etc.	80.59
15	Neritic limestone	342.50
16	Schist	66.65
17	Quartzite, quartzschist	13.75
18	Amphibolite	31.03
19	Gneiss, schist	1000.37

3.1.2. The 24 January 2020 Elazig (Turkiye) earthquake event

On January 24, 2020, at local time 20:55, an earthquake with a moment magnitude of Mw. 6.8 occurred as a result of the rupture of the NE-SW strike-slip fault along the Hazar-Sincik Segment on the EAFZ [126]. According to the AFAD report (see also Figure 3.1), the epicenter of the earthquake was 37 km south-southwest of Elazig and 64 km east of Malatya (N38.359°, E39.063°) and the earthquake's focal depth was 8.06 kilometers. The effects of the Elazig- Sivrice earthquake were observed in a wide area in the Elazig and Malatya regions, from Lake Hazar in the east to Malatya city center in the west. According to the preliminary report of field observations published by MTA, the surface deformations associated with this earthquake were along a line of about 48 km from Lake Hazar to Pütürge (Malatya) [133]. The Anatolian Plate is tectonically active and thus, the region is frequently exposed to destructive earthquakes. According to AFAD data, unfortunately 41 people lost their lives and 1607 people were injured in the earthquake. 547 buildings were completely destroyed, 6270 buildings suffered severe damages, 962 buildings suffered moderate damages and 10273 buildings suffered minor damages [133]. In addition, secondary hazards such as lateral spreading, rockfalls, liquefaction and landslides were observed in the region after the earthquake. In the technical report published by Gokceoglu et al. [134], these secondary hazards, especially landslides, were discussed in detail.

3.1.3. Recent flood events in the Elazig study site

Due to the geographical characteristics and climatic conditions of Elazig and its surrounding basins, several floods have occurred before. The causes of these floods include sudden and heavy rains, overflowing of stream beds, disruption of stream flow regimes and streambed morphology by extracting material from stream beds, and settlement in stream beds due to unplanned urbanization. Flood events seriously affect settlements and agricultural areas in the region. The damage to homes and businesses, the destruction of agricultural produce, and the infrastructure damage have adverse effects on the local economy and the living standards of the community. Despite extensive efforts, no comprehensive inventory of flood events could be found to conduct the study analyses. Yet, based on the news and media reports, some inundated areas, which were found highly susceptible to flooding, could be found. The locations of inundated areas are presented in detail in Table 3.2.

Table 3.2. Locations of the inundated areas during the previous events occurred in Elazig and its surroundings.

Inundated Area No	Event Date	Location
1	15 April 2017	N38.609°, E39.302° [135]
2	20 June 2019	N38.681°, E39.257° [136]
3	20 June 2019	N38.675°, E39.206° [137]
4	4 May 2022	N38.669°, E39.185° [138]
5	4 May 2022	N38.667°, E39.246° [139]
6	13 June 2022	N38.683°, E39.395° [140]
7	13 June 2022	N38.646°, E39.393° [140]
8	15 March 2023	N38.491°, E39.852° [141]
9	16 March 2023	N38.565°, E39.246° [142]
10	6 December 2023	N38.671°, E39.228° [143]

3.1.4. The landslide inventory for Elazig study site

It is of great importance to have information about both temporal and spatial frequency of landslides in order to create a map that reliably predicts landslide susceptibility, hazard and risk in a particular region. Therefore, it is necessary to start by compiling a comprehensive and complete inventory of landslides for these studies. Landslide inventories can be provided using various techniques. Image interpretation (stereo aerial photographs), semi-automated classification based on spectral and altitude characteristics (high resolution satellite images, aerial photograps, LiDAR shaded relief maps, RADAR images, InSAR), field investigation methods (field mapping), archive studies (interviews, newspaper). archives, existing databases), dating methods for landslides (direct and indirect methods), monitoring networks (electronic distance measurements, GPS, ground-based InSAR, terrestrial LiDAR) are among these techniques [144]. Some attempts were made to standardize the landslide inventories obtained by naming classification types ([2, 145]), causes of landslides ([146]), landslide activity ([147]).

For landslides triggered after triggering conditions such as rainfall, earthquake, human impact, etc., landslide inventory preparation studies must be carried out frequently and the inventory in existing databases must be updated.

In this thesis study, a multi-temporal landslide inventory was utilized. The landslide inventory used was categorized into two groups: pre- and post-earthquake landslide inventories. Detailed information regarding the pre- and post-earthquake inventories in the Elazig study site is explained below.

3.1.4.1. Pre-earthquake landslide inventory for Elazig study site

The pre-earthquake landslide inventory used in the model training phase of the thesis study was obtained by visual interpretation of 3D models, orthophotos produced aerial photographs and from MTA's geosciences WebGIS portal. The “Türkiye Landslide Inventory Project” was initiated regionally by MTA in 1997 for the landslides in the portal

and was completed on a national scale in 2007 [148]. Existing landslides were identified and mapped as a result of aerial photo analysis and detailed field studies. The landslides mapped within the scope of this project were presented to users as an inventory on the geosciences WebGIS portal. Based on the classification of Varnes (1978) [149] in the classification of landslides, mass movements were classified as flow, slide and complex according to the type of movement. Fall and topple-type landslides could not be taken into consideration due to scale limitations. In addition, landslides were classified according to their activities, divided into active and inactive [148]. As can be seen in Figure 3.4, there are a total of 694 pre-earthquake landslides defined as polygons in the Elazig study site. The areas of these landslides vary from 0.0002 km^2 to 3.431 km^2. Additionally, the distribution of area sizes for the landslide inventory before the earthquake is presented in Table 3.3 and Figure 3.5. Generally, most of these landslides were observed along active fault segments.

Table 3.3. The distribution of area sizes for the Elazig study site's pre-earthquake landslide inventory.

Landslide Area (km^2)	**Landslide Counts**	**Percentage (%)**
<0.03	246	35.45
0.03 – 0.06	135	19.45
0.06 – 0.09	51	7.35
0.09 – 0.12	63	9.08
>0.12	199	28.67

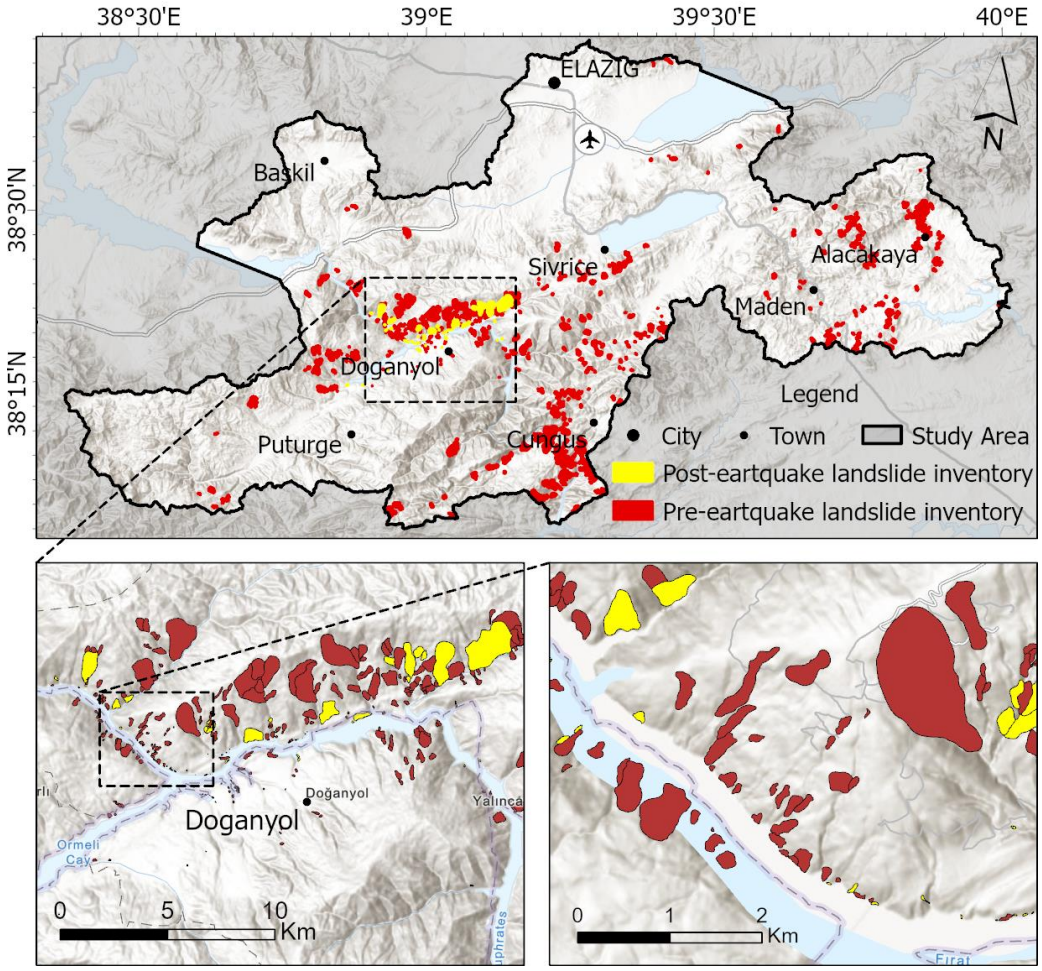

Figure 3.4**.** Pre and post-earthquake landslide inventory for Elazig study site.

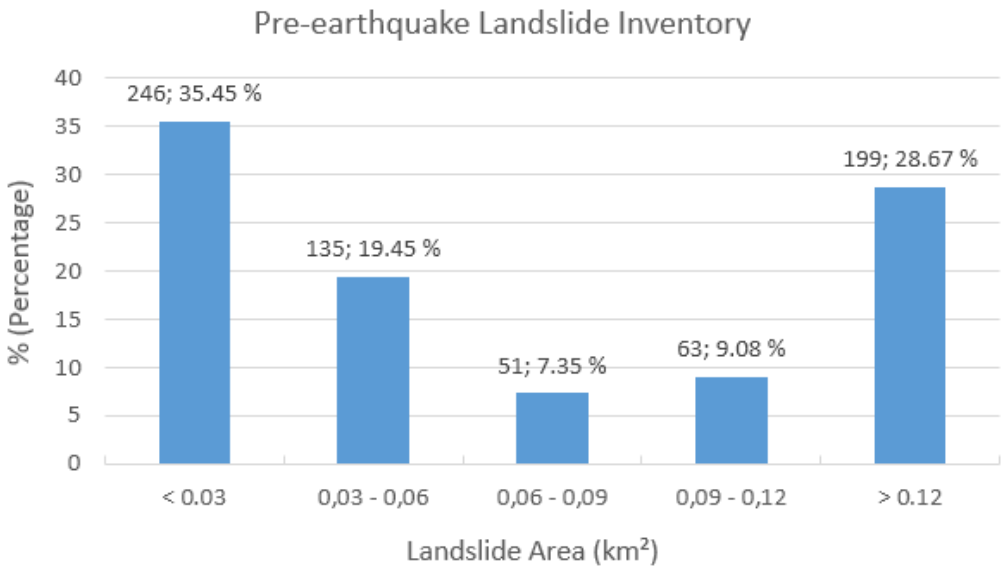

Figure 3.5. The pre-earthquake landslide inventory's size distribution as a percentage chart.

3.1.4.2. Post-earthquake landslides inventory for Elazig study site

The post-earthquake landslide inventory used in this thesis was obtained by visually interpreting orthophotos and 3D surface models produced from aerial photographs taken pre and post-earthquake (see Karakas et al. [71] for further details). Aerial photographs taken in three different years (2017, 2018, 2020) were used for photogrammetric processing. 142 pre-earthquake images of 2017 (Malatya flight) and 2018 (Elazig flight) with 80% forward overlap and 60% side overlap with 30 cm GSD were obtained from the General Directorate of Mapping (GDM). 1410 post-earthquake images were taken by the GDM on 26 January 2020, 2 days after the Elazig earthquake.

The GDM's photogrammetric data production process comprised steps such as flight planning, image acquisition, and aerial triangulation. The airplane's inertial navigation system (INS) and global navigation satellite system (GNSS) receivers were used to determine the external orientation parameters (EOPs). The interior orientation parameters (IOPs) of the UltraCam sensors [150] were established through laboratory calibration conducted by Vexcel Imaging. At the GDM, the photogrammetric bundle block adjustment method was employed across all datasets to enhance image georeferencing accuracy. This was achieved by recalculating the image exterior orientation parameters (EOPs) through a least squares estimation process, utilizing signalized and ground-surveyed control points as reference points. The digital surface models (DSMs) and orthophoto mosaics were produced using Agisoft Metashape Professional, developed by Agisoft LLC in St. Petersburg, Russia. Table 3.4 illustrates the characteristics of stereo datasets and photogrammetric products.

Table 3.4. The characteristics of stereo datasets and photogrammetric products.

Date	Province	Camera	#of photos	Flight altitude (m)	Raster DSM (cm)	Ortho GSD (cm)	Use purpose
2017 (Summer)	Malatya	UltraCam Eagle 1	88	7500	66	30	Pre-earthquake
2018 (Summer)	Elazig	UltraCam Eagle 1	54	6500	68	30	Pre-earthquake
26 Jan 2020	Malatya and Elazig	UltraCam Eagle M3	1410	6500	82	30	Post-earthquake

The area surrounding the segment damaged by the Elazig earthquake was found to have 328 landslides, which were detected and mapped by comparing the surface models and orthophotos taken pre and post-earthquake. These landslides were divided into four groups according to the classification proposed by Cruden and Varnes [145]. These groups were inactive mass movements (75), active mass movements (183), new active zone developed within the existing mass after 2018 (57), and newly developed after 2018 triggered by the Elazig earthquake (13) [71]. The observed activities within the masses typically occurred in a retrogressive manner, primarily concentrating on the crown sections of the landslides, leading to their backward development. Additionally, new activities were noted in the secondary failures of the large masses, characterized as sackung-type landslides. Since it was concluded that the 3rd and 4th group activities were triggered by the Elazig earthquake, 70 of these 328 landslides were used to test the the final LSM. Group 1 and 2 activities were included in the pre-earthquake landslide inventory data and used in model training. The areas of these 70 landslides vary from 0.0001 km^2 to 3.007 km^2. The landslides triggered by Elazig earthquake were mostly observed along lakeshore, road cuts and river terraces [71]. In Figure 3.6, examples of landslides triggered in the Elazig earthquake can be seen on orthophotos produced from aerial photographs pre and post-earthquake.

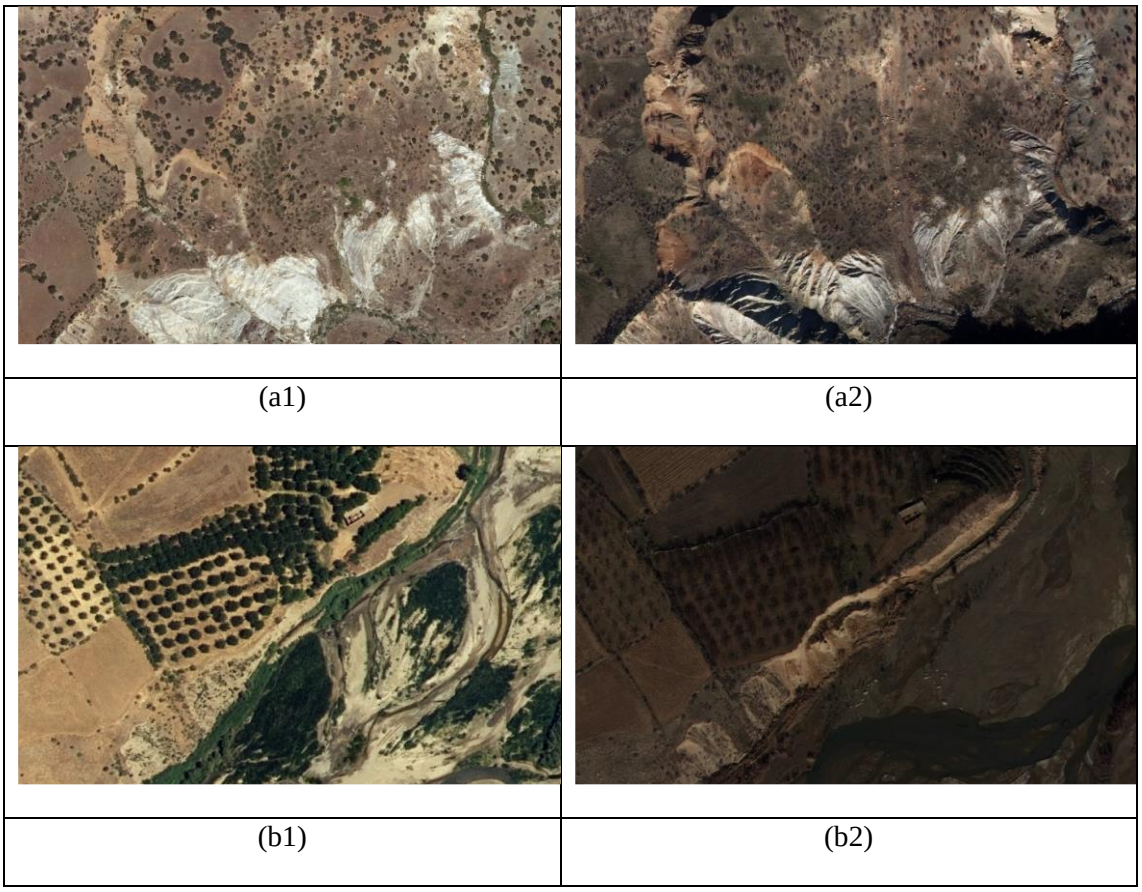

(a1) (a2)

(b1) (b2)

Figure 3.6. Examples of landslides triggered in the Elazig earthquake on orthophotos produced from aerial photographs pre (a1, b1) and post-earthquake (a2, b2).

3.2. The Adiyaman Study Site

In this section, the geographical and geological characteristics of the Adiyaman study site, the February 6, 2023 Kahramanmaras earthquake events, and various previous flood events in the region was explained. The site was selected due to data availability and also it is susceptible to multi-hazards, namely landslides, floods and earthquakes.

3.2.1. Location and geological characteristics for Adiyaman study site

Adıyaman and its surroundings, one of the 11 provinces affected by the Kahramanmaras earthquakes that occurred on February 6, 2023, was selected as the study site. Particularly

in the Tut region of Adıyaman, many landslides were observed as a secondary hazard triggered during the earthquakes. Subsequently, a flood event occurred in the region due to heavy rains. For the purpose and scope of the thesis study, since there are more than one multi-hazards affecting the same area in Adıyaman Tut region, this region was selected as an additional study site to test the applicability of the methodology. The model parameters and predictive variables were tuned for the site. The study area covers an area of approximately 1600 km^2 and Figure 3.7 shows the location of the study area together with the digital elevation model (DEM) obtained from EUDEM v1.1. The altitude of the site varies between 461 m and 2522 m. The mean annual temperature in Adiyaman Province is 17.4°C degrees, while the average annual precipitation is 715.1 mm [122]. According to global land cover map released by the ESA, the Adiyaman study site predominantly consists of 55% grassland. Subsequently, it encompasses 21% cropland, 12% bare/sparse vegetation, 8% tree cover, 3% built-up area, and 1% shrubland (Figure 3.8).

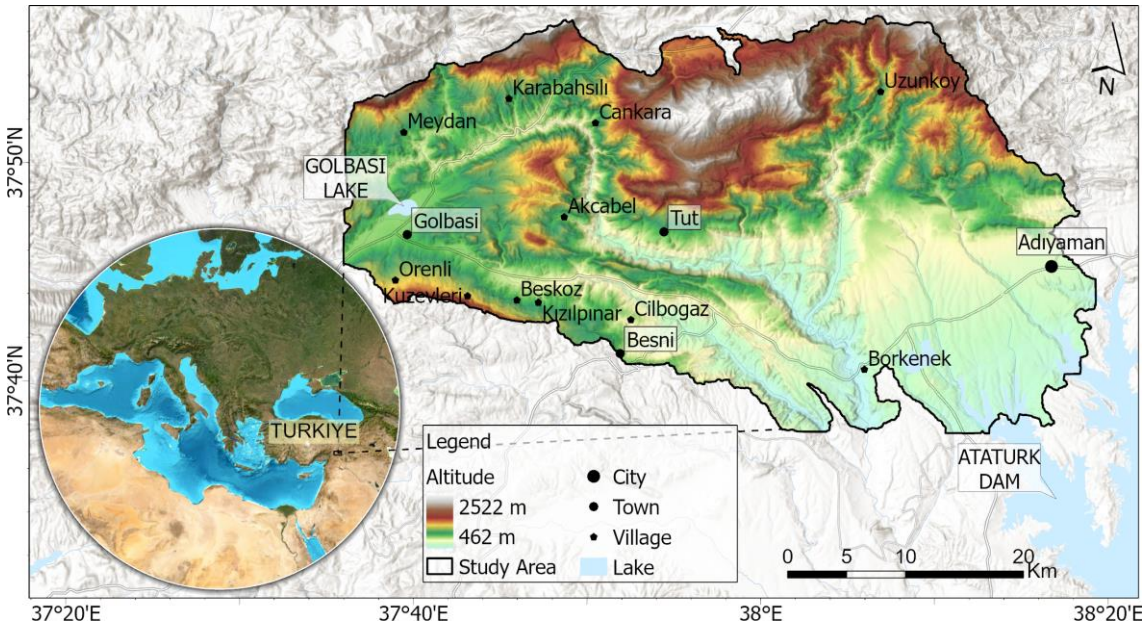

Figure 3.7. The Adiyaman study site with EUDEM v1.1 data and fault lines.

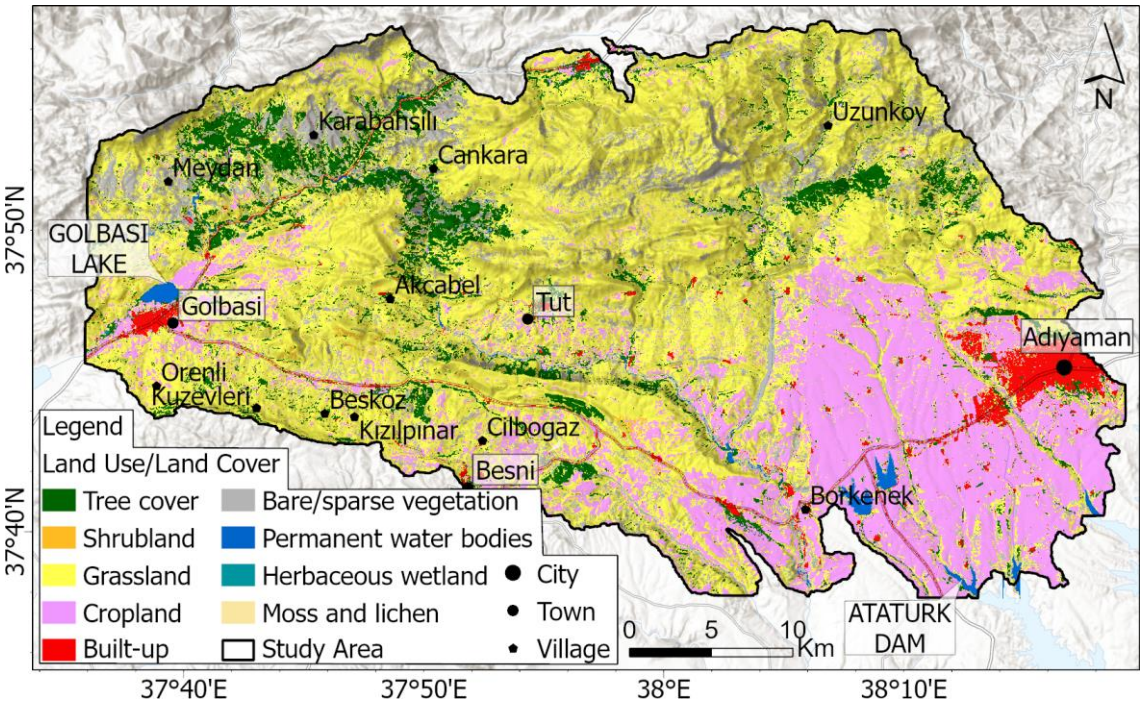

Figure 3.8. The LULC map of Adiyaman study site obtained from ESA WorldCover map [123].

The Adiyaman study site exhibits a complex structure due to its placement within the EAFZ, characterized by frequent seismic activity. It comprises diverse units consisting of igneous, metamorphic, and sedimentary rocks spanning from the Precambrian age to the present geological time periods. The geological map for the Adiyaman study site is provided in the Figure 3.9. A total of 27 geological units were available in the area. Yet, they were combined based on similar characteristics to reduce the dimensionality, thus 12 units were obtained. As depicted in Figure 3.9 (please also see Table 3.5), the unit of neritic limestone is the most commonly observed within these geological units. This is followed by units pelagic limestone, clastics and carbonates, non-graded terrigenous clastics, volcanites and sedimentary rocks and terrigenous clastics, respectively. The unit names are given in Table 3.5.

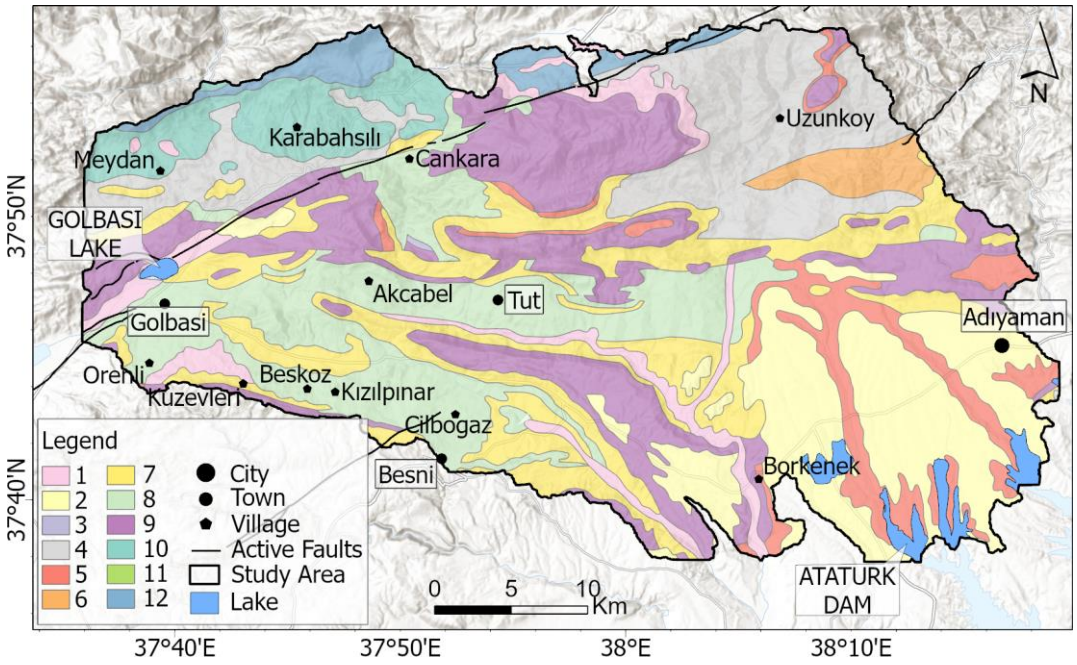

Figure 3.9. Geological map in the Adiyaman study site ([151-152]).

Table 3.5. Area sizes of the geological units in the Adiyaman study site.

Unit ID	Lithological Units	A_i (km²)
1	Undifferentiated Alluvial	74.08
2	Non-graded terrigenous clastics	234.87
3	Basalt	0.68
4	Volcanites and sedimentary rocks	205.84
5	Terrigenous clastics	98.82
6	Ophiolitic melange	28.24
7	Clastics and carbonates	247.58
8	Pelagic limestone	271.16
9	Neritic limestone	301.15
10	Undifferentiated basic and ultrabasic rocks	84.93
11	Peridotite	0.01
12	Marble, schist in places	42.01

3.2.2. The 6 February 2023 Kahramanmaras (Turkiye) earthquake events

On February 6, 2023, two major devastating earthquakes occurred at local times 04:17 and 13:24, with their epicenters located in the Pazarcik (N37.288, E37.043) and Elbistan (N38.089°, E37.239°) districts of Kahramanmaras, known as the catastrophic events of the century. The magnitudes of these earthquakes were Mw. 7.7 and Mw. 7.6, respectively. According to the AFAD report, the focal depth of the first earthquake, located in the primary branch of the EAFZ between the Narlı segment and the Pazarcık segment of the Dead Sea Fault Zone, was 8.6 km. The focal depth of the second earthquake, which caused surface rupture along the Cardak Fault, a part of the northern branch of the EAFZ, was determined to be 7.0 km. The these seismic events resulted in catastrophic devastation across 11 provinces situated in the Southeastern and Eastern Anatolia Region of Türkiye. The earthquakes led to immeasurable damages and casualties numbering in tens of thousands. In addition to the devastating earthquakes, the region witnessed numerous secondary hazard occurrences, including rockfalls, landslides, rock avalanches, surface ruptures, liquefaction, and more, all triggered by the seismic activity. Adiyaman and its surrounding areas are also among the provinces most affected by these earthquakes and secondary hazards. Furthermore, several parts of the region frequently experience flooding, a meteorological hazard related to climate conditions, which may also trigger landslides.

3.2.3. Recent flood events in the Adiyaman study site

On March 15, 2023, approximately one month after the earthquakes in Kahramanmaraş on February 6, 2023, a second disaster occurred in the Tut district of Adıyaman due to heavy rainfall, namely a flood event. Due to the overflow of the stream passing through the center, many houses and agricultural areas were damaged, resulting in losses of lives. Again, as in the Elazig site, no comprehensive flood inventory was obtained despite extensive efforts. Yet, based on the news and media reports, some inundated areas, which are highly susceptible to flooding, were identified. These inundated areas are presented in Table 3.6.

Table 3.6. The inundated areas that have occurred previously in Adiyaman and its surroundings.

Inundated Area No	Event Date	Location
1	1 May 2022	N37.759°, E38.279° [153]
2	15 March 2023	N37.795°, E37.914° [154]
3	11 April 2023	N37.794°, E38.240° [155]

3.2.4. The landslide inventory for Adiyaman study site

In the Adiyaman study site, a multi-temporal landslide inventory was also used. The inventory was categorized as pre- and post-earthquake landslide. Detailed information regarding the pre- and post-earthquake inventories in the Adiyaman study site are given below.

3.2.4.1. Pre-earthquake landslides inventory for Adiyaman study site

The pre-earthquake landslide inventory used in the model training phase in the Adiyaman study site was obtained from MTA's geosciences WebGIS portal. Landslide inventories in this region were also mapped within the scope of the "Türkiye Landslide Inventory Project", as explained in detail in Section 3.1.4. As seen in Figure 3.10, there were a total of 217 pre-earthquake landslide inventories in the Adıyaman study site. The smallest and largest landslide areas in the pre- earthquake landslide inventory varied between 0.0005 km^2 and 7.970 km^2. The distribution of area sizes for the landslide inventory before the earthquake is presented in Table 3.7 and Figure 3.11.

Table 3.7. The distribution of area sizes in the Adiyaman study site's pre-earthquake landslide inventory.

Landslide Area (km^2)	Landslide Counts	Percentage (%)
<0.02	111	51.15
0.02 – 0.04	52	23.96
0.04 – 0.06	9	4.15
0.06 – 0.08	8	3.69
>0.08	37	17.05

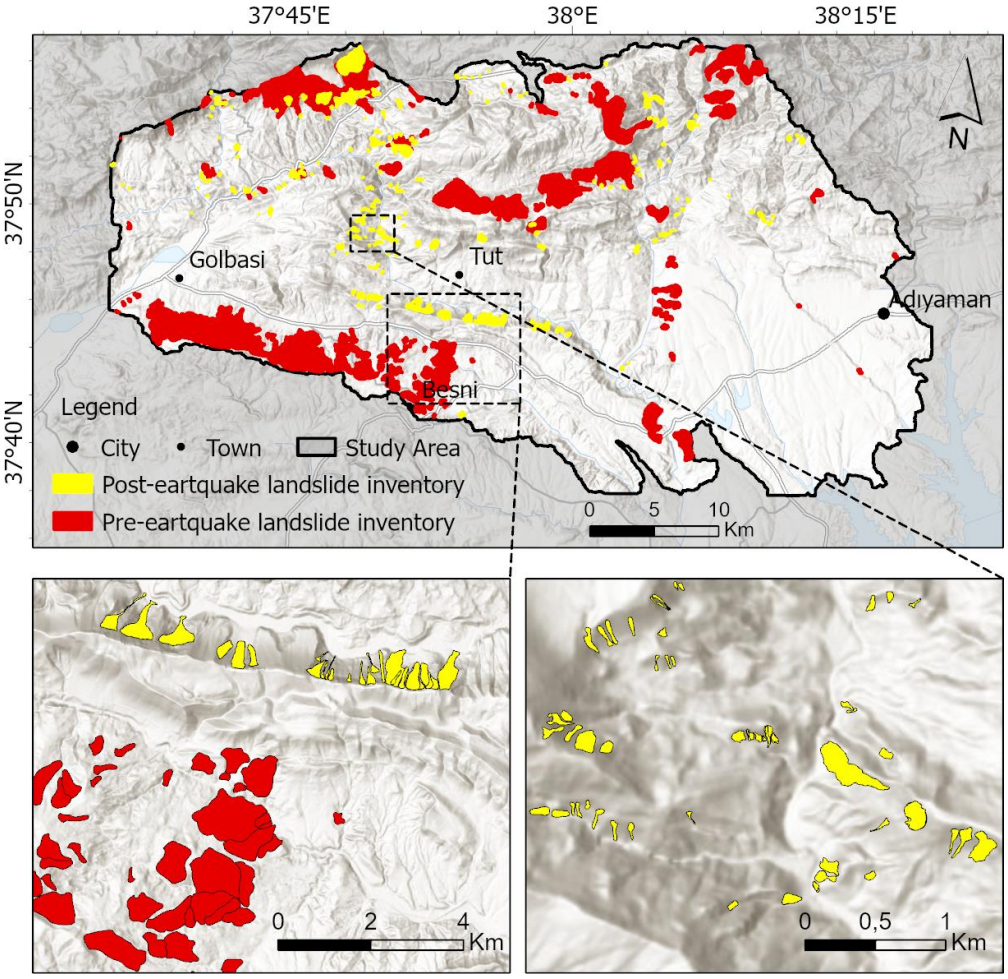

Figure 3.10. Pre-earthquake landslide inventory in the Adiyaman study site.

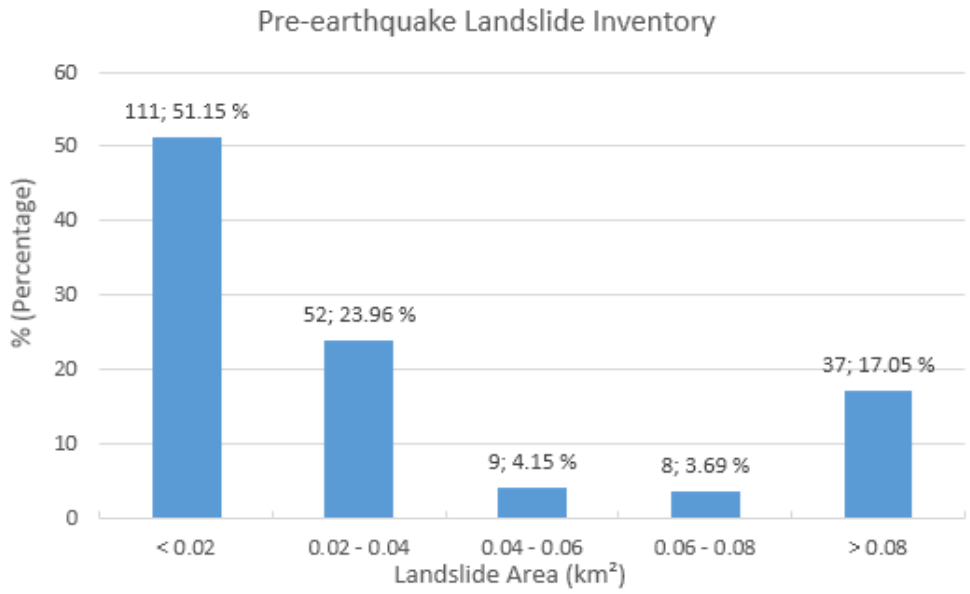

Figure 3.11. The pre-earthquake landslide size distribution as a percentage chart.

3.2.4.2. Post-earthquake landslides inventory for Adiyaman study site

The landslides in the Adiyaman study site triggered by the Kahramanmaraş earthquakes were determined by comparing the pre-earthquake and post-earthquake orthophotos in the HGM Küre application [156], which is a web-based GIS platform offered to the user by the GDM. These orthophotos were produced by processing the aerial photographs obtained as a result of the aerial photogrammetric flight mission carried out by GDM in the earthquake region (see Karakas et al. [73] and Kocaman et al. [157] for further details). The GDM continued its flight missions for a week, starting from February 7, 2023, one day after the earthquake. Aerial photograps were generally taken from rural and mountainous areas. All aerial stereo images with an average GSD of 25 cm were captured with an Ultracam Eagle M3 camera [150]. These images were rapidly processed and presented to the user in the HGM Küre application. In these orthophotos presented in 3D, there was only a DEM representing the pre-earthquake situation. The geometric quality of these orthophotos is suitable for identifying and mapping landslides.

Due to seasonal conditions, it was observed that the images obtained from flights after the earthquake show dense cloud cover shadows and snow cover. Despite these

challenging situations, a total of 2611 landslides triggered by Kahramanmaraş earthquakes were mapped in the HGM Küre application by[72], [73], [157]. In addition, some of these landslides have been validated with field observations in the earthquake region. Mass movements such as flow (debris flow), slide (translational and bedrock rotational), fall (rock fall) and spread were observed in landslide types triggered after the earthquake.

There were 530 landslides triggered after the earthquake in the Adıyaman study site. Observations also revealed certain failures in talus materials, identified as debris flows. Such landslides have been encountered especially in the east of the Tut region. Talus material originated from limestone formations located at higher elevations of the slope, gradually accumulating on the lower slopes. The areas of these landslides varied from 0.0001 km^2 to 2.47 km^2. These landslides triggered after the earthquake were not included in the model training. It was used to validate the LSM produced for the Adıyaman study site. Examples from the pre- and post-earthquake landslides were illustrated as perspective images shown on Google Earth platform [158] in Figure 3.12.

	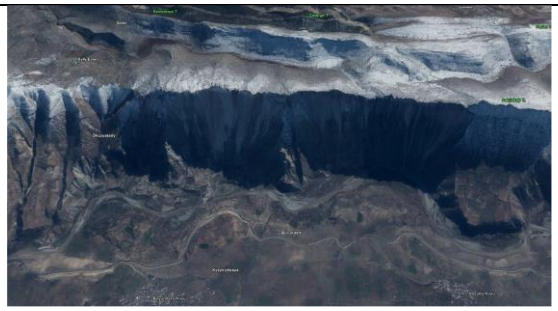
(a1)	(b1)
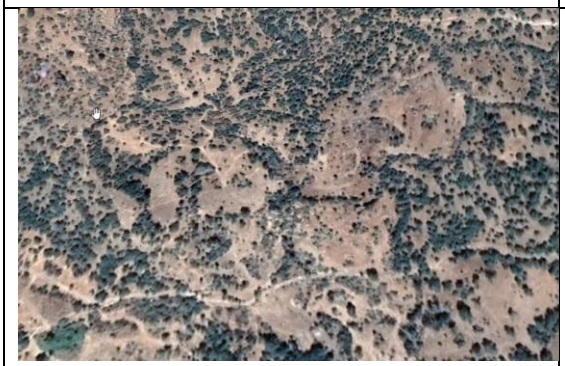	
(a2)	(b2)

(a3) (b3)

Figure 3.12. The pre (a1, a2, a3) and post (b1, b2, b3) 3D image perspective of the identified post-earthquake landslides on the Google Earth platform.

3.3. Geospatial Datasets

The first stage of obtaining the univariate susceptibility maps used in the thesis study was the collection of data from which the conditioning factors associated with landslides were produced. The main data, data sources, resolution/scale and formats used for this thesis study are presented in Table 3.8.

Table 3.8. The main data, data sources, resolution/scale and format used in the study sites.

Data	**Data sources**	**Source format**	**Resolution/Scale**
DEM	EUDEM v1.1	Grid	25 m
Lithology	Geological maps from MTA	Polygon	1/100.000
Faults	MTA Geosciences WebGIS portal	Polyline	1/25.000
Pre-earthquake Landslide Invertories	MTA Geosciences WebGIS portal	Polygon	1/25.000
LULC	ESA WorldCover	Grid	10 m
River Vector data	TopoVT of HGM	Polyline	1/25.000

Arias Intensity values	AFAD earthquake database	Point	-

The DEM data, which is one of the main data sources in the study, was extracted from EUDEM v1.1. The EUDEM v1.1 published by CLMS represents an upgraded version of EU-DEM v1.0., incorporating improvements such as rectifying geopositioning discrepancies, minimizing artifacts, and enhancing vertical accuracy by utilizing data from the Ice, Cloud, and land Elevation Satellite (ICESat) mission operated by NASA. The product was obtained by combining ASTER GDEM datasets and the Shuttle Radar Topography Mission (SRTM). It has a spatial resolution of 25 m and a vertical accuracy of 7 m, and consists of a total of 27 tiles, covering a 1000 km × 1000 km area (CLMS 2022). The study area corresponds to the tile with the ID number E60N20. This tile was clipped to be used in other processes according to the study area. The EUDEM v1.1 data was preferred because it has high spatial resolution and high elevation accuracy. The lithology, pre-earthquake landslide inventory and fault data were obtained from the MTA. The worldwide land cover mapping published by ESA was used for LULC data. The river vector data was acquired from the TopoVT geodatabase of the General Directorate of Mapping and visually detailed drawings of the rivers in the Elazig study site. Arias intensity values for seismic hazard were downloaded from the AFAD earthquake database based on records of accelerometric stations in the study sites and its surroundings.

4. METHODOLOGY

In this chapter, the methodology proposed in the thesis was explained. The chapter begins with an overview of the workflow proposed in the thesis. Then, data preprocessing methods for landslide and flood susceptibility map production were explained. The explanations for the production methods of each univariate susceptibility map and also the MHS map are also provided.

4.1. Overview of the Proposed Workflow

In this section, the overall workflow proposed for the thesis study is explained. The proposed methodology for the MHS map production consists of three basic stages: (i) a-data pre-processing, (ii) the production of univariate susceptibility maps, and (iii) the MHS map production, as shown in Figure 4.1.

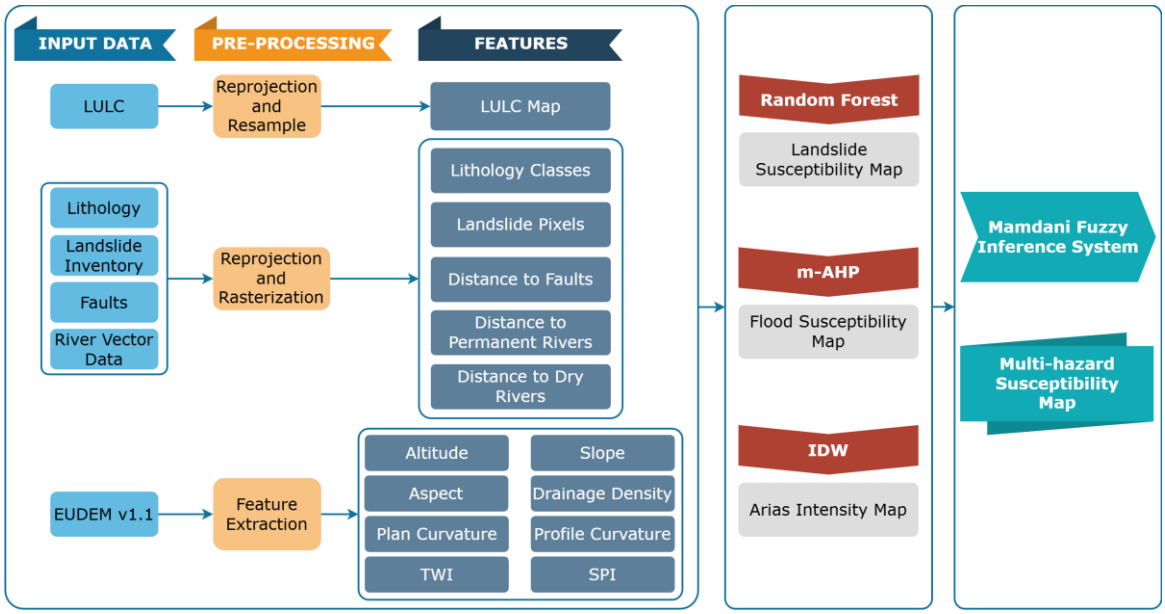

Figure 4.1. The overall workflow proposed for the thesis study

In the first stage, the main data used in the study were obtained from various sources. These data were pre-processed and features representing the conditioning factors were derived to produce the univariate susceptibility maps. At the second stage, the univariate susceptibility maps for natural hazards such as landslides, floods and earthquakes were produced using different methods depending on the data availability. The RF algorithm was used for the LSM production due to its ability to handle complex interactions between terrain features. The flood susceptibility was evaluated with the m-AHP method, which takes various factors into account, such as slope, land use, distance to drainage network etc. The seismic hazard map was created based on Arias intensity values using Inverse Distance Weighted (IDW) technique to interpolate the spatial variations. At the third stage, a MHS map was produced using the Mamdani FIS method. These stages are explained in detail in the following sections. The effectiveness and accuracy of the proposed methodology was analyzed by applying it in two different study areas selected after the Elazig and Kahramanmaras earthquakes.

4.2. Data Pre-processing for the Univariate Susceptibility Map Production

The main data sources used in the study were DEM, lithology, LULC, pre-earthquake landslide inventory, faults, rivers (as vector data) and Arias Intensity values. During the data preprocessing stage, features used to produce each univariate susceptibility map were extracted by applying geometric preprocessing & rasterization, and feature extraction steps for topographical parameters to this main data.

A geological map is a type of thematic map that shows the types, compositions, structures, and the other characteristics of the exposed rocks in a region. Lithology plays a crucial role in evaluating the risks of landslides, floods, and earthquakes. Lithological properties have an impact on rock type, permeability, and surface runoff [159]. Lithology is one of the factors that has a direct effect on the landslide potential. Because different geological units have different characteristics, which affect the possibility of landslide occurrence, movement and propagation. Properties of geological units such as water permeability and water holding capacity affect the rate of penetration of precipitation into the soil and the surface flow of water.

The geological formations in the study sites were acquired by digitizing the geological formation map published on the Geosciences WebGIS portal of MTA, which had a scale of 1/100,000. The vector polygons were combined to form a single geometry of geological units with similar characteristics. Before the rasterization process, each geological unit was assigned an ID ranging from 1 to the number of units in the study sites as a preparation step for method application. According to these ID values, a rasterized geology map was obtained and stored in GeoTIFF format.

The different LULC types within a region display various influences in natural hazard events. For this reason, it is necessary to use up-to-date LULC data. The global WorldCover product [123] with a resolution of 10 m provided by ESA was used in the thesis study. This LULC map was resampled to the 25 m grid size used in the study and clipped according to study sites.

Due to the study site locations within the EAFZ that are prone to landslides induced by seismic activity, the distance to faults factor was incorporated. This distance is used to determine the proximity of a point or an area to an active fault line. The faults used in the study were digitized from the MTA geosciences WebGIS portal. These distances to faults were calculated based on Euclidean.

Distance to river beds plays an important role in flood events. Water overflowing from river beds can cause serious damage to environment. The distances to permanent rivers and dry drainage channels were considered for susceptibility, as nearby places are more susceptible to flooding. Permanent and dry river datasets from the GDM TopoVT database were used to calculate these distances. Additional updates were carried out through manual delineations based on recent orthoimages. Multiple buffers were created at certain distances around the permanent rivers and dry drainage vector dataset to have discrete values in modeling (not continuous or gradually increasing). These distances were classified into six groups. The first five groups have equal intervals of 20 m, while the last group included area with a distance greater than 120 m.

The pre- and post-earthquake landslide inventory, which was in vector format, was converted to raster format to be used in model training, testing and validation. For this process, a value of 1 was assigned to the pre and post-earthquake landslide inventory and a value of 0 was assigned to non-landslide areas.

The topographic features mentioned in Figure 4.1 were derived from the EUDEM v1.1 data used as DEM data. Among those, slope refers to the degree of steepness or gradient of a terrain. It has a critical role in the LSM and the FSM production. In areas with steep slopes, the risk of soil erosion and landslides is higher. As the slope increases, downward forces that can cause water to flow more rapidly across the surface and trigger soil erosion also increase. Moreover, in steeply sloped areas, fast-flowing water increases the likelihood of forming water puddles. This may increase the risk of floods and cause puddles to form in low-lying areas. Areas with lower slopes and flat terrain are at higher risk of flooding due to the potential for increased surface inundation levels in these regions [102], [124].

Aspect feature describes the direction a surface faces downhill and is expressed in degrees clockwise from north. The duration of sunlight exposure and cycles of freezing and thawing, which impact the breakdown and erosion of slope materials facing various directions, may be associated with the aspect [102]. For instance, northern slopes tend to be more humid and shaded, whereas southern slopes can be warmer and drier. This condition affects soil moisture and vegetation, potentially resulting in different landslide hazards.

Surface curvature, the second derivative of a DEM, can be split as plan and profile curvatures. While plan curvature refers to the horizontal curvature of the surface (in two directions such as left and right, or X and Y curvatures), profile curvature refers to the vertical curvature of the surface (upward and downward curvature). The direction of the highest slope is perpendicular to the plan curvature. The direction of the highest slope is where profile curvature is found. In profile curvature, a negative value signifies upward convexity at the cell, resulting in flow deceleration. A positive profile indicates upward concavity at the cell, leading to flow acceleration. A value of zero indicates a linear

surface. In plan curvature, a positive value indicates lateral convexity at the cell, while a negative value indicates lateral concavity. A linear surface is indicated by a value of zero. Areas with steep curvature often indicate elevation changes at the surface and can affect the flow of water. Regarding the FSA, plan curvature illustrates the acceleration of flow and the rate of erosion/deposition, whereas profile curvature indicates variations in flow velocity [159].

Drainage density is a measure of the proportion between the total length of all streams and rivers and the overall area of the catchment. A high drainage density indicates that a region has a dense river and stream network. This suggests that the area is subject to intensive erosion and shaping processes, potentially leading to soil erosion. Therefore, a high drainage density may indicate that an area may be susceptible to erosion and runoff.

The Stream Power Index (SPI) quantifies the erosive capacity of water in motion. The SPI is calculated using the gradient and catchment area as its foundation. With increasing catchment area and slope gradient, the volume of water originating from upslope areas and the speed of water flow both increases. Consequently, stream power index and the risk of erosion rise.

Topographic wetness index (TWI) is widely used to express locations and sizes of water-saturated areas in a topographic sense. High TWI values indicate areas where water tends to accumulate and drainage systems have developed. Low TWI values indicate drier areas where water flows away quickly and less puddles occur. Regions with high TWI values indicate areas where rainfall causes water accumulation and stream flow is intense. This is useful for identifying areas at high risk of flooding. The SPI and TWI were calculated using Equation 4.1 [160].

$$\mathrm{SPI} = A_s * \tan\beta \qquad TWI = \ln\left(\frac{A_s}{\tan\beta}\right) \tag{4.1}$$

where A_s refers to the specific catchment area and β is the slope gradient.

All topogtaphic features were derived from EU-DEM v1.1 using open source SAGA GIS software and ArcGIS software from ESRI [161-162].

4.3. The univariate Susceptibility Maps Production

In this section, the univariate susceptibility maps produced for landslide, flood and earthquake are explained together with the respective methods.

4.3.1. Landslide Susceptibility Map Production with Random Forest Method

As mentioned in Chapter 2 of this thesis, diverse methods have been used for the LSM production in the literature. In recent years, with the advancement of technology and availability of accurate inventories, there has been an increase in the use of data-driven methods. Especially, the RF algorithm is among the most commonly used methods based on the literature review. Thus, the RF was preferred to produce the LSMs.

A number of statistical analyses were performed on the features selected for the LSM before the modeling phase. For this purpose, variance inflation factor (VIF), tolerance (TOL), and Pearson coefficients were computed to determine the multicollinearity among input features. The correlation levels between parameters were analyzed. In addition, the Information Gain Rate (IGR) method, which has been frequently used in the literature, was applied to analyze the importance of features, measure predictive abilities and determine the most effective ones.

The term *multicollinearity* in landslide research describes the non-independence among features within datasets, which arises from their high correlation. This condition can lead to inaccuracies in system analysis [163]. Minimizing the correlation between factors can be crucial for enhancing the precision of landslide prediction. Various methods have been suggested to assess multicollinearity, including Pearson's correlation coefficients [164], conditional index [165], variance decomposition proportion [166] and metrics like

variance inflation factor (VIF), and tolerance [167-168]. However, novel ML methods have the potential to reduce or avoid the adverse effects of the multicollinearity as well.

The VIF and tolerance values of an independent variable can be used to identify and assess the magnitude of the relationship between variance of a variable and the other independent variables. High VIF values indicate a high probability of multicollinearity. VIF and tolerance are inversely related to each other. A high tolerance value indicates the absence of multicollinearity, whereas a low tolerance value may indicate the presence of multicollinearity. If a VIF value is greater than 10 or the tolerance is less than 0.1, it suggests a potential multicollinearity issue in the dataset. If the VIF values are high, this may negatively affect the accuracy and reliability of the model. Therefore, it is important to check the VIF values and take appropriate measures to eliminate the multicollinearity problem when necessary. The formula used to compute the VIF is as follows:

$$VIF_i = \frac{1}{TOL} = \frac{1}{1-R_i^2} \tag{4.2}$$

where the VIF_i represents the VIF value of the i^{th} independent variable, and R_i^2 denotes the percentage of variance explained by regressing the i-th independent variable against the other independent variables.

In the LSM production, the correlation coefficient of two features can also be evaluated using the Pearson coefficient method. The linear relationship between two features is measured. Pearson's coefficient values vary between -1 and 1. A linear relationship is positive when it is closer to 1; negative when it's closer to -1; and nonexistent when it is closer to 0. As shown in Equation 4.3, the covariance of two features is divided by the product of their standard deviations to obtain the result. Pearson's correlation values above 0.7 indicate high collinearity.

$$r_{XY} = \frac{\sum_{a=1}^{n}(X_a-\bar{X})(Y_a-\bar{Y})}{\sqrt{\sum_{a=1}^{n}(X_a-\bar{X})^2}\sqrt{\sum_{a=1}^{n}(Y_a-\bar{Y})^2}} \tag{4.3}$$

where X and Y denote two features related to landslides, r_{XY} represents the correlation coefficient between factor X and factor Y, n signifies the count of input training data, while X_a and Y_a stand for the values of the a-th training data in X_a and Y_a, respectively and $\bar{X}$ and $\bar{Y}$ represent the mean values of the variables $\bar{X}$ and $\bar{Y}$, respectively.

In addition to defining multicollinearity, the features in the initial set may not have similar predictive ability. There are some techniques such as Relief [169], Fuzzy-Rough sets [170], Information Gain [171] and Information Gain Ratio (IGR) [172] to measure the predictive abilities between features and to determine the most effective ones. Among these techniques, the IGR technique was used in this thesis study. The IGR represents an enhancement over the conventional information gain approach. The information gain measures the ability of an attribute to partition a dataset. The IGR, on the other hand, considers how information gain relates to the diversity of the dataset, that is, the homogeneity of an attribute in dividing the dataset. The IGR value serves as an indicator of a feature's significance: the greater the IGR value, the more crucial the information provided by the feature for predicting landslide susceptibility.

After the statistical analyses of the features selected for landslide susceptibility map production, the model training phase was started. The RF algorithm, as proposed by Breiman (2001) [173], is commonly employed for both regression and classification tasks, and it was utilized for the LSM production in the thesis study. The RF consists of multiple Decision Trees (DTs) built on different subsamples of the data, ensuring robustness against outliers and noise. To get the RF output, it uses a voting system that takes into account the outcomes of multiple DTs [52]. A random selection of characteristics and a subset of the training dataset are used to build each DT in the RF, resulting in variability among the trees.

The RF algorithm utilizes the bagging (or Bootstrap Aggregating) technique to generate these varied subsets. Throughout the training stage, each tree is constructed through iterative partitioning of the data according to the features. At each division, the algorithm

chooses the most suitable feature from the random subset, aiming to optimize information gain or Gini impurity. This procedure persists until a predefined stopping condition is fulfilled, such as reaching a maximum depth or achieving a minimum number of samples within each leaf node. After training, the random forest can make predictions by having each tree *vote* for a class, and the class with the highest number of votes is designated as the predicted class for the input data. Figure 4.2 illustrates a generalized structure for the RF. Figure 4.3 shows the workflows for the LSM approach, which was developed in a Python programming environment.

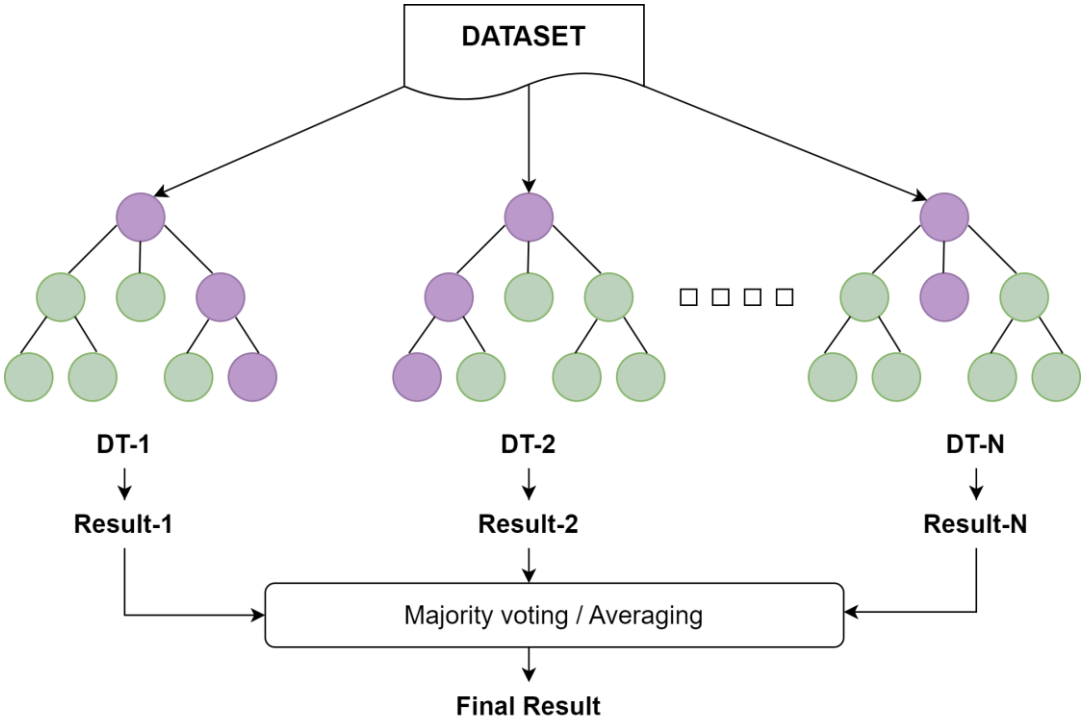

Figure 4.2. A generalized structure for the RF algorithm [174].

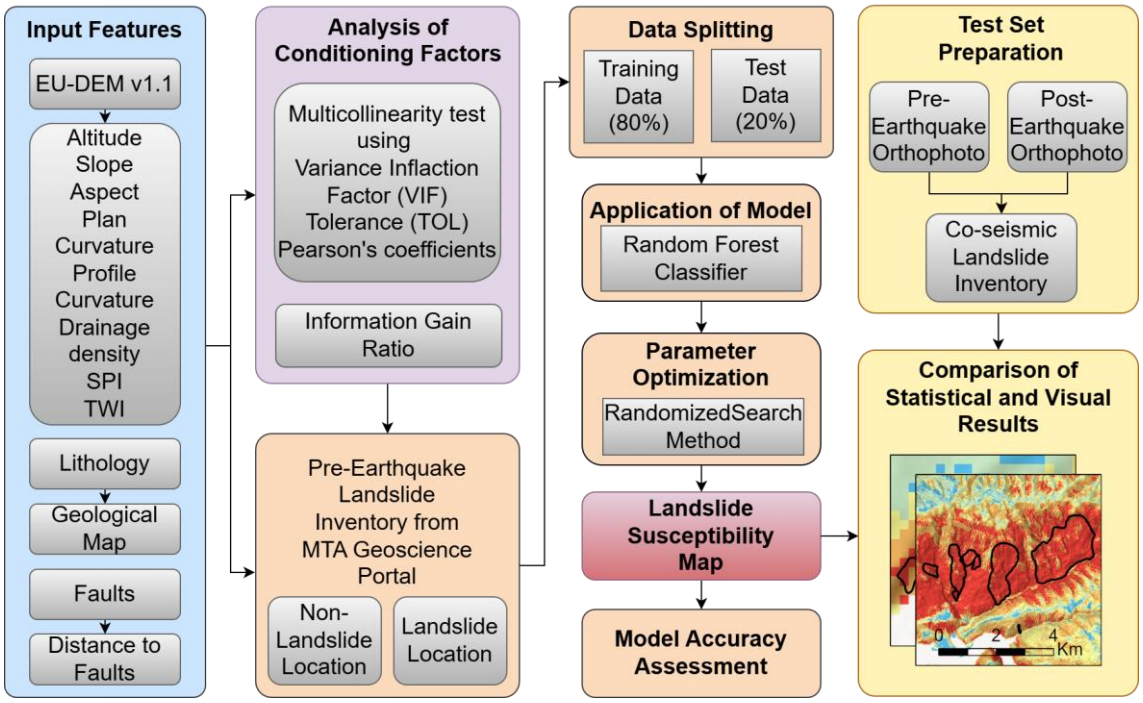

Figure 4.3. The workflow implemented for the landslide susceptibility map production.

As can be seen in Figure 4.3, a total of 10 input features were used for the LSM production. These features were selected based on previous LSA studies conducted in the area and expert opinions. Before applying the RF model, the VIF, the TOL, Pearson's coefficient and the IGR were used to identify the relationship between features. To achieve reliable and accurate results, choosing suitable parameters within the model is crucial. For optimizing the model parameters, this study employed a random search approach, which was considered to be more efficient than grid search due to the large data volumes [175-176]. The random search algorithm randomly selects various combinations of parameters from predefined ranges or values, then assesses the model performances using cross-validation (as shown in Table 4.1) and appropriate metrics such as accuracy, precision, recall, or F1 score and the AUC values.

Table 4.1. Parameter optimization values

Model	Parameter	Value	
		Elazig Study Site	**Adiyaman Study Site**
Random Forest	n_estimators	426	344
	criterion	‘entropy’	‘entropy’
	max_depth	16	16
	min_samples_split	2	2
	min_samples_leaf	1	2
	max_features	‘auto’	‘auto’

The precision parameter quantifies how many predicted positive instances are truly positive, gauging the classifier's skill in avoiding misclassifying negative samples as positive. Recall, on the other hand, exhibits the classifier's efficacy in capturing all positive instances. The F1 Score, as the harmonic mean of precision and recall, provides a well-balanced evaluation of both criteria. Support denotes the frequency of each class within the ground truth values. It shows that optimizing parameters has a notable effect on the performance of the RF algorithm. By fine-tuning parameters such as the number of trees, maximum tree depth, and the number of features considered in each split, the aim is to increase prediction accuracy while reducing overfitting. Furthermore, the SHapley Additive exPlanations (SHAP) methodology was used to evaluate the relationships of the input features with the model predictions and the most effective parameters in model prediction were determined [177].

The pre-earthquake landslide inventory was used in model training. For the Elazig site, landslide samples used for training were selected from pixels within the inventory, with 175,219 landslide and 262,829 non-landslide pixels, totaling 4,380,480 pixels across all features. In the training data set within the Adiyaman study site, there were 188,619 pixels identified as landslide and 282,929 pixels categorized as non-landslide. As can be seen from the pixel counts, the training data from non-landslide areas were randomly selected

outside landslide polygons with a ratio of 1:1.5. The distribution and balance of landslide and non-landslide samples are important to ensure fair and accurate model performance. There are some studies in the literature on the determination of the sample ratio between landslide and non-landslide data. In these studies, experiments with different sample size ratios were performed and discussed (e.g. [178-179]). In the comparisons, it was stated that the selection ratio of landslide and non-landslide areas affected the model accuracy (specificity, sensitivity). In general, it has been found that the use of 1:1.5 and 1:2 ratios is suitable for the accuracy of susceptibility map production. Therefore, based on the studies in the literature and previous experience (e.g.[69], [124]), it was preferred to employ a ratio of 1:1.5 in this study. In addition, an 80/20 split ratio was applied to divide the training and test samples.

The LSMs produced in this thesis study were validated with landslides triggered during the Elazig and Kahramanmaraş earthquakes. Most studies in the literature have been validated with the test data separated from learning data due to the absence of multi-temporal landslide inventory. Considering that earthquakes trigger many landslides in this study, there is an opportunity for a study to evaluate the performance limits of LSMs. In this study, post-earthquake landslide inventories were used only for validation purposes rather than model training. Class values of pixels in the intersection areas of the susceptibility maps and post-earthquake landslide inventories were compared using statistical metrics and visual interpretation for expert-based validation.

4.3.2. Flood Susceptibility Map Production with m-AHP

The FSM of the study sites was produced with the M-AHP method, which is an expert-based method. The reason for using this method was the lack of learning data. Figure 4.4 shows the workflows for the FSM approach, which was developed in a Python programming environment.

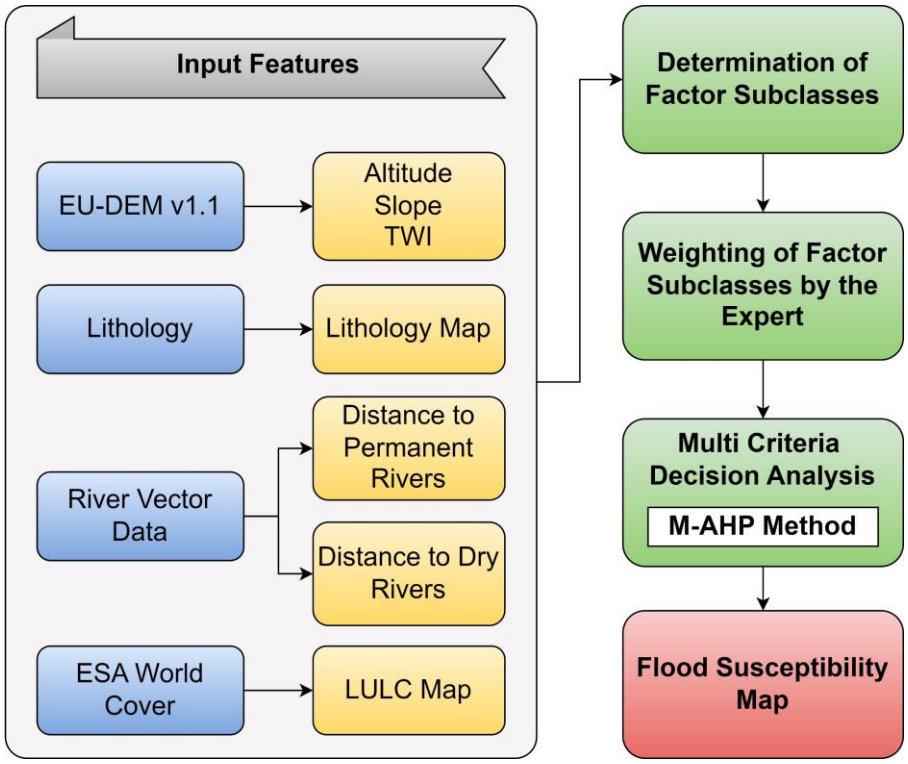

Figure 4.4. The workflow implemented for the flood susceptibility map production.

A modified form of the conventional AHP approach, called M-AHP, was proposed by Nefeslioglu et al. [63]. This method has been modified to eliminate expert subjectivity in pairwise comparison. In the M-AHP method, each classified conditioning factor in the system is weighted according to expert opinion. These weights are given according to factor importance. Expert knowledge and experience are important in assigning weights. This knowledge and experience helps them accurately determine the importance of factors. Experts weight factors using evidence based on available scientific data, study site characteristics, and past events. Weight values of each parameter class used in this study are given in Appendix A. A normalised factor score difference matrix is created for each factor, based on the highest weight assigned to each factor. A factor comparison matrix is then created, taking into account the modified importance value chart. Factor comparison consistency is measured. Finally, the percentage importance distributions of the factors at the decision points are found. For this, each factor is normalised according to its maximum score. The linear distances between the normalised factor score and the decision points are measured. At this stage, the modified importance value chart is again taken into account. Finally, the percentage importance distributions of the factors at the determined decision point are found. Since a different weight vector is calculated for each

grid cell in the M-AHP method, it is not ignored that the weight vector will not be constant in that grid cell. A total of 7 features (see Figure 4.4 above) were used as input features in the FSM production based on literature analysis and expert opinion. An expert (Dr. Candan Gokceoglu), who has long term experience in the region, provided support to define the class weights for the study sites.

4.3.3. Seismic Hazard Map Production with Inverse Distance Weighting

Assessing earthquake effects and classifying regions in terms of earthquake risk is a critical issue in earthquake engineering. Various parameters and criteria are used for this purpose. However, visualizing earthquake effects on a single map and thus preparing regional MHS maps still remains a challenging problem. Since local ground conditions significantly impact earthquake shaking, Kotha et al. [180] explained that the current seismic code provisions consider this effect by defining appropriate elastic design spectra based on different site categories. In this context, the main recommended parameter for soil classification is Vs30 [181]. However, there is no unanimous agreement on whether Vs30 is a valid criterion for earthquake amplification [182]. At the same time, However, it is emphasized that the basic characteristics of earthquake shaking cannot be fully expressed with a single parameter [183]. Therefore, it has been suggested to use several engineering parameters simultaneously to obtain more accurate results in terms of earthquake engineering. However, it should be noted that standard methods cannot accurately assess the amount of peak horizontal acceleration amplification expected for site classification [184].

Another parameter utilized in ground motion prediction equations is the horizontal component of cumulative absolute velocity. This parameter has been used as an indicator to indicate the possible onset of structural damage and liquefaction of saturated soils [185].

Arias intensity represents the release of energy, encompassing both the duration of earthquake shaking and the time-varying changes in frequency content [186]. The

intensity of the shaking is calculated by quantifying the acceleration of transient seismic waves. It was proposed by Arturo Arias in 1970 [187]. As shown in Equation 4.4, it is the sum of the horizontal and vertical components of the acceleration record.

$$I_A = I_{xx} + I_{yy} = \frac{\pi}{2g}\int_0^{td} a_x^2(t)dt + \frac{\pi}{2g}\int_0^{td} a_y^2(t)dt \quad (4.4)$$

where g denotes the acceleration of gravity, t represents time, and td stands for the total recording length.

Studies have indicated that among the parameters measuring ground shaking, the Arias Intensity is closely associated with the distribution and density of landslides [188-190]. It is a reliable parameter used to describe the earthquake shaking required to trigger landslides.

The Arias Intensity is widely used as a parameter to determine earthquake effects. The Arias Intensity and cumulative absolute velocity are successfully used in earthquake engineering problems because they reflect many characteristics of ground motion [191]. These parameters enable the relative determination of earthquake effects and are thus used in the production of multi-MHS maps. For this reason, because reliable data is accessible, the thesis study utilized Arias Intensity to comparatively classify the study site regarding earthquake effects. In other words, the Arias Intensity map categorized the area in relation to earthquake impact. This classification does not indicate the absolute effect of a potential earthquake but rather illustrates the relative influence within the study sites. Hence, the Arias Intensity utilized to depict earthquake effects in the production of MHS map is represented by the susceptibility map. Figure 4.5 shows the workflow for the seismic hazard map production.

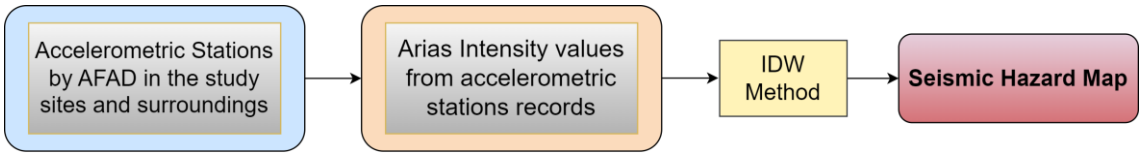

Figure 4.5. The workflow implemented for seismic hazard map production

In this thesis, the Arias Intensity values of accelerometric station records of the study site and its surroundings were obtained from the AFAD earthquake database [192]. The unit of arias intensity values is cm/s. The Arias Intensity values from twenty-five accelerometric station records were utilized for the Elazig study site, while fourty-six accelerometric stations were employed for the Adiyaman study site to determine the Arias Intensity values. Accelerometric stations obtained from AFAD earthquake database in Elazig (left) and Adiyaman (right) study sites are given in Figure 4.6. After obtaining the Arias Intensity values, the seismic hazard map was produced using the IDW interpolation. Kriging interpolation method, one of the other interpolation types, was also tested for the study areas. Since similar results were obtained and IDW interpolation method is preferred more frequently in such studies in the literature, it was decided that it would be appropriate to use the IDW interpolation method.

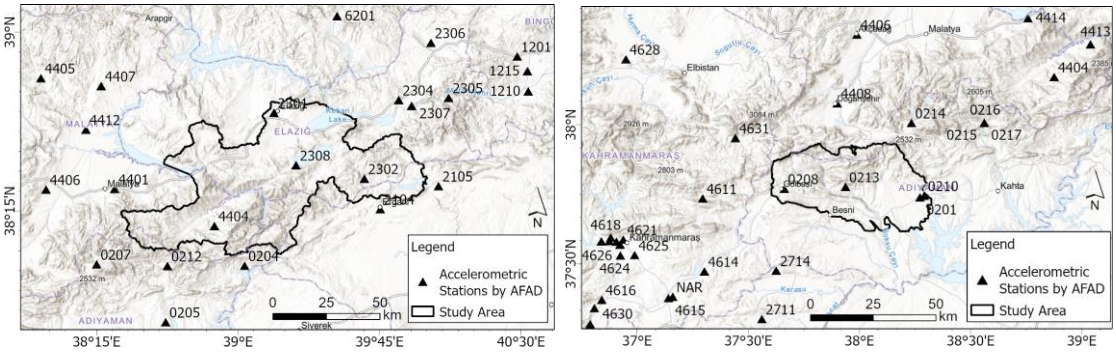

Figure 4.6. Accelerometric stations obtained from AFAD earthquake database in Elazig (left) and Adiyaman (right) study sites.

4.4. Multi-Hazard Susceptibility Map Production with Fuzzy Inference System

The fuzzy inference involves interpreting the values within an input vector and assigning values to the output vector, guided by specific rules. In fuzzy logic, the validity of a statement is determined by a degree of truth rather than being strictly binary [193]. Fuzzy inference entails using fuzzy logic to establish the relationship between a given input and an output. This process encompasses all the components, including membership functions, fuzzy logic operators, and if-then rules. The FIS have the ability to mitigate uncertainties encountered in tackling complex problems.

One of the three basic types of FIS, the Mamdani FIS [194] is a method of creating a control system using linguistic control rule sets based on the opinion of experienced experts. This method has more intuitive and easy to understand rules for solving complex and nonlinear problems. In this study, the univariate susceptibility maps (landslide, flood, seismic) were synthesized for a MHS map production using the Mamdani FIS. When the literature was analyzed, it was observed that various studies employed the Mamdani FIS for landslide susceptibility mapping, rock mechanics and engineering geology [195], [196], [197], [49]. Matlab Fuzzy Logic Toolbox was used in the MHS assessment to combine the univariate susceptibility maps [198].

A Mamdani FIS comprises four main steps: fuzzification, rule assessment, aggregation, and defuzzification. The output of each rule is a fuzzy set. In the fuzzification part, crisp inputs are determined by the experts. The selection of crisp inputs in multi-hazard assessments requires consideration of more than one hazard (e.g. landslide, flood, earthquake). In such assessments, experts select crisp inputs by considering various factors. Hazards that have occurred frequently in the study area before and have a negative impact on people and the environment are identified. For this, the knowledge of experienced and seasoned experts is very important. In addition, past events in the area and literature studies reveal which hazards need to be assessed. In the thesis study, the LSM, the FSM and the seismic hazard map were used as inputs. Each input has three membership functions (low, moderate, high). Membership boundaries were determined by giving different weights to these membership functions for each input. The reason for

this was that the damaging effect of each of the natural hazards were not the same in the study sites. Considering the statistics in AFAD reports and earthquake catalogue, Table 4.2 shows the number of occurrences of landslide, flood and earthquake hazards in the study sites during the specified years. For landslide and flood hazard, AFAD reports between 1950 and 2019 were evaluated. For earthquake hazard, the number of earthquakes between Mw. 5.0 and Mw. 8.0 in 1950 and 2024 was included. Although the number of earthquake hazards is low, the type of disaster that caused the most loss of life and property in the study area was earthquake. It was followed by landslides and floods [5]. In addition, the histograms of the univariate susceptibility maps were analyzed for probability distribution and the ranges of the membership functions were determined. Various membership functions exist in the literature, including triangular, sigmoidal, trapezoidal, bell-shaped, pi-shaped, and Gaussian combination functions. Triangle style membership functions are used for each membership (see Figure 4.7). Triangular shape is a simple and common type of membership function used to transform the values of a given variable into fuzzy sets. Triangular membership functions are frequently preferred in natural hazard studies due to their simplicity, computational efficiency and openness to direct interpretation. The x - y axes in the membership function graphs indicate the susceptibility level ranges and membership degrees, respectively. Figure 4.7 illustrates a susceptibility level represented by a probability ranging from 0 to 1 (normalized), which falls within two membership classes. For instance, a value of 0.6 in the landslide membership function corresponds to moderate and high susceptibility levels to varying degrees.

Table 4.2. The number of occurrences of landslide, flood and earthquake hazards in the study sites

Study Sites	**The number of occurrences of natural hazards**		
	Landslide	**Flood**	**Earthquake**
Elazig	988	123	38
Adiyaman	478	96	92

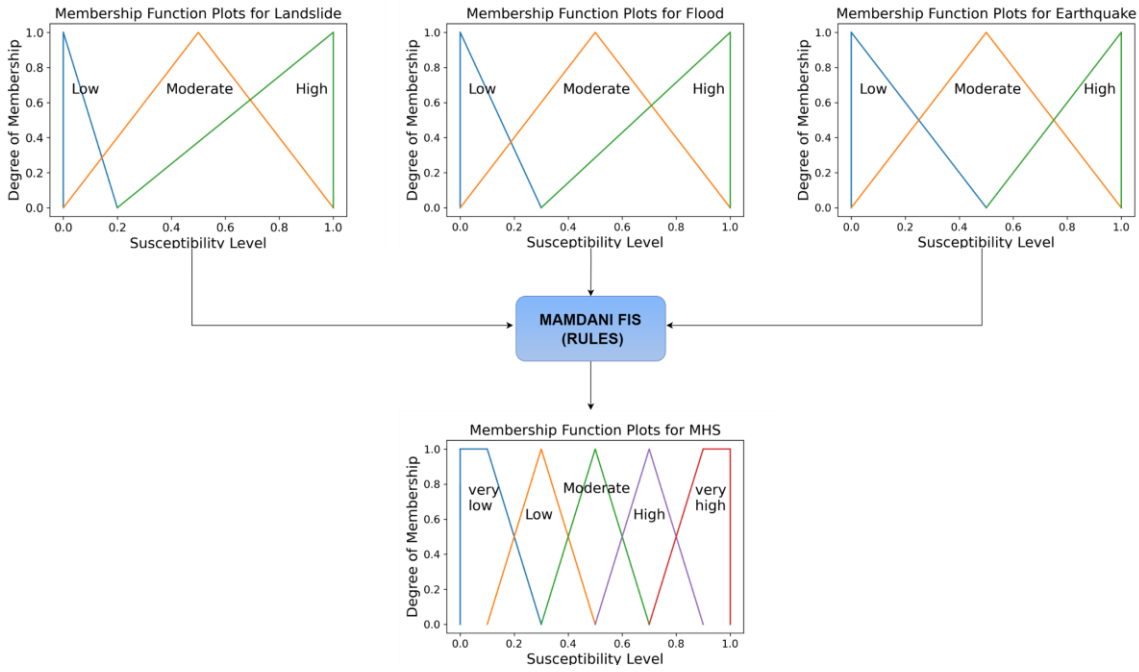

Figure 4.7. The Mamdani FIS's membership functions and boundaries.

Linguistic if-then rules, rule evaluation part, is one of the most important stages for Mamdani FIS. These rules, which were created based on the knowledge of experienced experts, were prepared again with the support of Dr. Gokceoglu due to his experience in the region. In the Mamdani Fuzzy Inference System, when there are three inputs and three membership functions for each input, the total number of possible rules depends on the number of all possible combinations of these membership functions. If there are n inputs and each input has m membership functions, the number of possible rules is calculated by the formula in Equation 4.5:

$$Number\ of\ possible\ rules = m^n \tag{4.5}$$

Here, m indicates number of membership functions for each input and n is number of inputs in the system. Since there are three inputs, each of which consists of three membership functions, a total of twenty-seven rules have been created. Experts define rules based on their knowledge and experience to determine the appropriate output for each possible combination. These rules are given in Table 4.3.

Table 4.3. Mamdani FIS's if-then rules (Rule evaluation part)

No	Mamdani FIS Rules
1	If (LS is high) and (FS is high) and (AI is high) then (MHSL is very_high)
2	If (LS is high) and (FS is high) and (AI is moderate) then (MHSL is very_high)
3	If (LS is high) and (FSis high) and (AI is low) then (MHSL is high)
4	If (LS is high) and (FS is moderate) and (AI is high) then (MHSL is very_high)
5	If (LS is high) and (FS is low) and (AI is high) then (MHSL is high)
6	If (LS is high) and (FS is moderate) and (AI is moderate) then (MHSL is high)
7	If (LS is high) and (FS is low) and (AI is low) then (MHSL is moderate)
8	If (LS is high) and (FS is low) and (AI is moderate) then (MHSL is moderate)
9	If (LS is high) and (FS is moderate) and (AI is low) then (MHSL is moderate)
10	If (LS is moderate) and (FS is high) and (AI is high) then (MHSL is very_high)
11	If (LS is moderate) and (FS is high) and (AI is moderate) then (MHSL is high)
12	If (LS is moderate) and (FS is high) and (AI is low) then (MHSL is moderate)
13	If (LS is moderate) and (FS is moderate) and (AI is high) then (MHSL is high)
14	If (LS is moderate) and (FS is low) and (AI is high) then (MHSL is moderate)
15	If (LS is moderate) and (FS is moderate) and (AI is moderate) then (MHSL is moderate)
16	If (LS is moderate) and (FS is low) and (AI is low) then (MHSL is low)
17	If (LS is moderate) and (FS is low) and (AI is moderate) then (MHSL is moderate)
18	If (LS is moderate) and (FS is moderate) and (AI is low) then (MHSL is moderate)
19	If (LS is low) and (FS is high) and (AI is high) then (MHSL is high)
20	If (LS is low) and (FS is high) and (AI is moderate) then (MHSL is moderate)
21	If (LS is low) and (FS is high) and (AI is low) then (MHSL is moderate)
22	If (LS is low) and (FS is moderate) and (AI is high) then (MHSL is moderate)
23	If (LS is low) and (FS is low) and (AI is high) then (MHSL is moderate)
24	If (LS is low) and (FS is moderate) and (AI is moderate) then (MHSL is low)
25	If (LS is low) and (FS is low) and (AI is low) then (MHSL is very_low)
26	If (LS is low) and (FS is low) and (AI is moderate) then (MHSL is low)
27	If (LS is low) and (FS is moderate) and (AI is low) then (MHSL is low)

In the aggregation part, the fuzzy output of the model was obtained by collecting all the results in the rule evaluation section. The max operator was used for this aggregation [197]. The output was classified in five membership functions (very low, low, moderate, high, very high). In the last part, the defuzzification part, the result produced in the aggregation part was converted to crisp output with the fuzzy output centroid technique. The geocoding process was applied to the crisp outputs for MHS map production.

The method proposed in this thesis was first applied to the Elazig study site. In Mamdani FIS, the input data used, membership functions, appropriate rules, and the weight of each membership function were adjusted primarily by considering the Elazig study site. The applicability of the proposed model was tested for the Adiyaman study site, which was exposed to multi-hazards after the Kahramanmaras Earthquakes. The input data used,

membership functions, rules and membership function weights were considered similar due to the close proximity of natural hazard types and areas.

5. RESULTS

In this chapter, the qualitative and quantitative assessment results of the univariate susceptibility and MHS assessments of the two study sites (Elazig site and Adiyaman site) are presented.

5.1. Results from Elazig Study Site

This section presents the results maps produced for the Elazig study site in detail. In the next subheading, the features map used to produce univariate sensitivity maps and multicollinearity among features results are given. The univariate susceptibility maps produced for each hazard are given in Section 5.1.2, and MHS map results are given in Section 5.1.3.

5.1.1. Input Feature Maps Produced for Elazig Study Site

The input feature map results used in the production of landslide and flood susceptibility maps for the Elazig study area are given in Figure 5.1. For landslide susceptibility, 10 features (see Figure 4.4) were utilized, whereas for flood susceptibility, 7 features (see Figure 4.5) were employed. The statistical analysis results for the features are given in Table 5.1. Additionally, Tables 5.2 and 5.3 present statistical summary of the input features contained within the pre and post-earthquake landslide inventory, respectively. Visual and statistical analyses play crucial roles in understanding the characteristics of the study area and assessing the outputs of the model.

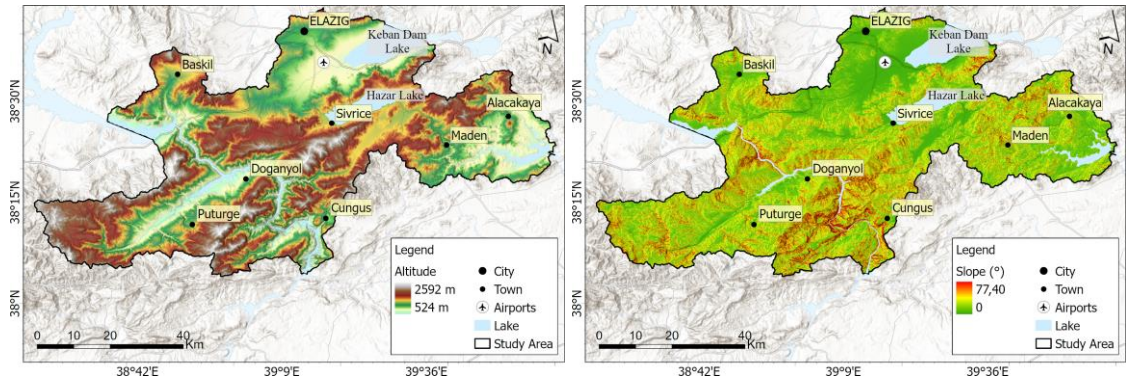
ELAZIG
Keban Dam Lake
Baskil
Hazar Lake
Sivrice
Alacakaya
Maden
Doganyol
Puturge
Cungus
N
38°30'N
38°15'N
38°N
0 10 20 40 Km
38°42'E
39°9'E
39°36'E
Legend
Altitude
2592 m
524 m
Slope (°)
77,40
0
City
Town
Airports
Lake
Study Area

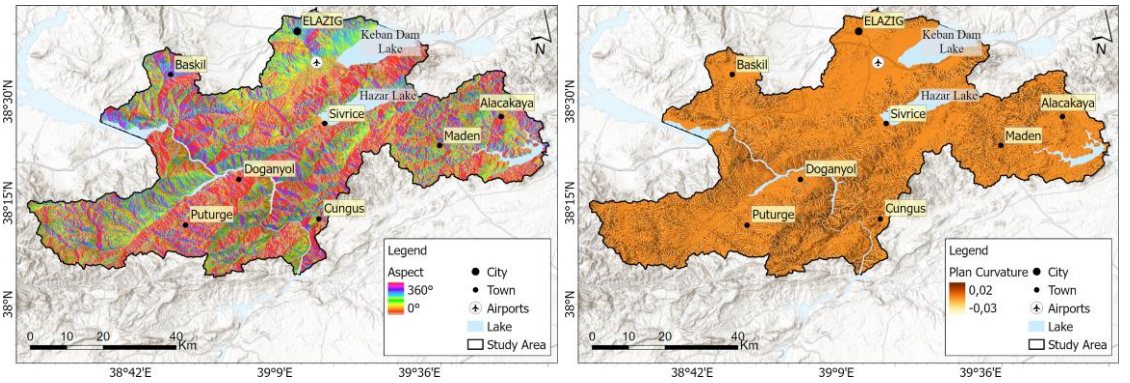
ELAZIG
Keban Dam Lake
Baskil
Hazar Lake
Sivrice
Alacakaya
Maden
Doganyol
Puturge
Cungus
N
38°30'N
38°15'N
38°N
0 10 20 40 Km
38°42'E
39°9'E
39°36'E
Legend
Aspect
360°
0°
Plan Curvature
0,02
-0,03
City
Town
Airports
Lake
Study Area

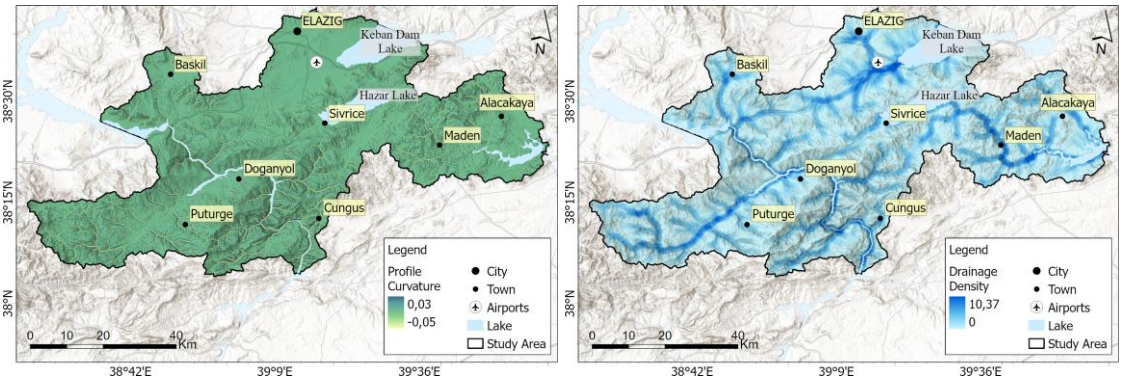
ELAZIG
Keban Dam Lake
Baskil
Hazar Lake
Sivrice
Alacakaya
Maden
Doganyol
Puturge
Cungus
N
38°30'N
38°15'N
38°N
0 10 20 40 Km
38°42'E
39°9'E
39°36'E
Legend
Profile Curvature
0,03
-0,05
Drainage Density
10,37
0
City
Town
Airports
Lake
Study Area

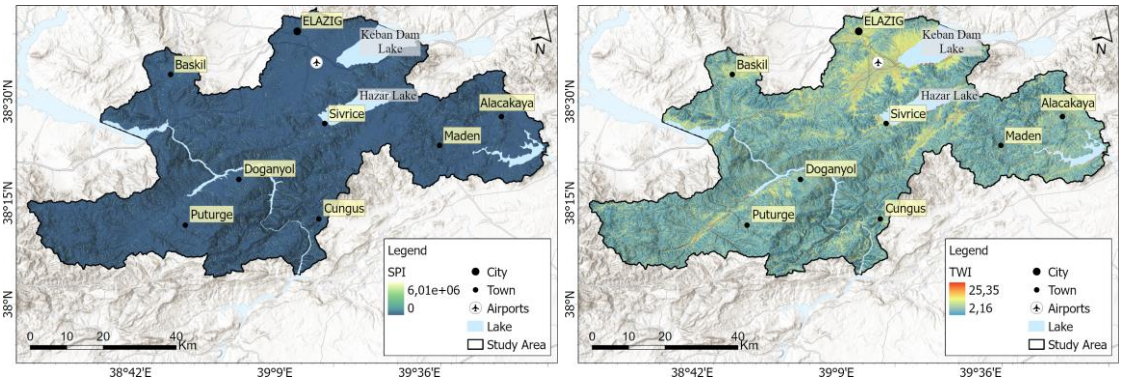
ELAZIG
Keban Dam Lake
Baskil
Hazar Lake
Sivrice
Alacakaya
Maden
Doganyol
Puturge
Cungus
N
38°30'N
38°15'N
38°N
0 10 20 40 Km
38°42'E
39°9'E
39°36'E
Legend
SPI
6,01e+06
0
TWI
25,35
2,16
City
Town
Airports
Lake
Study Area

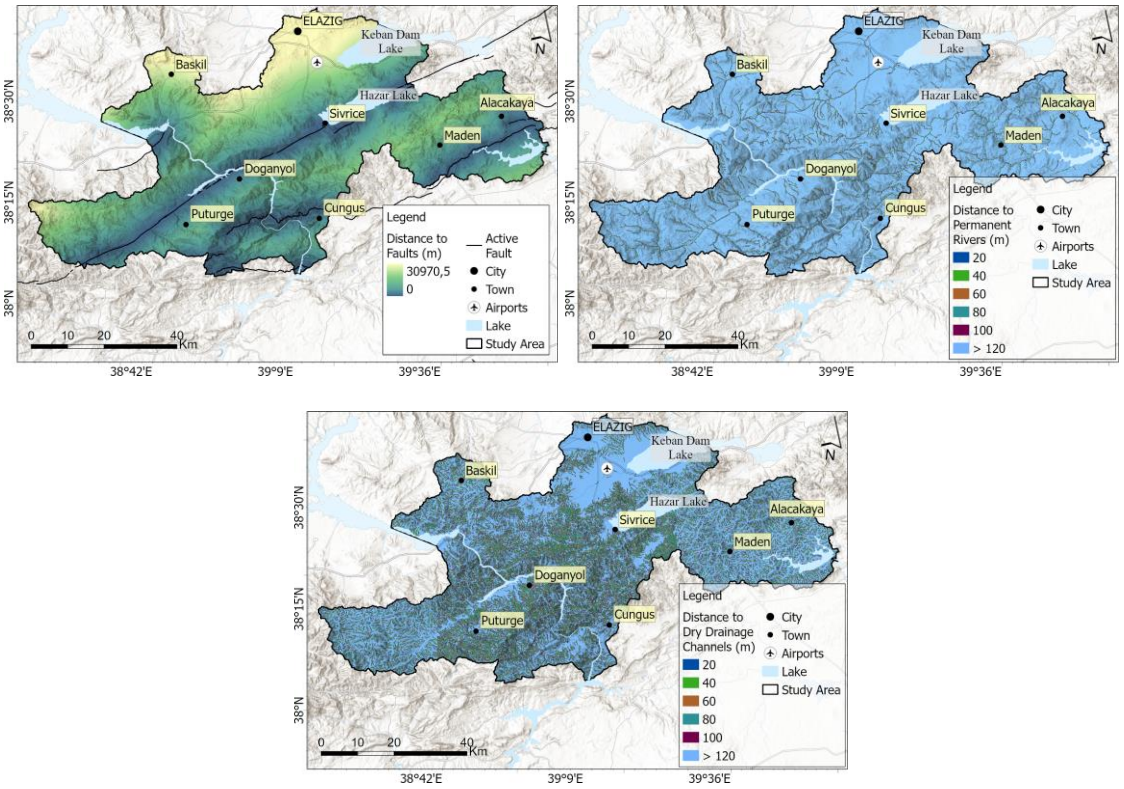

Figure 5.1. The feature map results for landslide and flood susceptibility assessment in the Elazig site: (a) Altitude, (b) Slope, (c) Aspect, (d) Plan curvature, (e) Profile curvature, (f) Drainage density, (g) SPI, (h) TWI, (i) Distance to faults, (j) Distance to premanent rivers, (k) Distance to dry rivers

Table 5.1. Statistical summary of all the input features for Elazig study site.

Features	Min	Max	Mean	Std. Dev.	Median
Altitude (m)	524.341	2592.429	1288.098	346.726	1263.897
Slope (°)	0	77.398	13.242	9.436	12.115
Aspect (°)	0	360.00	171.458	110.295	167.106
Distance to faults (m)	0	18842.946	2718.551	2891.037	1811.249
Drainage Density	0	10.375	1.270	1.506	0.765
Plan Curvature	-0.033	0.019	6.096	0.001	$1.95*10^{-7}$
Profile Curvature	-0.048	0.033	-6.753	0.001	-6.166
SPI	0	$6.016*10^{6}$	4546.271	31147.524	330.348

TWI	2.164	25.349	7.845	3.023	6.883

Table 5.2. Statistical summary of the input features inside pre-earthquake landslide inventory for Elazig study site.

Features	**Min**	**Max**	**Mean**	**Std. Dev.**	**Median**
Altitude (m)	524.341	2309.859	1211.941	340.611	1178.391
Slope (°)	0	56.556	17.601	8.164	16.889
Aspect (°)	0	360.00	167.881	98.035	156.075
Distance to faults (m)	0	8902.598	1497.741	1544.953	989.002
Drainage Density	0	8.012	1.146	1.510	0.447
Plan Curvature	-0.014	0.008	-0.001	0.001	-0.001
Profile Curvature	-0.014	0.010	-0.001	0.001	-0.001
SPI	0	$2.242*10^6$	9781.630	52329.520	589.148
TWI	3.154	25.073	7.565	2.019	7.213

Table 5.3. Statistical summary of the input features inside post-earthquake landslide inventory for Elazig study site.

Features	**Min**	**Max**	**Mean**	**Std. Dev.**	**Median**
Altitude (m)	680.691	1721.290	1167.282	231.791	1191.918
Slope (°)	2.117	54.119	23.084	6.688	22.746
Aspect (°)	5.077	333.271	165.207	27.986	164.644
Distance to faults (m)	0	4119.617	817.667	794.929	575.00
Drainage Density	0	6.847	1.307	1.316	1.154
Plan Curvature	-0.010	0.005	4.276	0.001	8.904
Profile Curvature	-0.009	0.006	-0.001	0.001	-7.462
SPI	0	$3.997*10^6$	13828.59	85209.558	771.859

TWI	3.895	21.190	7.091	1.404	6.856

Additionally, this study identified multicollinearity among the input features by employing VIF and TOL (see Table 5.4), as well as Pearson's correlation coefficient (see Figure 5.2). For the dataset to be considered acceptable, the VIF value should be below 10, and the TOL value should exceed 0.1. As can be seen in Table 5.4, the VIF values of all input features, except altitude, are less than 10 and the TOL values are greater than 0.1. Altitude exhibits the highest VIF, suggesting significant multicollinearity. However, since altitude is an important feature in model training and DT-based methods are relatively immune to the multicollinearity problem, all input features were used in model training [199], [124], [69]. The final analysis results will be unbiased, with no collinearity effects of the feature maps influencing landslide occurrence. The IGR results applied to analyze the importance of features are given in Table 5.4. The results show that lithology has the greatest importance (0.192), followed by distance to faults (0.080), altitude (0.045) and slope (0.032). Since the IGR value of these features is greater than the other features, the information they provide for estimating landslide susceptibility is considered to be more important than the other features.

Table 5.4. Collinearity analysis results between the input features for Elazig study site.

No	**Input Features**	**Collinearity Statistics**		**IGR**
		VIF	**TOL**	
1	Altitude	13.238	0.075	0.045
2	Slope	4.053	0.246	0.032
3	Aspect	5.291	0.189	0.004
4	Lithology	1.662	0.601	**0.192**
5	Plan Curvature	1.281	0.780	0.010
6	Profile Curvature	1.189	0.841	0.006
7	SPI	1.075	0.930	0.020
8	TWI	9.311	0.107	0.021

9	Distance to Faults	1.940	0.515	**0.080**
10	Drainage Density	2.205	0.453	0.011

Pearson coefficient results are given in Figure 5.2. The highest absolute correlation coefficient is observed between TWI and slope features with a value of 0.53. Here, it indicates a moderate inverse relationship between two variables. That is, one variable tends to increase while the other tends to decrease. Slope indicates how step the land is, generally water flow is faster on steep terrain, leading to lower TWI values because TWI is a measurement of how long water stays in the soil. The rapid flow of water on steep terrain results in less water interacting with the soil and therefore lower wetness values. If the coefficient value is greater than 0.7, it indicates that there is a strong correlation between the two factors. All values in the Pearson coefficient matrix are less than 0.7, indicating that the collinearity between features is negligible.

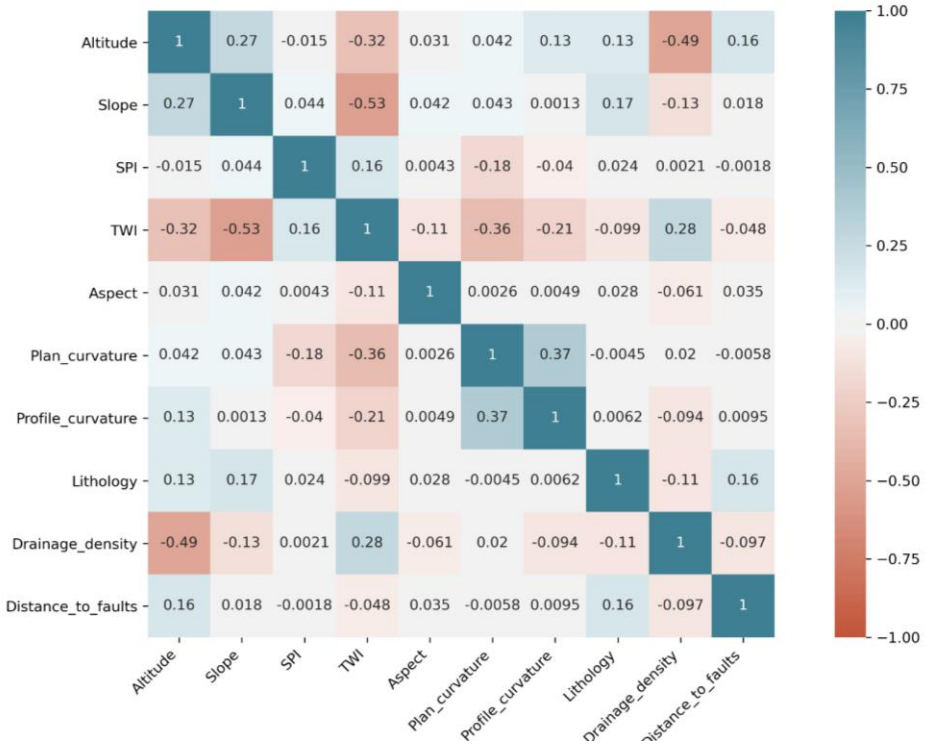

Figure 5.2. Pearson's coefficient results between the input features for Elazig study site.

5.1.2. The Univariate Susceptibility Maps for Elazig Study Site

The univariate susceptibility maps are presented in Figure 5.3. The predicted susceptibility values of the LSM produced using the RF algorithm were classified into five classes with the natural breaks classification (Jenks) [200]. Furthermore, Table 5.5 presents the sizes and probability percentages associated with these classes. The table shows that 36.4% of the Elazig study site demonstrates susceptibility to landslides at very high, high, and moderate classes. The results for landslide susceptibility showed that mountainous regions often have a high probability of landslides. In addition, the surroundings of Karakaya and Kralkızı dams are areas highly susceptible to landslides.

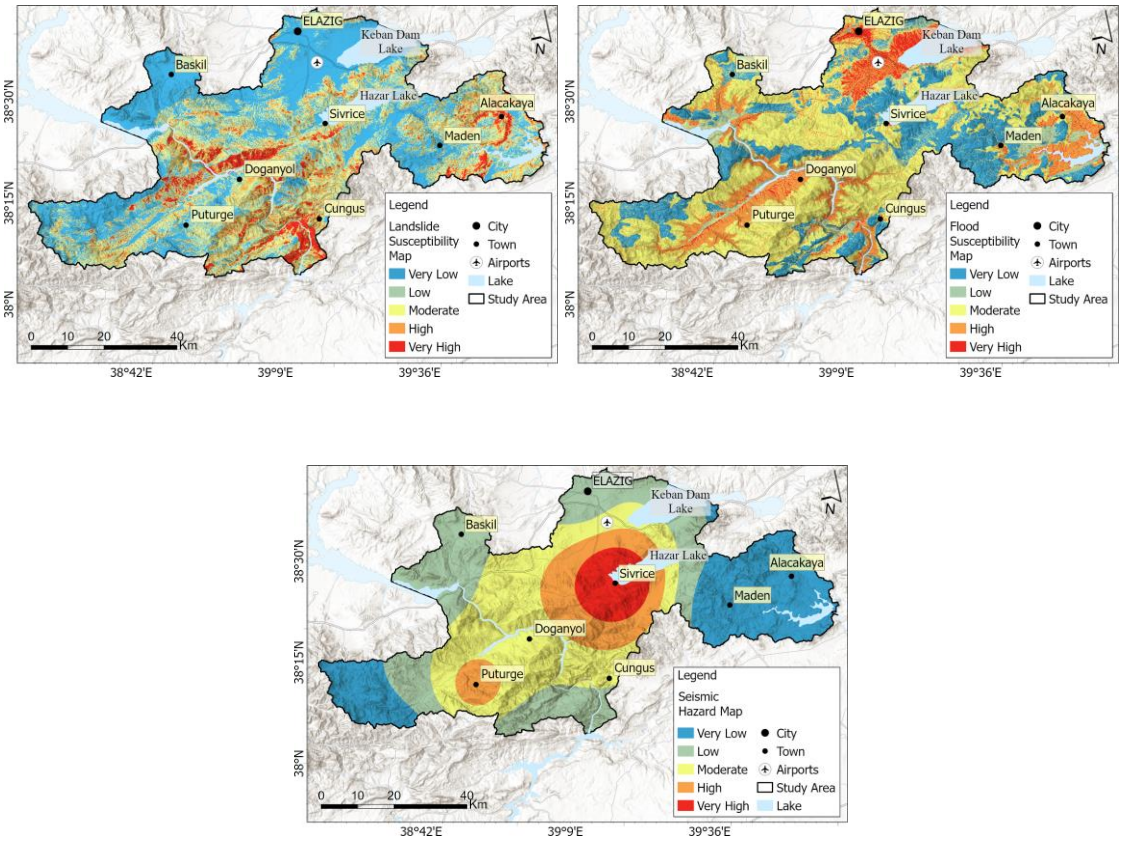

Figure 5.3. The univariate susceptibility result maps for Elazig site

Table 5.5. The landslide probability, size and their percentages predicted by the RF algorithm

Class	Probability (%)	Size (km^2)	Percentage (%)
Very Low	0 - 11	1900.88	39.28
Low	11 - 26	1176.03	24.30
Moderate	26 - 44	877.29	18.13
High	44 - 66	574.76	11.87
Very High	66 - 100	309.66	6.40

Table 5.6 summarizes the statistical performance measures produced by the RF algorithm using the test dataset, which was split and not used for model training. The table also includes the number of test pixels (support). Figure 5.4 shows the ROC curve. The AUC value derived from the RF is 0.96, indicating a high level of classification accuracy, which is further supported by the overall accuracy (90.0%) and F-1 score (0.88).

Table 5.6. Statistical performance measures of the RF algorithm for Elazig site

Classes	Precision	Recall	F1-score	Support
Non-landslide (0)	0.95	0.87	0.91	52362
Landslide (1)	0.83	0.93	0.88	35248

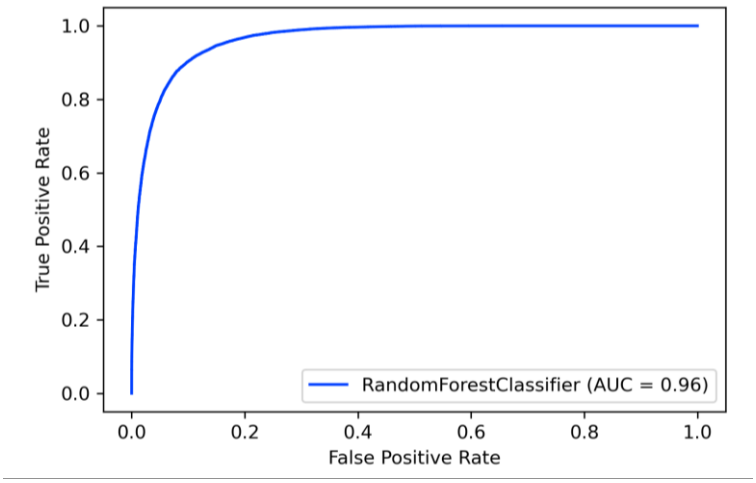

Figure 5.4. The ROC curve evaluation with AUC value of the RF algorithm

Figure 5.5 shows the SHAP value plot and the feature importance plot. In the SHAP value plot, which shows the relationship between the model prediction and the input features, the x-axis shows the effect of the value that causes the higher or lower prediction, while the y-axis indicates which input feature defines. The color indicates whether the input feature is high or low in that row of the dataset. Input features are ranked according to their importance. When the plot is analyzed, it shows that slope, distance to faults and lithology have larger influence among other features, respectively. It was observed that low distances to faults have a positive contribution to the model output. The closer a point to the faults, the more positively correlated it with landslide occurrence. As can be seen in the plot, the impacts of various lithological units, indicated by their ID numbers, were varied and mixed. Additionally, higher slope values positively increase the model output. SHAP values are a powerful tool for understanding a model's predictions and explaining the decision process of the model. These values provide a detailed visualization of the contribution of each feature to the output.

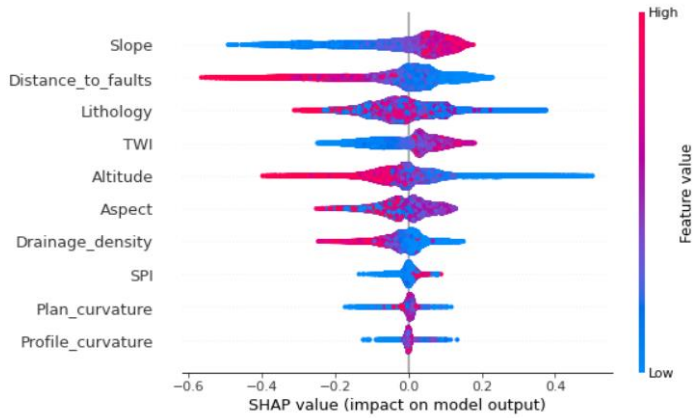

(a)

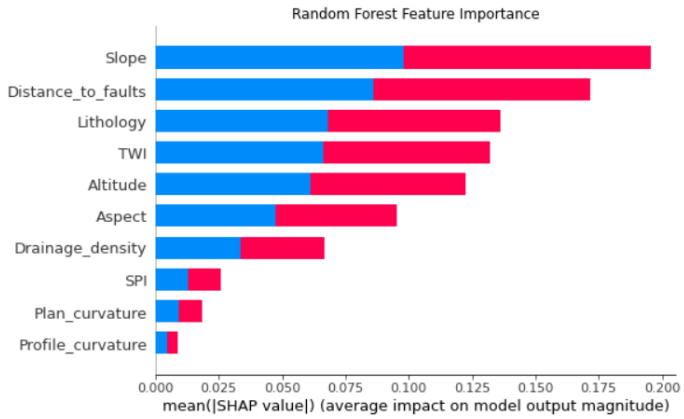

(b)

Figure 5.5 Summary (a) and feature importance (b) plots of SHAP values.

In this thesis, the validation of the LSM produced for the Elazig study site was evaluated with earthquake-triggered landslides. The analysis yielded an overall accuracy of 85%, with additional measures detailed in Table 5.7. The evaluations were specifically conducted on landslide pixels categorized as having moderate, high, and very high probability values. According to the F1 score, the accuracy obtained for the Elazig study area is high. Although the LSM was produced using EUDEM v.1.1 with 25 m resolution, the landslides triggered after the earthquake were detected with higher accuracy because the size of the landslides triggered after the earthquake was larger in this study area.

Table 5.7. Statistical performance measures for the external validation using the post-earthquake landslide inventory in Elazig study site.

Classes	Precision	Recall	F1-score	Support
Non-landslide (0)	0.99	0.70	0.82	12,909
Landslide (1)	0.77	1.00	0.87	12,909

Figure 5.6 shows sub-areas of the LSM with the post-earthquake landslides to facilitate visual evaluation. It is important to highlight that the resolution of the DEM (25 m) utilized for LSM production differs from the DSM depicted in the figure. The EU-DEM has proved to be well-suited for the production of regional LSMs.

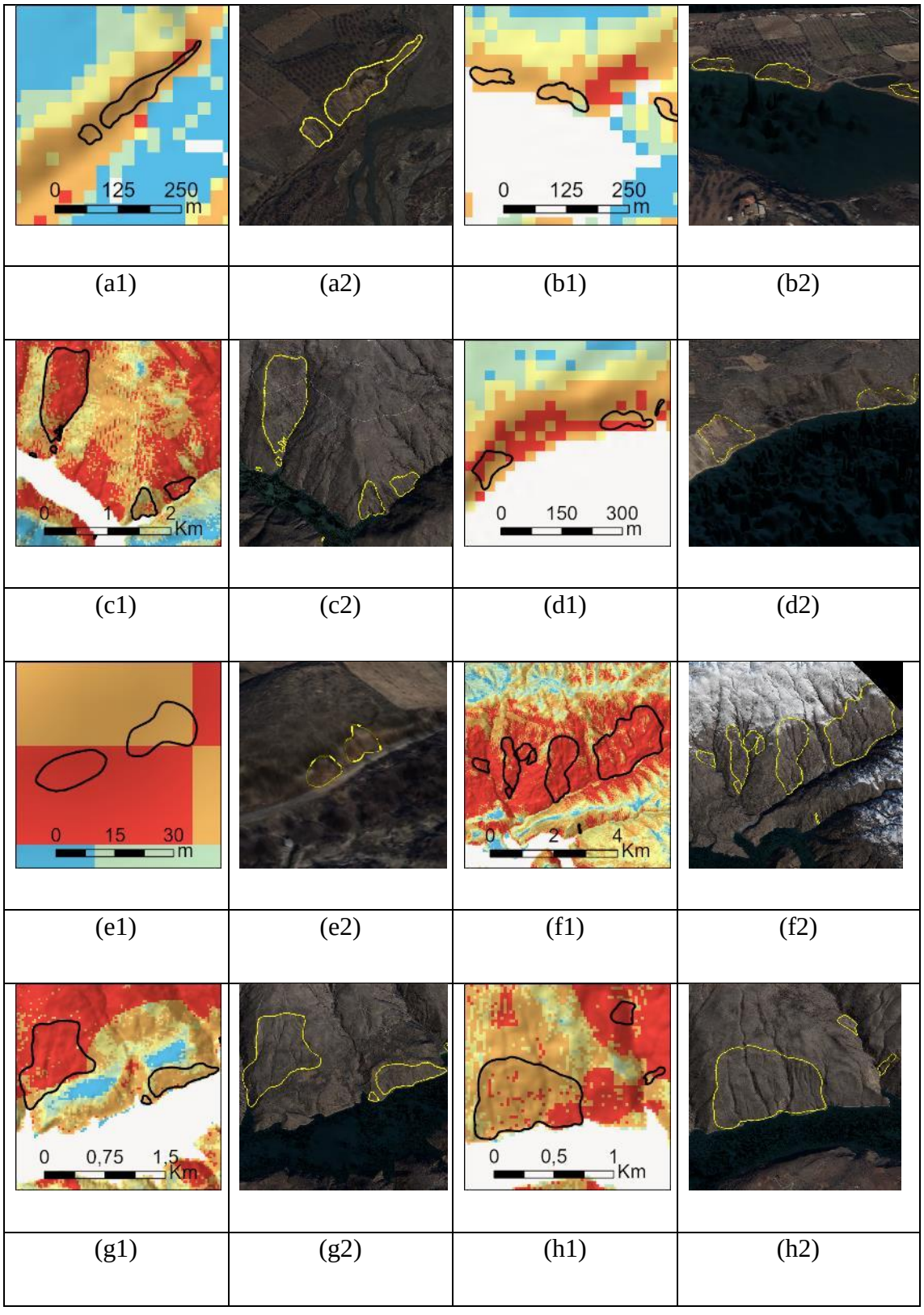

(a1) (a2) (b1) (b2)

(c1) (c2) (d1) (d2)

(e1) (e2) (f1) (f2)

(g1) (g2) (h1) (h2)

Figure 5.6. The LSM result with the post-earthquake landslides shown in sub-areas (a1, b1, c1, d1, e1, f1, g1, h1) and post-earthquake orthophotos (a2, b2, c2, d2, e2, f2, g2, h2)

Flood size and probability percentages for each class regarding the flood susceptibility result map seen in Figure 5.1 (b) are given in Table 5.8. According to the table, 69.9% of the Elazig study site exhibits susceptibility to flood across the very high, high, and moderate susceptibility classes. The flood susceptibility map indicates that Elazig city center and airport areas are more prone to floods. The dams in the Elazig study site have flood susceptibility as well. In addition, a preliminary assessment after the flood event occurred in the region on different dates (see Section 3.1.3) indicated that the map accurately illustrate the flood-prone areas.

Table 5.8. The flood probability, size and their percentages produced by the m-AHP method

Class	Probability (%)	Size (km^2)	Percentage (%)
Very Low	0 - 25	1124.59	21.88
Low	25 - 48	420.36	8.17
Moderate	48 - 66	2041.75	39.72
High	66 - 82	1061.80	20.65
Very High	82 - 100	491.95	9.57

When the seismic hazard map (Figure 5.1c) was analyzed, it was observed that the Elazig study site generally showed high-intensity values, especially in Sivrice district and its surroundings. Values exceeding the shaking threshold established by Keefer and Wilson [201] indicate susceptibility to seismically triggered landslides and lateral flows. High arias intensity values in the Elazig study site are above this threshold value.

5.1.3. The Multi-hazard Susceptibility Map for Elazig Study Site

The multi-hazard susceptibility map produced with Mamdani FIS in the Elazig study site is presented in Figure 5.7. Table 5.9 shows the multi-hazard probability, size and their percentages for the multi-hazard susceptibility map produced by Mamdani FIS. According to the MHS map, the southern parts of the study area show very high

susceptibility classes due to the higher AI and landslide susceptibility values. The settlements of Sivrice, Cungus, Alacakaya, Doganyol, and Puturge were found to be extremely prone areas according to the results of the MHS analysis.

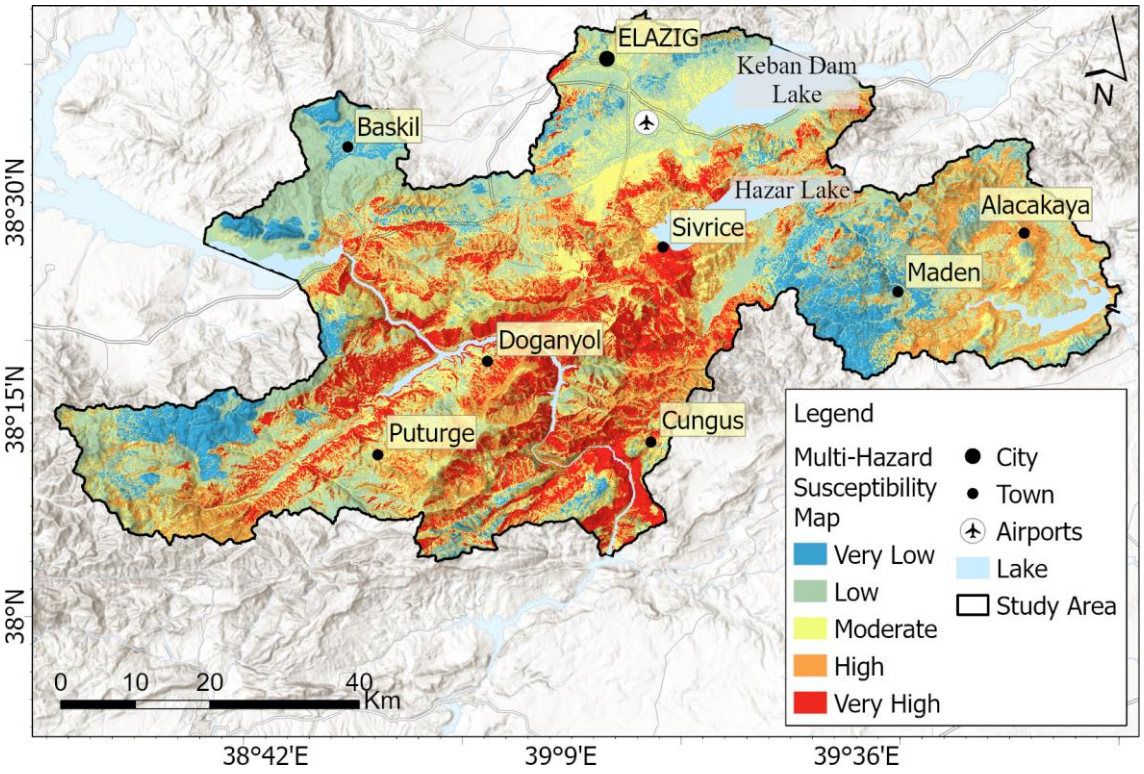

Figure 5.7. The MHS map of the Elazig study site.

Table 5.9. The multi-hazard probability, size and their percentages produced by the Mamdani FIS.

Class	Probability (%)	Size (km^2)	Percentage (%)
Very Low	0 - 27	439.22	9.08
Low	27 - 42	1368.38	28.29
Moderate	42 - 55	1010.05	20.88
High	55 - 68	1250.51	25.85
Very High	68 - 100	769.09	15.89

5.2. Results from Adiyaman Study Site

This section provides a detailed overview of the results maps generated for Adiyaman study site. In the subsequent subheading, emphasis is placed on the feature maps utilized for producing the univariate susceptibility maps and analyzing multicollinearity among features. The univariate susceptibility maps produced for each hazard are delineated in Section 5.2.2, while the result of multi-hazard susceptibility mapping is elaborated upon in Section 5.2.3.

5.2.1. Input Feature Maps Produced for Adiyaman Study Site

In the context of the Elazig study area, Figure 5.8 illustrates the input feature maps utilized in the production of landslide and flood susceptibility maps. For landslide susceptibility assessment, a set of 10 features as depicted in Figure 4.4 was employed, while flood susceptibility mapping utilized 6 features. Since the process of applicability of the method proposed in the thesis study in Adiyaman study site was carried out quickly after the Kahramanmaras earthquakes, permanent and dry river datasets could not be obtained immediately from HGM's TopoVT database. Only the distance to drainage network feature was produced in this site. Therefore, 6 features were used to produce flood susceptibility in Adiyaman study site. Detailed statistical analyses of these features are provided in Table 5.10. Furthermore, Tables 5.11 and 5.12 present statistical summaries of input features in both pre and post-earthquake landslide inventory polygons.

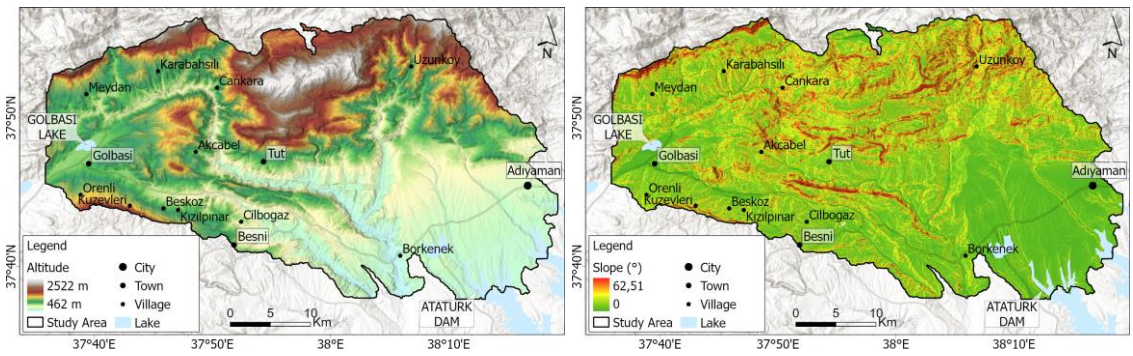

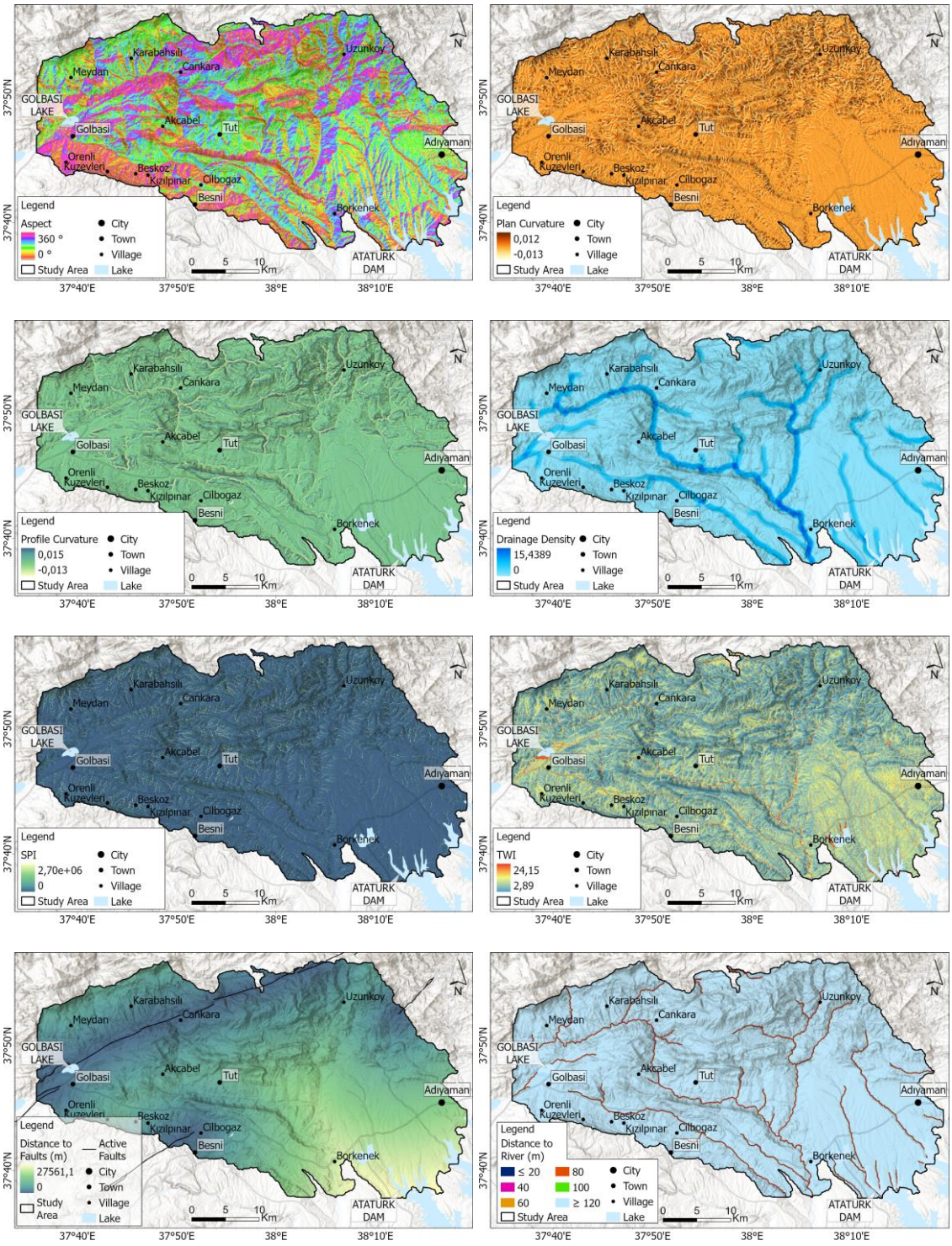

Figure 5.8. The feature map results for landslide and flood susceptibility assessment in Adiyaman site: (a) Altitude, (b) Slope, (c) Aspect, (d) Plan curvature, (e) Profile curvature, (f) Drainage density, (g) SPI, (h) TWI, (i) Distance to faults, (j) Distance to rivers

Table 5.10. Statistical summary of all the input features for Adiyaman study site.

Features	Min	Max	Mean	Std. Dev.	Median
Altitude (m)	461.964	2522.258	1030.864	397.404	936.908
Slope (°)	0	62.514	11.917	8.836	9.992
Aspect (°)	0	360.00	176.177	94.609	176.514
Distance to faults (m)	0	27561.125	8817.079	6524.592	7148.864
Drainage Density	0	15.438	0.817	1.882	0
Plan Curvature	-0.013	0.012	5.667	0.001	$2.18*10^{-5}$
Profile Curvature	-0.013	0.015	-6.526	0.001	-3.62.166
SPI	0	$2.705*10^{6}$	3769.335	24685.334	303.572
TWI	2.890	24.151	7.519	2.196	7.052

Table 5.11. Statistical summary of the input features inside pre-earthquake landslide inventory for Adiyaman study site.

Features	Min	Max	Mean	Std. Dev.	Median
Altitude (m)	489.403	2519.906	1298.595	386.149	1278.98
Slope (°)	0	60.749	14.272	8.399	11.974
Aspect (°)	0	360.00	161.039	104.768	156.616
Distance to faults (m)	0	22894.664	6140.725	3847.446	5905.929
Drainage Density	0	11.173	0.315	1.133	0
Plan Curvature	-0.011	0.009	-3.882	0.001	$-5.28*10^{-5}$
Profile Curvature	-0.008	0.011	-9.399	0.001	$-9.63*10^{-5}$
SPI	0.378	$1.533*10^{6}$	6322.083	32803.556	429.032
TWI	3.442	23.150	7.563	1.711	7.322

Table 5.12. Statistical summary of the input features inside post-earthquake landslide inventory for Adiyaman study site

Features	Min	Max	Mean	Std. Dev.	Median
Altitude (m)	534.677	1536.470	962.225	221.939	931.439
Slope (°)	0	62.514	27.866	10.212	27.965
Aspect (°)	0	360.00	140.028	114.025	130.099
Distance to faults (m)	0	16957.373	6421.754	2855.204	6283.709
Drainage Density	0	10.604	1.404	2.228	0
Plan Curvature	-0.011	0.010	-0.0003	0.002	-0.0004
Profile Curvature	-0.013	0.008	-0.0005	0.002	-0.0006
SPI	1.412	$6.79*10^5$	7559.072	26913.197	1001.404
TWI	3.058	23.037	6.505	1.847	6.171

Furthermore, the multicollinearity analyses for the 10 LSM features were performed using VIF, TOL and Pearson's coefficient, and the results are presented in Table 5.13. The analyses indicated that among the landslide input features, altitude has the lowest tolerance value at 0.085, while SPI has the highest tolerance value at 0.930. The maximum VIF value observed was 11.763, while the minimum VIF value recorded was 1.075 (Table 5.13). Nevertheless, the tolerance values for the landslide conditioning factors exceed 0.1, and the VIF values fall below 10, indicating the absence of collinearity issues among these factors. This condition is met except for the altitude feature. Altitude was used in the model training as it is one of the important features for the LSM production. According to the IGR results in Table 5.13, distance to faults has the most significant influence on the predictive performance of the model (0.126), followed by altitude (0.106) and lithology (0.086).

Table 5.13. Collinearity analysis results between the input features for Adiyaman study site

No	Input Features	Collinearity Statistics		IGR
		VIF	TOL	
1	Altitude	11.763	0.085	**0.106**
2	Slope	4.267	0.234	0.042
3	Aspect	6.957	0.144	0.014
4	Lithology	2.598	0.384	**0.086**
5	Plan Curvature	1.266	0.789	0.007
6	Profile Curvature	1.199	0.834	0.003
7	SPI	1.075	0.930	0.024
8	TWI	9.800	0.102	0.009
9	Distance to Faults	3.685	0.271	**0.126**
10	Drainage Density	1.384	0.722	0.017

Figure 5.9 shows Pearson's coefficient results for Adiyaman study site. A Pearson correlation coefficient below 0.7 suggests a weak or nearly no correlation. The highest absolute correlation coefficient among the factors is between distance to faults and altitude (-0.6). When the results were analyzed, it was determined that the correlation coefficients between the features were lower than 0.7. This indicates that there is not a strong relationship between the factors used. These results support the suitability of the factors used in the production of the LSM in terms of ensuring diversity and independence.

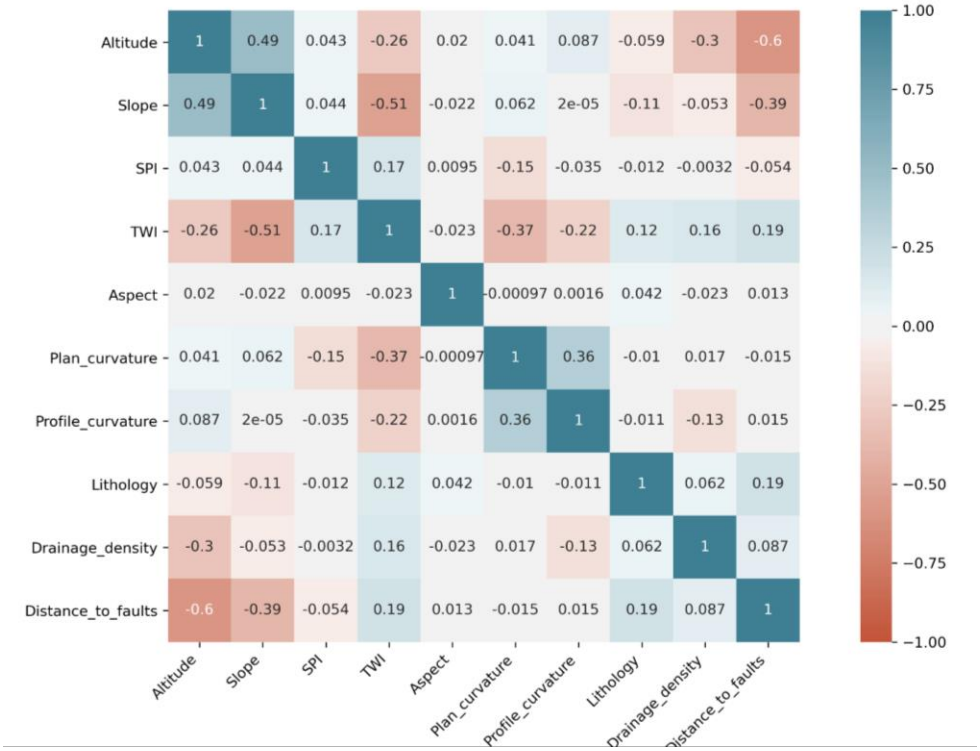

Figure 5.9. Pearson's coefficient results between the input features for Adiyaman study site.

5.2.2. The Univariate Susceptibility Maps for Adiyaman Study Site

The univariate susceptibility maps produced from Adiyaman study site are presented in Figure 5.10. The size and probability percentages of the predicted susceptibility values for each class in the landslide susceptibility map are given in Table 5.14. According to the table, 22.8% of Adiyaman study site exhibits susceptibility to landslides across very high, high, and moderate classes. During the assessment of landslide susceptibility results, it became apparent that the probability of landslides is notably high in the mountainous regions to the north of Tut town and the south of Golbasi town. Visual similarity was noted between steeper slopes (see Figure 5.8 (b)) and increased values of landslide susceptibility (Figure 5.10 (a)) across Adiyaman study site.

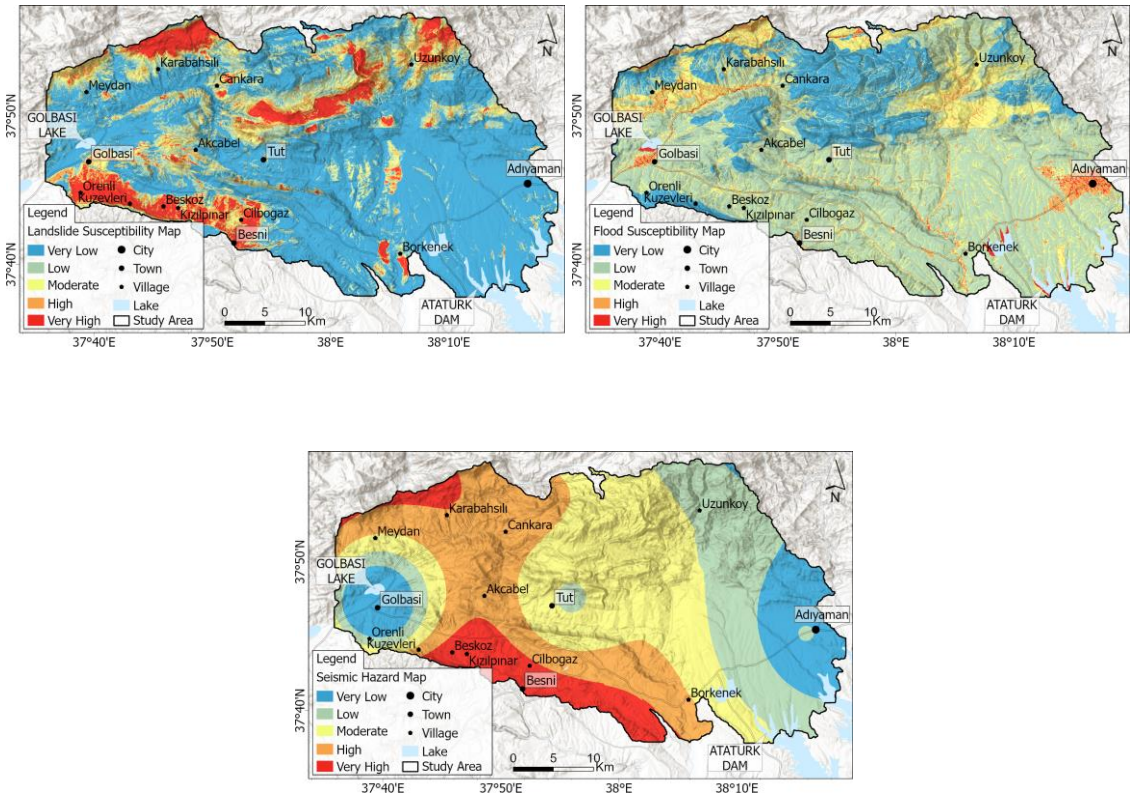

Figure 5.10. The univariate susceptibility result maps for Adiyaman site

Table 5.14. The landslide probability, size and their percentages predicted by the RF algorithm

Class	Probability (%)	Size (km^2)	Percentage (%)
Very Low	0 - 9	975.13	60.89
Low	9 - 26	261.22	16.31
Moderate	26 - 50	125.65	7.85
High	50 - 76	100.21	6.26
Very High	76 - 100	139.06	8.68

Table 5.15 provides a statistical summary of the precision, recall, and F1-score performance measures generated by the RF algorithm using the test dataset. The model achieved an overall accuracy of 94%. As anticipated, the performance metrics for the non-landslide class outperformed those for the landslide class. Additionally, Figure 5.11 illustrates ROC, revealing a notably high AUC (=0.98).

Table 5.15. Statistical performance measures of the RF algorithm for Adiyaman study site

Classes	Precision	Recall	F1-score	Support
Non-landslide (0)	0.98	0.91	0.94	56448
Landslide (1)	0.88	0.97	0.92	37862

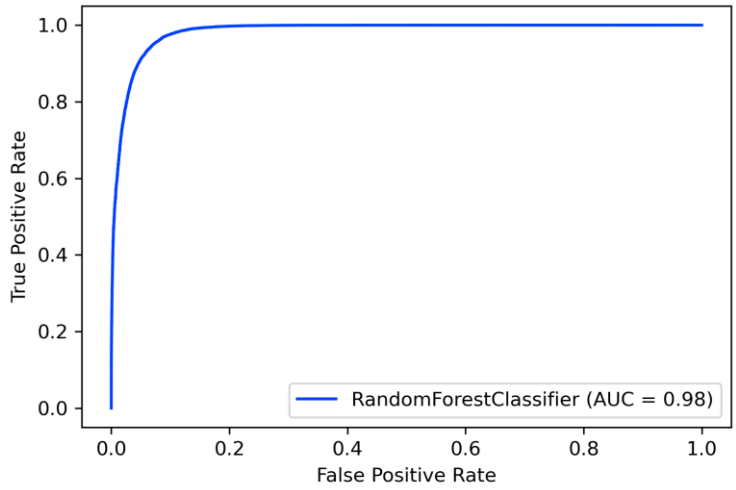

Figure 5.11. The ROC curve evaluation with AUC value of the RF algorithm

Feature importance results for the Adiyaman study site are shown in Figure 5.12. In the feature importance analysis evaluated using SHAP, the summary plot shows the correlation and contribution of feature values to the model prediction. From the summary plot, it can be concluded that higher values of distance to faults direct model predictions towards the non-landslide class. Low values of distance to faults contribute positively to landslide prediction. High altitude values are positively related to landslide occurrence. In the feature importance plot, the most predictive features were identified as altitude, distance to faults and lithology.

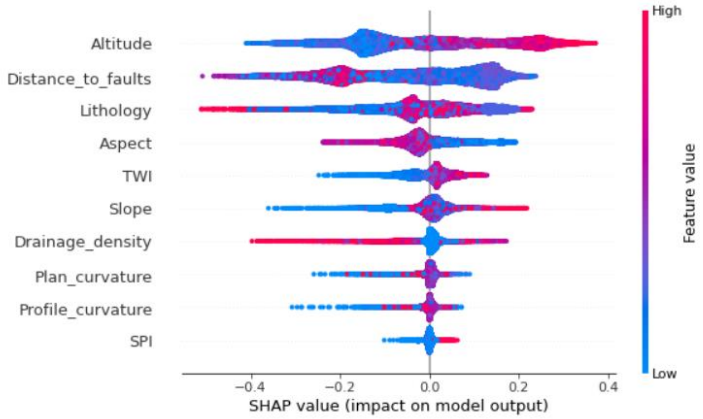

(a)

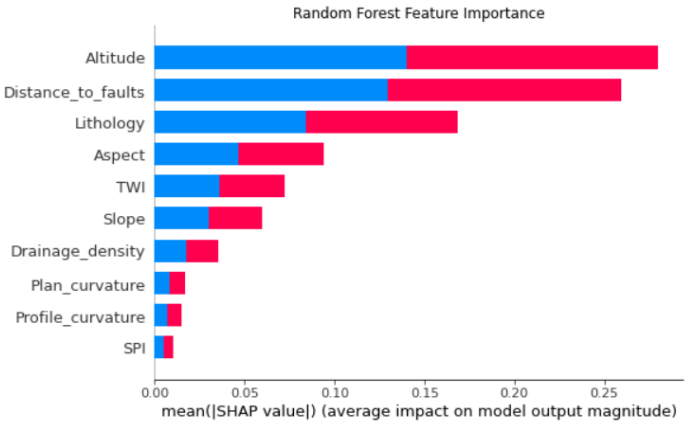

(b)

Figure 5.12. Summary (a) and feature importance (b) plots of SHAP values

Statistical results of the LSM validated with the post-earthquake landslide inventory in Adiyaman study site are given in Table 5.16. The analysis resulted in an OA rate of 72%. The lower F1-scores observed in comparison to those in Table 5.15 may be attributed to the severity of the event, indicating the need for further research to understand landslide dynamics fully. Moreover, while the post-earthquake landslides were delineated using aerial photogrammetric DSMs with sub-meter resolution and high accuracy, the LSM was developed using the EU-DEM with a resolution of 25 meters. Since the post-earthquake landslides defined for this region are smaller in size, this accuracy is acceptable considering the DEM resolution (25 m). As mentioned in the study by Karakas et al. [202], the detectability of landslide sizes within LSMs is associated with the quality of DEMs, specifically their density and distribution. Additionally, Figure 5.13 shows the post-earthquake inventory and LSM results in the sub-areas of the Adiyaman study site.

Table 5.16. Statistical performance measures for the external validation using the post-earthquake landslide inventory in Elazig study site.

Classes	Precision	Recall	F1-score	Support
Non-landslide (0)	0.70	0.79	0.74	16628
Landslide (1)	0.76	0.66	0.70	16628

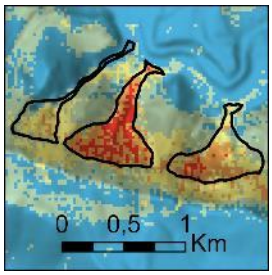

(a1)

(a2)

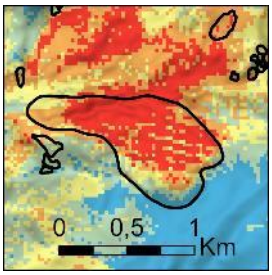

(b1)

(b2)

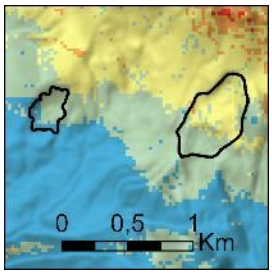

(c1)

(c2)

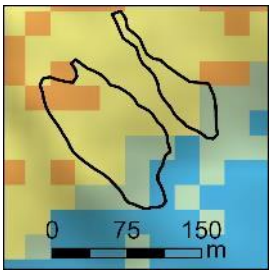

(d1)

(d2)

Figure 5.13 The LSM result with the post-earthquake landslides shown in sub-areas (a1, b1, c1, d1) and post-earthquake orthophotos (a2, b2, c2, d2).

Table 5.17 presents flood size and probability percentages for each class based on the flood susceptibility result map depicted in Figure 5.10 (b). As seen from the table, 25.6% of Adiyaman study site demonstrates susceptibility to floods across the very high, high, and moderate susceptibility classes. The flood susceptibility map suggests that regions surrounding Tut and Golbasi towns, as well as the central area of Adiyaman Province, are

highly prone to floods. An initial evaluation following a flood event in the region on March 15, 2023, indicated that the map accurately depicts areas susceptible to flooding.

Table 5.17. The flood probability, size and their percentages produced by the m-AHP method

Class	Probability (%)	Size (km^2)	Percentage (%)
Very Low	0 - 17	270.55	16.95
Low	17 - 40	916.06	57.40
Moderate	40 - 57	300.50	18.83
High	57 - 74	87.80	5.50
Very High	74 - 100	20.84	1.31

Upon analysis of the seismic hazard map, Adiyaman study site exhibited predominantly high-intensity values, with particularly high values observed in the northern and southern regions. The impact of the Kahramanmaras earthquakes in this region also confirms this situation.

5.2.3. The Multi-hazard Susceptibility Map for Adiyaman Study Site

The MHS map generated from the Mamdani FIS revealed significantly high susceptibility levels in both the southern and northern regions of the study area (Figure 5.14). The MHS assessment identified several highly hazard-prone areas, including the settlements of Karabahsili, Cankara, Uzunkoy, Orenli, Beskoz, Kuzevleri, Cilbogaz, and Borkenek. Moreover, the northern parts of Tut town and the southern parts of Golbasi town were identified as susceptible areas to multi-hazard. Table 5.18 presents the probabilities, sizes, and their respective percentages for the MHS map in Adiyaman site.

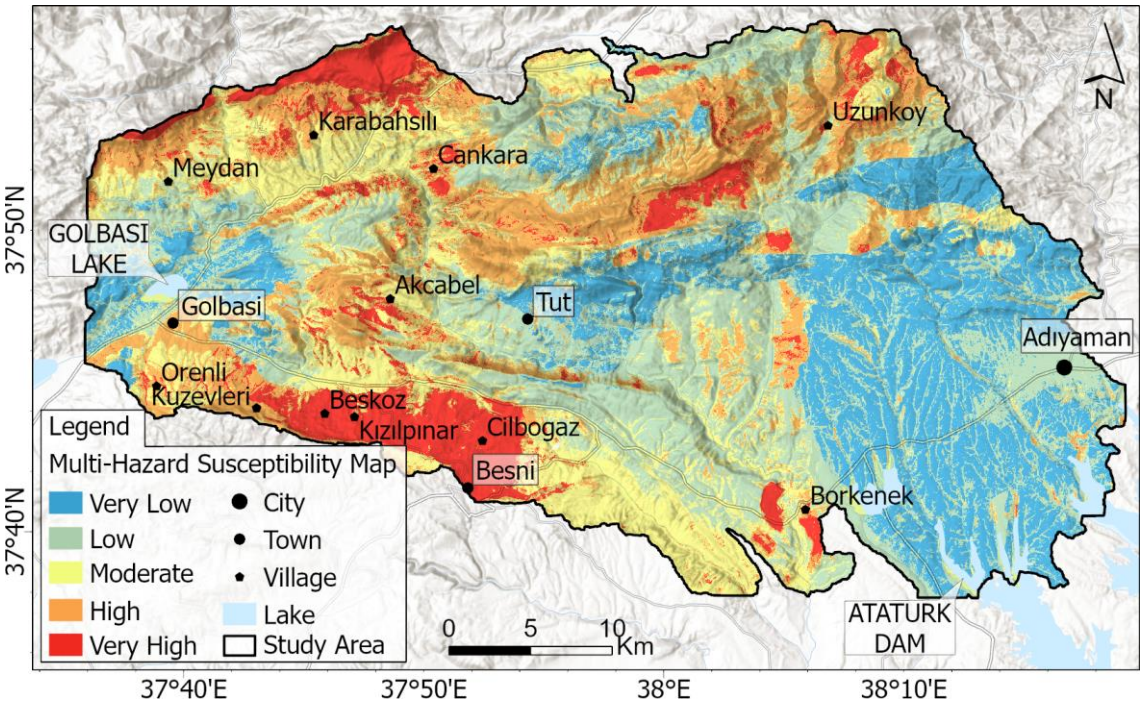

Figure 5.14. The multi-hazard susceptibility map for Adiyaman study site.

Table 5.18.The multi-hazard probability, size and their percentages produced by the Mamdani FIS

Class	Probability (%)	Size (km^2)	Percentage (%)
Very Low	0 - 21	324.48	20.33
Low	21 - 34	496.89	31.14
Moderate	34 - 49	330.06	20.68
High	49 - 69	301.97	18.92
Very High	69 - 100	142.37	8.92

6. DISCUSSIONS

In this chapter, the results produced from the thesis are discussed from different perspectives, such as the selection and use of input features, the suitability and importance of the methods used to produce the univarite and multi-hazard susceptibility maps.

The aim of this thesis was to develop a novel approach for conducting multi-hazard assessments at a regional scale by integrating landslide, flood, and earthquake hazards using a combination of machine learning and expert-based methods. The results and recommendations of this study aim to contribute to the literature and future research. To achieve this objective, multi-hazard susceptibility assessment was applied to two study sites. One of these study sites was determined as a result of the observation of landslides triggered after 24 January 2020 Elazig earthquake (Mw=6.8) and the region's frequent exposure to flood events. The other study area was selected to evaluate the impact of the 6 February 2023 Kahramanmaras earthquakes (Mw=7.7 and Mw=7.6), the largest disaster our country has ever seen, and to test the applicability of the proposed methodology. In the thesis study, the results obtained using datasets obtained from different sources were evaluated with both qualitative and quantitative analyses.

6.1. Input Features and Landslide Susceptibility Map Production

The input features (also known as conditioning factors) used in the production of the LSMs are important factors that influence and determine the occurrence of potential landslides. These include various factors such as geological, topographic, hydrological, environmental and anthropogenic factors that play a role in the occurrence of landslides. There is no standardized selection of these factors in the literature, which differ in each study. Accurate identification and evaluation of the conditioning factors is important for predicting the possible locations of landslides and producing more accurate susceptibility maps. The selection of influential factors relies heavily on the specific geoenvironmental

conditions. The selection of input features for the LSM was determined following a review of studies conducted between 2017 and 2023, taking into account the specific characteristics of the study sites. For the Elazig study site, slope, distance to faults, and lithology characteristics were identified as the most significant features. In the case of the Adıyaman study site, altitude, distance to faults, and lithological features were found to be important. The selected factors were considered suitable considering the availability of high-quality maps for LSM. On the other hand, According to the multicollinearity results tested among the features, although the VIF value of the altitude feature was high, this feature was not eliminated due to its importance. It was emphasized by Piramithu [199] that DT based algorithms are known to be immune to multicollinearity. Additionally, Piramithu [199] mentioned that eliminating parameters due to multicollinearity issues might decrease classification accuracy in DTs.

The preparation of a reliable and comprehensive landslide inventory is another important consideration in the production of landslide susceptibility maps. The landslide inventory used in model training in the thesis was obtained from the MTA geo-sciences portal. The landslide data in the portal (as stated in sub-section 3.1.4.1) were produced within the "Turkey Landslide Inventory Project" of the MTA, which was completed in 2007. Landslides triggered during Elazig and Kahramanmaras earthquakes were used to validate the LSMs produced for the study sites. A post-earthquake landslide inventory was compiled by interpreting orthophotos and 3D surface models produced from aerial photographs taken pre- and post-earthquake. A comprehensive inventory of landslides triggered by the Elazig earthquake was compiled using aerial photogrammetric datasets. The study conducted by Karakas et al. [71] presented the first comprehensive inventory of earthquake-triggered landslides in Türkiye. The landslides triggered by the Kahramanmaras earthquake were also mapped [73] by comparing the pre- and post-earthquake orthophotos published on the HGM Küre platform. Detailed information about these landslides was given by Kocaman et al. [157]. Additionally, Gorum et al. [203] also conducted a study on the preliminary documentation of landslides triggered by the Kahramanmaras earthquakes. New data to be obtained from Türkiye is important for international landslide literature. Complete landslide inventories can contribute greatly to the production of more accurate and up-to-date LSMs. In addition, Compiling the

inventory of landslides induced by the Elazig and Kahramanmaras earthquakes on a regional scale helped address the deficiency in landslide inventory.

Several classification algorithms have been used in the literature to produce the LSMs. There is no widely accepted algorithm to use for this purpose. However, recent research indicated a prevailing tendency to employ different ML algorithms to generate precise and up-to-date susceptibility maps. One of the most commonly utilized algorithms among these is the RF [45], [46], [48], [204], [50]. The RF has features such as high accuracy, ability to work effectively with large data sets, ability to handle interactions between features, and reducing overfitting. Consequently, although both the RF and MLP algorithms were employed during the thesis study to produce LSMs in Elazig site, only the RF was applied to Adiyaman site and presented here as it ensures high accuracy and efficiency.

The evaluation of the model quality for the produced LSM was conducted using ROC curves and statistical measures consistent with common practice in many studies. As expected, the RF method exhibited strong performance in Elazig (90% OA) and Adiyaman (94% OA) study sites for the landslide susceptibility assessment. When the visual and statistical results were evaluated together, the RF algorithm has been proven to be successful.

One of the important issues in LSMs produced by RF and different methods is the collection of training and test samples. It was observed that different sampling strategies are used in the literature. These strategies determine the selection and distribution of data samples used in the training and testing phase of the model, which may affect its performance and the accuracy of the resulting map. Aktas and San [205] proposed two-level random sampling to select train and test samples strategy. In their study, Aktas and San [205] stated that if the training datasets randomly selected samples happen to fall within the same seed cell as the landslide, then both training and testing should identify the same landslide. They emphasized that the sampling strategy is important to produce a realistic LSM. In this thesis study, automatic random sampling algorithm was presented, as in most studies in the literature. However, the performance and accuracy of the models

were also analyzed using different sampling strategies during the thesis work and published in different platforms. As stated by Karakas et al. [50], in the study area covering Ikizce and Caybası districts of Ordu Province, landslide samples were randomly selected from only a part of the area and model training was carried out. The model, which was trained in approximately 1/3rd of the study region, was then applied to the entire field (also unseen regions). In the resulting susceptibility map, it was observed that landslides in the southern parts of the study area, which were not included in the model training, were correctly detected. In another study conducted by Karakas et al. [70], the study area was split into two parts containing the boundaries of Malatya and Elazig Provinces. In the study, the model was trained with landslide samples selected from the Malatya part, and used directly in the Elazig part. The resulting maps were evaluated with different methods and landslides that the model did not see in Elazig part were predicted. In addition, this demonstrates the ability of RF model parameters to be transferred to similar regions. It can be concluded that in this thesis and other studies, when the amount of data is large, the sampling strategy does not affect the prediction results, which proves again the importance of high quality and complete inventories.

An important contribution of this study was that it was based on the use of earthquake-triggered landslide inventory in the testing phase. Although the susceptibility map was produced using the pre-earthquake landslide inventory, the post-earthquake landslide inventory was utilized, which was not incorporated into the model during the testing phase. Incorporating external data for validating the result susceptibility map in such studies can provide more realistic and accurate insights [73]. As a result of validating the LSMs produced for the Elazig and Adiyaman study sites with the post-earthquake inventory, the OA was found to be 85% and 72%, respectively. It can be interpreted that the reason for higher accuracy with external data in the Elazig study site is that the landslide sizes triggered here are larger than those in the Adiyaman site.

Mountainous areas that experience strong and destructive earthquakes tend to have a greater probability of landslides occurrence when compared to the state before the earthquake. The phenomenon is known as the earthquake legacy effect, and a thorough understanding of it is necessary to evaluate post-seismic landslide hazards precisely

[206]. The evaluation of the earthquake legacy effect mostly involves the continuous monitoring of either sudden landslide events or gradual landslides over a period of time [206]. Especially after the Kahramanmaras Earthquakes, comprehensive research is needed to understand the earthquake legacy effect, which plays an important role in assessing the long-term impacts in the region. These effects can be evaluated for the Adiyaman study site, where many landslides were triggered after the earthquake. This study site allows for the long-term investigation of how hillslopes respond to earthquakes.

In the study conducted by Karakas et al. [202], it was observed how DEM quality and resolution affected the results both qualitatively and quantitatively. In the study, susceptibility maps were produced using high-resolution DEM data produced from aerial photographs and the EU-DEM. In the resulting maps presenting similar spatial patterns, larger landslide areas were successfully detected. It can be said that smaller activities are better detected using the DEM produced with aerial photographs. Nevertheless, the EU-DEM was considered suitable for producing regional LSMs, as higher-resolution DEMs would bring about computational complexities for such an extensive area. For this reason, in this study, considering both the model performance results and the validation results obtained using external data, it was decided that the use of EUDEM data was appropriate.

6.2. Flood Susceptibility Map Production and Seismic Hazard Map

There are fewer studies in the literature on flood susceptibility assessment than landslide susceptibility assessment studies. However, flood events in recent years have increased the trend in this direction. As stated in Section 2.3, different methods and datasets are used in flood susceptibility assessment. Due to the general lack of complete flood inventories, the use of MCDM methods is common. Especially the AHP method has been frequently used [79], [80], [89]. In this thesis, it was found appropriate to use the M-AHP method recommended by Nefeslioglu et al. [63], which provided more accurate results than AHP because it eliminates expert subjectivity and creates a weight matrix for each pixel. The usability of the method was also confirmed through expert validation of the FSM produced with the M-AHP. This observation was consistent with the research

conducted by Sozer et al. [207] (2018), which utilized the M-AHP methodology for FSM development on a regional scale in Ankara, Türkiye.

With their knowledge and experience, experts can better understand the factors affecting flood risk and determine the importance of these factors. Therefore, weighting and evaluation processes created with the participation of experts can provide more accurate results. Additionally, an expert-based method can better take into account local conditions and environmental factors. Experts can gain in-depth knowledge of site-specific topographical, hydrological and geological features and integrate this knowledge into the modeling process. However, there is a risk of subjectivity in an expert-based method. Therefore, along with the use of expert-based methods, it is important that validation processes are carried out meticulously and the results are carefully evaluated.

When a flood susceptibility map is produced, it is aimed to identify areas with high flood risk based on various conditioning factors specific to the study area. In other words, areas susceptible to flood risk are identified. According to the flood susceptibility map produced, areas close to rivers, lakes, dams in the study areas, or other water bodies appear to be at high risk. Additionally, low-elevation areas and floodplains are also at high risk of flooding. Areas with poor drainage systems may also be at risk of flooding. Moderate risk zones can be characterized by moderately sloping terrain that might lead to the formation of puddles, as well as areas with a moderate amount of vegetation cover. Low-risk areas will be areas with high elevations or steep slopes where it is difficult for water to accumulate. These areas generally have well-established drainage systems and infrastructure. These maps, produced for the Elazig and Adiyaman study sites, provide important information for risk assessment and management by identifying flood-prone areas and infrastructure. It can also provide the basis for urban planning, development studies and implementation of flood prevention measures. It helps to develop strategies to minimize the impacts of potential flood events.

In this study, inundation areaswith high flood risk were determined in the Elazig and Adiyaman study sites using the information obtained from the news and media reports. These inundation areas were given with their locations in Table 3.2 and Table 3.6.

Additionally, the locations of these areas are shown in Figures 6.1 and 6.2 along with the sub-areas of the susceptibility maps produced. In the preliminary evaluation made after previous flood events in the study sites, it was revealed that the flood susceptibility maps produced accurately showed the areas that would be exposed to flood. This proves the applicability of this expert-based method.

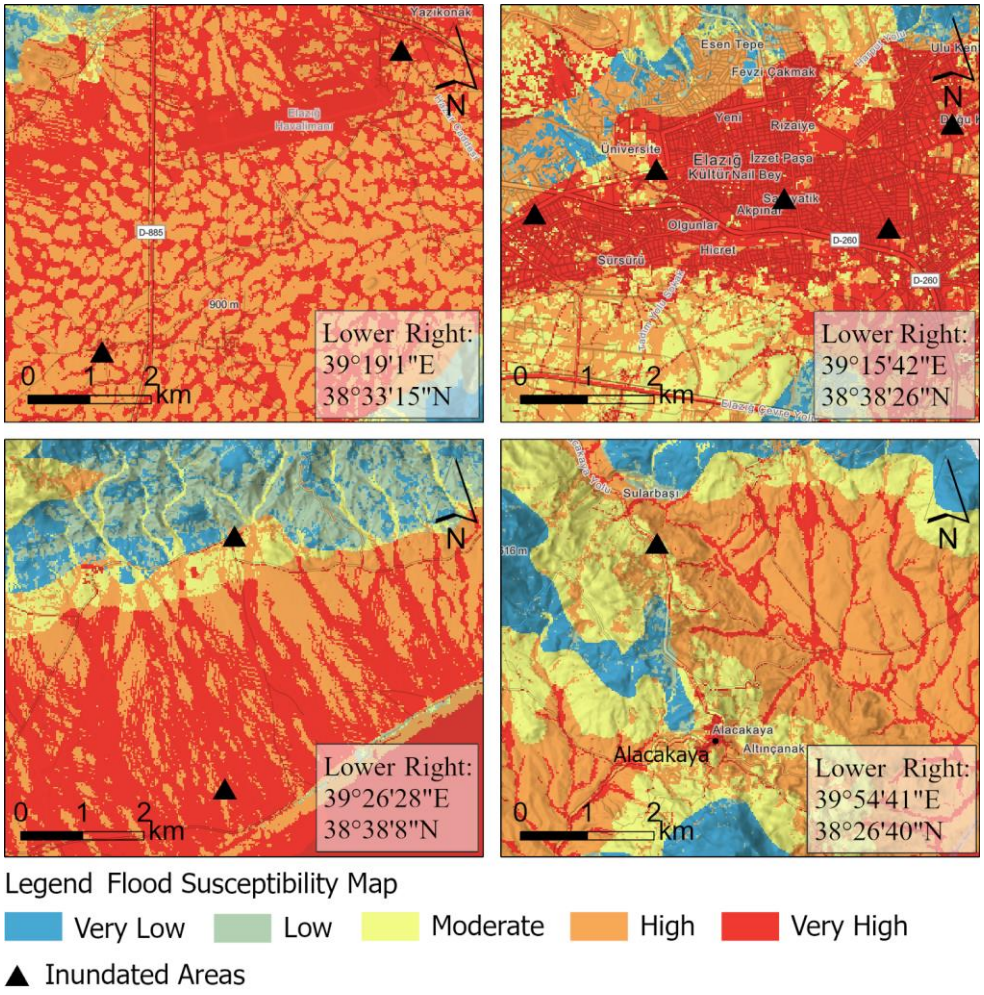

Figure 6.1. Inundated areas determined with the flood susceptibility map produced for the Elazig study site

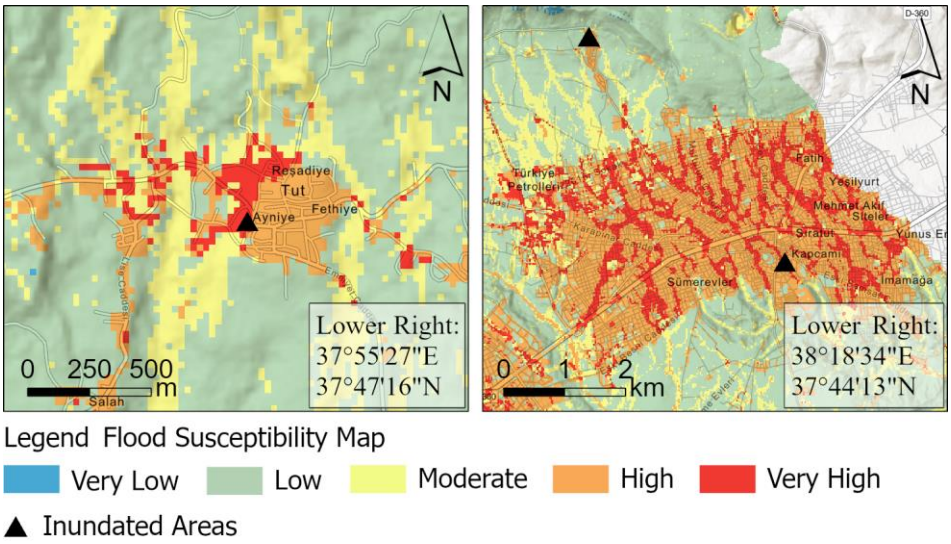

Figure 6.2. Inundated areas determined with the flood susceptibility map produced for the Adiyaman study site

In recent years, the Arias Intensity has become a popular choice for seismic hazard assessment studies, frequently used in producing seismic hazard maps [208], [80], [108]. As the parameter employed to evaluate the degree of earthquake shaking for landslide initiation, it is extensively utilized in the literature and was chosen for this thesis study.

In addition, in this thesis study, the study area was selected by delineating the basin boundaries. The univariate and multi-hazard susceptibility maps were produced and modeling was according to the basin boundaries. Modeling at the basin scale provides a holistic perspective necessary to fully understand flood and landslide risks and develop effective management strategies. Delineating the boundaries of the basin is important to understand how water is collected in this area and how it is drained. This helps determine water flow paths and flood risks. Additionally, it provides an understanding of geological features and formations as a whole.

6.3. Multi-hazard Susceptibility Map Production

In recent years, there has been a growing recognition of the significance of multi-hazard assessments in understanding natural hazards. This highlights the necessity for a more

inclusive approach [209], [110], [120]. Although there is a growing interest in the MHS modeling, communities concerned with the topic still perform independent assessments. Various methodologies have been employed to study multi-hazards globally in order to accomplish this [116]. Within the framework of this thesis, an approach that will facilitate the identification of regions that are under threat of more than one hazard (such as landslides, floods, and earthquakes) at the same time is proposed. This goal has been achieved by integrating machine learning and expert-based approach.

The utilization of the Mamdani FIS for the MHS assessment constituted a significant contribution to this thesis study. Producing a MHS map remains a very difficult task because of the complicated nature of different regions and the absence of ground truth data, which hinders the application of data-driven ML techniques. Typically, raster arithmetic operations or fundamental spatial analysis approaches, including accumulating the individual hazard levels per pixel, have been used to integrate univariate susceptibility maps in the literature [119], [114], [117], [120]. Ullah et al. [120] combined flash flood, landslide and debris flow hazard maps using addition arithmetic to produce MHS map. In each hazard map, low and moderate classes were reclassified by assigning 0 (low hazard) conditions and high and very high classes were assigned 1 (high hazard) conditions, and then combined. Pourghasemi et al. [119] and Bordbar et al. [1] also combined three hazard maps in the ArcGIS environment in their study.

In the thesis study, the utilization of Mamdani FIS through the establishment of rules for each specific hazard has significantly enhanced the sophistication level and usability of the resulting maps. However, the implementation of this methodology is not possible in just any desktop GIS program. It necessitates the use of specialized software and a certain level of expertise. Furthermore, as there are no generally acknowledged processes or standards, the rules and membership functions need to be defined by an expert with knowledge in the field. Additional applications and case studies would contribute to the expansion of knowledge, maybe resulting in the establishment of a standardized method. The resulting maps in Figures 5 and 14 demonstrate that a significant percentage of the study sites are prone to landslides, floods, and earthquakes. According to the MHS maps, no hazard affects around 37.77% and 51.47% of the Elazig and Adiyaman study sites,

respectively. The remaining 62.63% and 48.53% of the Elazig and Adiyaman study sites are susceptible to all three hazards, as shown in Tables 5.8 and 5.16.

Furthermore, a MHS model can provide greater utility compared to the univariate susceptibility maps when it comes to selecting sites for roadways, trains, settlements, and similar purposes. It provides authorities and policymakers with estimates of where to concentrate their efforts and respond after disasters, enabling them to have a more comprehensive understanding of how many hazards are likely to happen [210]. Additionally, the acquired MHS map can enhance the effectiveness of emergency response agencies in both the pre and post-disaster stages. The intuitive structure of the Mamdani FIS has emerged as an advantage in this study for MHS assessments. The system processes uncertain and variable natural disaster data, providing robust and comprehensible outputs under complex real-world conditions. However, the subjective decisions in system design and the computational intensity may impose limitations on the model's applicability. Therefore, in the application of Mamdani FIS, additional work is required to optimize the accuracy and performance of the model. The accuracy of the Mamdani fuzzy logic system is determined by the rule set's comprehensiveness and precision. Reviewing existing rules and extending them with new rules as needed can help to produce more accurate and precise results. To make the system more applicable to real-world situations, it is recommended to reevaluate and update the current set of rules based on expert feedback. The accuracy of the system's outputs is influenced by the configuration and characteristics of the membership functions. Optimizing these functions can improve the accuracy of the model. Experimental analysis can be performed to determine the most appropriate membership functions for each natural hazard and the shape of these functions can be optimized.

7. CONCLUSIONS AND FUTURE WORKS

This chapter, which is divided into two parts, includes the main findings of the thesis and comments on the limitations in the first section. In the second section, suggestions for future studies are given.

7.1. Conclusions

In recent years, the increasing frequency of natural hazards and the expectation of their continuation in the future emphasizes the critical importance of natural hazard research. Considering the devastating effects of landslides, floods and earthquakes, it can be seen that the damage caused by these hazards triggering each other is greater than the damage they cause alone. As such, assessing these hazards separately could not fairly depict the possible risks. It is essential and suitable to use a holistic and comprehensive approach that uses a multi-hazard assessment framework to investigate these interrelated hazards. This necessity forms the basis for the methodological approach and analyses conducted in this thesis, aiming to contribute effectively to disaster risk reduction strategies.

Considering the recent natural disasters in Türkiye, especially the devastating earthquakes in Kahramanmaraş occurred on 6 February 2023, the importance of assessing earthquake, flood and landslide hazards together becomes even more urgent. Turkiye has complex tectonic dynamics and geological structure due to its location on many active fault lines, especially the North and East Anatolian Fault Zone. This makes our country extremely vulnerable to earthquakes. Moreover, variable topography and climate conditions throughout the country cause frequent and severe floods and landslides, especially in regions with steep slopes and high rainfall intensity. As demonstrated by previous occurrences where earthquakes caused landslides and changed riverbeds, resulting in floods, these interrelated dangers can intensify one another. Therefore, it is of great

importance to integrate and evaluate these hazards by taking into account Türkiye's complex geological and hydrological dynamics.

In this thesis, a new approach that combines and evaluates these hazards in an area susceptible to landslide, flood and earthquake hazards was proposed. In selecting the study site, it was taken into consideration that it is susceptible to multi-hazards that trigger each other and is tectonically activated. The methodology proposed in the thesis was first applied to the Elazig study site due to the landslides triggered after the Elazig earthquake on January 24, 2020 and the frequent flooding in the region. Then, many provinces were affected by the February 6, 2023 Kahramanmaras earthquakes and numerous landslides were triggered. Due to the flood event that occurred as a result of heavy rainfalls in Adiyaman and Tut regions approximately one month after the earthquakes, the methodology proposed in the thesis was performed in the Adiyaman study site and the applicability of the method was proved.

The RF is a powerful algorithm for accurate and up-to-date LSM production. This algorithm has been proven to be effective, as a result of LSM production with 90% and 94% overall acuracy in the Elazig and Adiyaman study sites. The FSM was obtained by the M-AHP method since there was no suitable flood inventory. For the FSMs produced, a preliminary evaluation was made with the flood points that previously occurred in the study sites and it was determined that the FSMs were suitable. In addition, seismic hazard assessment of the study sites was obtained with maps produced using Arias Intensity values.

The univariate susceptibility maps were integrated using the Mamdani FIS to produce the MHSM, marking a novel instance in the literature. The FSM and MHSM were visually evaluated by the expert. The results showed that the suggested approach for the MHSA performed well, and it is recommended for use in future studies of a similar nature. The produced maps can be utilized by local authorities to identify regions susceptible to multi-hazards, strategize sustainable land utilization, choose suitable locations for engineering structures, and implement effective disaster management. In addition, this approach not only reflects a more comprehensive understanding of the risk landscape, but also

increases the effectiveness of disaster preparedness and mitigation strategies that are vital to protecting lives and infrastructure.

However, regional MHSA remains an extremely challenging problem, and data-driven techniques are nearly always ineffective in solving it. Therefore, a FIS based on expert knowledge was chosen. While the present study achieved good and promising results, there is still a considerable and challenging path ahead in producing MHS maps. It is necessary to conduct MHS assessment studies in various regions using diverse approaches in order to enhance the accuracy and dependability of these evaluations.

7.2. Future Works

Based on the results of the detailed literature review and the proposed multi-hazard assessment methodology within the scope of this thesis study, recommendations for future works are listed below.

- It could be recommended to track the long-term performance of the approach created in this study for MHS evaluation. This is essential to assess the efficacy of the methodology and adaptability over time. The monitoring and assessment process gives rise to a foundation for recognizing possible problems the methodology might run into over time and coming up with proactive remedies. Furthermore, scaling and generalization of the methodology allow it to be appropriate for wider applications and other geographies, therefore raising the total effectiveness of disaster risk management.

- It has been observed that there are some limitations in the use of data in such natural hazard assessment studies, and it is important to evaluate the existing data and their properties appropriately. It is recommended to use expert-based methods, especially in the production of flood susceptibility maps, due to the lack of inventory. Experts' field experience is important in increasing the realism and accuracy of the model. As experts may not always be available, flood areas can

be determined using pre-event and post-event satellite optical and radar data and a flood inventory can be created. Thus, flood susceptibility maps can be produced with data-driven methods. However, timeliness of the maps would be important. In addition, such inventories would be insufficient in areas with rugged topography as the drainage channels would not have any inundation.

- In future research, it is advisable to perform studies on natural hazard assessments with the aim of not only identifying the hazards themselves, but also assessing the specific elements at risk that are exposed to these hazards. Additionally, it would be beneficial to produce multi-hazard risk maps for a more comprehensive understanding. Understanding where and when risks might occur, as well as who or what structures might be impacted by them and how much of an impact, is part of such an evaluation. Consideration of elements at risk is especially important for risk mitigation strategies and emergency management planning. In disaster risk management, more comprehensive and informed decisions can be made, thus achieving more effective results in both protecting human life and minimizing economic losses. Future works may aim to develop methodologies and tools to analyze these at-risk elements in more detail and develop strategies accordingly.

- To enhance the effectiveness of this methodology, it is recommended to incorporate an early warning system in future works. Data from existing susceptibility models should be integrated with real-time observation data. The early warning system will contribute to reducing the damages before and during the disaster by providing early detection of hazards and rapid intervention.

- The results obtained from the thesis can be converted into regional base maps and made available to users. Such data can be quickly integrated into various analysis and processing techniques, saving time and resources and allowing users to work with the data more effectively. Such base maps can support fast and effective decision-making in disaster management and planning processes.

8. REFERENCES

[1] M. Bordbar, H. Aghamohammadi, H.R. Pourghasemi and Z. Azizi, Multi-hazard spatial modeling via ensembles of machine learning and meta-heuristic techniques, Sci Rep *12*, 1451, **2022**.

[2] IAEG Commission on Landslides. Suggested nomenclature for landslides. Bulletin of the International Association of Engineering Geology, 41, p:13–16, **1990**.

[3] IPCC, Global Warming of 1.5°C. An IPCC Special Report on the impacts of global warming of 1.5°C above pre-industrial levels and related global greenhouse gas emission pathways, in the context of strengthening the global response to the threat of climate change, sustainable development, and reorts to eradicate poverty. **2018**.

[4] AFAD Açıklamalı Afet Terimleri Sözlüğü, https://www.afad.gov.tr/aciklamali-afet-yonetimi-terimleri-sozlugu, Last Access: 27 April 2024.

[5] AFAD, Afet Yönetimi Kapsamında 2019 Yılına Bakış ve Doğa Kaynaklı Olay İstatistikleri, **2020**.

[6] AFAD, Afet İstatistikleri, https://www.afad.gov.tr/afet-istatistikleri, Last Access: 27 April 2024.

[7] UN SDGs, **2020**. Global indicator framework for theSustainable Development Goals and targets of the 2030 Agendafor Sustainable Development. Technical report,https://unstats.un.org/sdgs/indicators/Global%20Indicator%20Framework%20after%202020%20review_Eng.pdf, Last Access: 27 April 2024.

[8] UN, Environment Program, https://www.un.org/en/conferences/environment, Last Access: 27 April 2024.

[9] A. Carrara, G. Crosta, and P. Frattini, Comparing models of debris-flow susceptibility in the alpine environment, Geomorphology, 94(3):p. 353-378, **2008.**

[10] Z. Xie, G. Chen, X. Meng, Y, Zhang, L. Qiao, and L. Tan, A comparative study of landslide susceptibility mapping using weight of evidence, logistic regression and support vector machine and evaluated by SBAS-InSAR monitoring: Zhouqu to Wudu segment in Bailong River Basin, China, Environmental Earth Sciences, 76(8):p. 313, **2017.**

[11] X.Yang, R. Liu, M. Yang, J. Chen, T. Liu, Y. Yang, W. Chen, Y. Wang, Incorporating Landslide Spatial Information and Correlated Features among

Conditioning Factors for Landslide Susceptibility Mapping, Remote Sensing, 13, **2021**.

[12] T. Lewandowski, and K. Pawluszek-Filipiak, Landslide susceptibility mapping by using various selection strategies of landslide conditioning factors and XGBoost, EGU General Assembly 2022, Vienna, Austria, 23–27 May 2022, EGU22-12676, **2022.**

[13] S. R. Meena, S. Puliero, K. Bhuyan, M. Floris, and F. Catani, Assessing the importance of conditioning factor selection in landslide susceptibility for the province of Belluno (region of Veneto, northeastern Italy), Natural Hazards Earth System Science, 22(4):p.1395–1417, **2022**.

[14] S. B. Gazibara, M. Sinčić, M. Krkač, H. Lukačić and S. M. Arbanas, Landslide susceptibility assessment on a large scale in the Podsljeme area, City of Zagreb (Croatia). Journal of Maps, 19(1):p. 1-11, **2023.**

[15] S. Wang, S. Ling, X. Wu, H. Wen, J. Huang, F. Wang and C. Sun, Key predisposing factors and susceptibility assessment of landslides along the Yunnan–Tibet traffic corridor, Tibetan plateau: Comparison with the LR, RF, NB, and MLP techniques, *Frontiers in Earth Science, 10:*1100363, **2023**.

[16] E. Bravo-López, T. Fernández Del Castillo, C. Sellers, J. Delgado-García, Analysis of Conditioning Factors in Cuenca, Ecuador, for Landslide Susceptibility Maps Generation Employing Machine Learning Methods. Land. 12(6): p. 1135, **2023**.

[17] P. Reichenbach, M. Rossi, B. D. Malamud, M. Mihir, F. Guzzetti, A review of statistically-based landslide susceptibility models. *Earth-Science Reviews*. 180: p. 60-91, **2018**.

[18] C. Gokceoglu, and E. Sezer, A statistical assessment on international landslide literature (1945–2008). Landslides. 6(4): p. 345, **2009.**

[19] C.J. van Westen, D. Alkema, M.C.J. Damen, N. Kerle, N.C. Kingma, Multi-hazard risk assessment : Distance education course : Exercise book. International Institute for Geo-Information Science and Earth Observation, **2011**.

[20] J. Corominas, C.J. van Westen, P. Frattini, L. Cascini, J.-P. Malet, S. Fotopoulou, F. Catani, M. Van Den Eeckhaut, O. Mavrouli, F. Agliardi, K. Pitilakis, M. G. Winter, M. Pastor, S. Ferlisi, V. Tofani, J. Hervás and J. T. Smith, Recommendations for the quantitative analysis of landslide risk. Bulletin of Engineering Geology and the Environment, 73(2): p. 209-263, **2014.**

[21] R. Soeters, and C.J. van Westen, Slope instability Recognition, analysis and zonation. In: Turner, A.K., Schuster, R.L. (Eds.), Landslide: Investigations and Mitigation. Special Report, vol. 247. Transportation Research Board, National Research Council, National Academy Press, Washington, *D.C.*: p. 129–17, **1996.**

[22] F. Guzzetti, A. Carrara, M. Cardinali, P. Reichenbach, Landslide hazard evaluation: a review of current techniques and their application in a multi-scale study, Central Italy. Geomorphology. 31(1): p. 181-216, **1999.**

[23] F.C. Dai, C.F. Lee, and Y.Y. Ngai, Landslide risk assessment and management: an overview. Engineering Geology. 64(1): p. 65-87, **2002.**

[24] R. Fell, J. Corominas, C. Bonnard, L. Cascini, E. Leroi, and W. Z. Savage, Guidelines for landslide susceptibility, hazard and risk zoning for land use planning. Engineering Geology. 102(3): p. 85-98, **2008.**

[25] J.L. Zêzere, S. Pereira, R. Melo, S.C. Oliveira, R.A.C. Garcia, Mapping landslide susceptibility using data-driven methods, Science of The Total Environment. 589: p. 250-267, **2017.**

[26] I. Yilmaz, Landslide susceptibility mapping using frequency ratio, logistic regression, artificial neural networks and their comparison: A case study from Kat landslides (Tokat—Turkey). Computers & Geosciences. 35(6): p. 1125-1138, **2009.**

[27] M. Kannan, E. Saranathan, and R. Anabalagan, Landslide vulnerability mapping using frequency ratio model: a geospatial approach in Bodi-Bodimettu Ghat section, Theni district, Tamil Nadu, India. Arabian Journal of Geosciences. 6(8): p. 2901-2913, **2013.**

[28] Y. Yi, Z. Zhang, W. Zhang, Q. Xu, C. Deng, and Q. Li, GIS-based earthquake-triggered-landslide susceptibility mapping with an integrated weighted index model in Jiuzhaigou region of Sichuan Province, China. Nat. Hazards Earth Syst. Sci. 19(9): p. 1973-1988, **2019.**

[29] H.R. Pourghasemi, B. Pradhan, and C. Gokceoglu, Application of fuzzy logic and analytical hierarchy process (AHP) to landslide susceptibility mapping at Haraz watershed, Iran. Natural Hazards. 63(2): p. 965-996, **2012.**

[30] P. Kayastha, S.M.Bijukchhen, M.R.Dhital, and F.D. Smedt, GIS based landslide susceptibility mapping using a fuzzy logic approach: A case study from Ghurmi-Dhad Khola area, Eastern Nepal. Journal of the Geological Society of India. 82(3): p. 249-261, **2013.**

[31] Z.A. Rostami, S. Al-modaresi, H. Fathizad, and M. Faramarzi Landslide susceptibility mapping by using fuzzy logic: a case study of Cham-gardalan catchment, Ilam, Iran. Arabian Journal of Geosciences. 9(17): p. 685, **2016.**

[32] Y. Thiery, J.P. Malet, S. Sterlacchini, A. Puissant, O. Maquaire, Landslide susceptibility assessment by bivariate methods at large scales: Application to a complex mountainous environment. Geomorphology. 92(1): p. 38-59, **2007.**

[33] R.K. Dahal, S. Hasegawa, A. Nonomura, M. Yamanaka, T. Masuda and K. Nishino, GIS-based weights-of-evidence modelling of rainfall-induced landslides

in small catchments for landslide susceptibility mapping. Environmental Geology. 54(2): p. 311-324, **2008.**

[34] P. Kayastha, M.R. Dhital, and F. De Smedt, Landslide susceptibility mapping using the weight of evidence method in the Tinau watershed, Nepal. Natural Hazards. 63(2): p. 479-498, **2012.**

[35] Q. Wang, D. Wang, Y. Huang, Z. Wang, L. Zhang, Q. Guo, W. Chen, W. Chen, M. Sang, Landslide Susceptibility Mapping Based on Selected Optimal Combination of Landslide Predisposing Factors in a Large Catchment. Sustainability. 7(12): p. 16653-16669, **2015.**

[36] R. Zine El Abidine, and N. Abdelmansour, Landslide susceptibility mapping using information value and frequency ratio for the Arzew sector (North-Western of Algeria). Bulletin of the Mineral Research and Exploration. 160(160): p. 197-211, **2019.**

[37] M.H. Tangestani, A comparative study of Dempster–Shafer and fuzzy models for landslide susceptibility mapping using a GIS: An experience from Zagros Mountains, SW Iran. Journal of Asian Earth Sciences. 35(1): p. 66-73, **2009.**

[38] N.W. Park, Application of Dempster-Shafer theory of evidence to GIS-based landslide susceptibility analysis. Environmental Earth Sciences. 62(2): p. 367-376, **2011.**

[39] M. Mohammady, H.R. Pourghasemi, and B. Pradhan, Landslide susceptibility mapping at Golestan Province, Iran: A comparison between frequency ratio, Dempster–Shafer, and weights-of-evidence models. Journal of Asian Earth Sciences. 61: p. 221-236, **2012.**

[40] S. Lee, and J.A. Talib, Probabilistic landslide susceptibility and factor effect analysis. Environmental Geology. 47(7): p. 982-990, **2005.**

[41] L.J. Wang, K. Sawada, and S. Moriguchi, Landslide susceptibility analysis with logistic regression model based on FCM sampling strategy. Computers & Geosciences. 57: p. 81-92, **2013.**

[42] L. Ermini, F. Catani, and N. Casagli, Artificial Neural Networks applied to landslide susceptibility assessment. Geomorphology. 66(1): p. 327-343, **2005.**

[43] M. Marjanović, M. Kovačević, B. Bajat, V. Voženílek, Landslide susceptibility assessment using SVM machine learning algorithm. Engineering Geology. 123(3): p. 225-234, **2011.**

[44] A.M. Youssef, H.R. Pourghasemi, Z.S. Pourtaghi, and M. M. Al-Katheeri, Landslide susceptibility mapping using random forest, boosted regression tree, classification and regression tree, and general linear models and comparison of their performance at Wadi Tayyah Basin, Asir Region, Saudi Arabia. Landslides. 13(5): p. 839-856, **2016.**

[45] L.L. Liu, J. Zhang, J.Z. Li, F. Huang, and L.C. Wang, A bibliometric analysis of the landslide susceptibility research (1999–2021). Geocarto International, 37(26):p. 14309-14334, **2022.**

[46] P. Lima, S. Steger, T. Glade, and F.G. Murillo-García, Literature review and bibliometric analysis on data-driven assessment of landslide susceptibility. Journal of Mountain Science. 19(6): p. 1670-1698, **2022.**

[47] H.A. Nefeslioglu, E. Sezer,C. Gokceoglu, S. Bozkir and T. Y. Duman, Assessment of Landslide Susceptibility by Decision Trees in the Metropolitan Area of Istanbul, Turkey. Mathematical Problems in Engineering. 2010: p. 901095, **2010.**

[48] E. Sevgen, S. Kocaman, H.A. Nefeslioglu, and C. Gokceoglu, A Novel Performance Assessment Approach Using Photogrammetric Techniques for Landslide Susceptibility Mapping with Logistic Regression, ANN and Random Forest. Sensors, **2019**.

[49] T. Yanar, S. Kocaman, and C. Gokceoglu Use of Mamdani Fuzzy Algorithm for Multi-Hazard Susceptibility Assessment in a Developing Urban Settlement (Mamak, Ankara, Turkey). ISPRS International Journal of Geo-Information, **2020**.

[50] G. Karakas, R. Can, S. Kocaman, H. A. Nefeslioglu, and C. Gokceoglu, Landslide Susceptibility Mapping With Random Forest Model For Ordu, Turkey. Int. Arch. Photogramm. Remote Sens. Spatial Inf. Sci. XLIII-B3-2020: p. 1229-1236, **2020.**

[51] Z. Wang, Q. Liu, and Y. Liu Mapping Landslide Susceptibility Using Machine Learning Algorithms and GIS: A Case Study in Shexian County, Anhui Province, China. Symmetry, **2020**.

[52] D. Sun, H. Wen, D. Wang, J. Xu, A random forest model of landslide susceptibility mapping based on hyperparameter optimization using Bayes algorithm. Geomorphology. 362: p. 107201, **2020.**

[53] P. Sajadi, Y.F. Sang, M. Gholamnia, S. Bonafoni and S. Mukherjee, Evaluation of the landslide susceptibility and its spatial difference in the whole Qinghai-Tibetan Plateau region by five learning algorithms. Geoscience Letters. 9(1): p. 9, **2022.**

[54] B. Pradhan, A comparative study on the predictive ability of the decision tree, support vector machine and neuro-fuzzy models in landslide susceptibility mapping using GIS. Computers & Geosciences. 51: p. 350-365, **2013.**

[55] C. Colesanti, and J. Wasowski, Investigating landslides with space-borne Synthetic Aperture Radar (SAR) interferometry. Engineering Geology. 88(3): p. 173-199, **2006.**

[56] F. Weirich, and L. Blesius, Comparison of satellite and air photo based landslide susceptibility maps. Geomorphology. 87(4): p. 352-364, **2007.**

[57] M. Jaboyedoff, T. Oppikofer, A. Abellán, M.H. Derron, A. Loye, R. Metzger and A. Pedrazzini, Use of LIDAR in landslide investigations: a review. Natural Hazards. 61(1): p. 5-28, **2012.**

[58] W. Chen, X. Li, Yanxin Wang, Gang Chen, Shengwei Liu, Forested landslide detection using LiDAR data and the random forest algorithm: A case study of the Three Gorges, China. Remote Sensing of Environment. 152: p. 291-301, **2014.**

[59] G. Karakas, S. Kocaman, and C. Gokceoglu, Aerial Photogrammetry and Machine Learning Based Regional Landslide Susceptibility Assessment For an Earthquake Prone Area In Turkey. Int. Arch. Photogramm. Remote Sens. Spatial Inf. Sci. XLIII-B3-2021: p. 713-720, **2021**.

[60] L. Nava, K. Bhuyan, S.R. Meena, O. Monserrat, and F. Catani, Rapid Mapping of Landslides on SAR Data by Attention U-Net. Remote Sensing, **2022**.

[61] M. Ercanoglu, O. Kasmer, and N. Temiz, Adaptation and comparison of expert opinion to analytical hierarchy process for landslide susceptibility mapping. Bulletin of Engineering Geology and the Environment. 67(4): p. 565-578, **2008.**

[62] H. Pourghasemi, B. Pradhan, C. Gokceoglu, and K.D. Moezzi, A comparative assessment of prediction capabilities of Dempster–Shafer and Weights-of-evidence models in landslide susceptibility mapping using GIS. Geomatics, Natural Hazards and Risk. 4(2): p. 93-118, **2013.**

[63] H.A. Nefeslioglu, E.A. Sezer, C. Gokceoglu and Z. Ayas, A modified analytical hierarchy process (M-AHP) approach for decision support systems in natural hazard assessments. Computers & Geosciences. 59: p. 1-8, **2013.**

[64] E. Sharifi Teshnizi, M. Golian, S. Sadeghi, and A. Rastegarnia, Chapter 4 - Application of analytical hierarchy process (AHP) in landslide susceptibility mapping for Qazvin province, N Iran, in Computers in Earth and Environmental Sciences, H.R. Pourghasemi, Editor. 2022, Elsevier. p. 55-95.

[65] C. Gokceoglu, H. Sonmez, H.A. Nefeslioglu, T.Y. Duman, and T. Can, The 17 March 2005 Kuzulu landslide (Sivas, Turkey) and landslide-susceptibility map of its near vicinity. Engineering Geology. 81(1): p. 65-83, **2005**.

[66] H.A. Nefeslioglu, and C. Gokceoglu, Probabilistic Risk Assessment in Medium Scale for Rainfall-Induced Earthflows: Catakli Catchment Area (Cayeli, Rize, Turkey). Mathematical Problems in Engineering. 2011: p. 280431, **2011.**

[67] S. Lari, P. Frattini, and G.B. Crosta, A probabilistic approach for landslide hazard analysis. Engineering Geology. 182: p. 3-14, **2014.**

[68] L.J. Wang, M. Guo, K. Sawada, J. Lin, and J. Zhang, A comparative study of landslide susceptibility maps using logistic regression, frequency ratio, decision tree, weights of evidence and artificial neural network. Geosciences Journal. 20(1): p. 117-136, **2016.**

[69] R. Can, S. Kocaman, and C. Gokceoglu, A Comprehensive Assessment of XGBoost Algorithm for Landslide Susceptibility Mapping in the Upper Basin of Ataturk Dam, Turkey. Applied Sciences. 11(11), **2021.**

[70] G. Karakas, S. Kocaman, and C. Gokceoglu, Comprehensive performance assessment of landslide susceptibility mapping with MLP and random forest: a case study after Elazig earthquake (24 Jan 2020, Mw 6.8), Turkey. Environmental Earth Sciences. 81(5): p. 144, **2022.**

[71] G. Karakas, H.A. Nefeslioglu, S. Kocaman, M. Buyukdemircioglu, T. Yurur and C. Gokceoglu, Derivation of earthquake-induced landslide distribution using aerial photogrammetry: the January 24, 2020, Elazig (Turkey) earthquake. Landslides. 18(6): p. 2193-2209, **2021.**

[72] G. Karakas, S. Kocaman, and C. Gokceoglu, Multi-Hazard Susceptibility Assessment With Hybrid Machine Learning Methods For Tut Region (Adiyaman, Türkiye). Int. Arch. Photogramm. Remote Sens. Spatial Inf. Sci. XLVIII-M-1-2023: p. 529-536, **2023.**

[73] G. Karakas, E.O. Unal, S. Cetinkaya, N. Tunar Ozcan, V.E. Karakas, R. Can, C. Gokceoglu and S. Kocaman, Analysis of landslide susceptibility prediction accuracy with an event-based inventory: The 6 February 2023 Turkiye earthquakes. Soil Dynamics and Earthquake Engineering. 178: p. 108491, **2024.**

[74] A. Merghadi, A. P. Yunus, J. Dou, J. Whiteley, B. ThaiPham, D.T. Bui, R. Avtar and B. Abderrahmane, Machine learning methods for landslide susceptibility studies: A comparative overview of algorithm performance. Earth-Science Reviews. 207: p. 103225, **2020.**

[75] S. Wang, J. Zhuang, J. Zheng, H. Fan, J. Kong and J. Zhan, Application of Bayesian Hyperparameter Optimized Random Forest and XGBoost Model for Landslide Susceptibility Mapping. FRONTIERS IN EARTH SCIENCE. 9, **2021.**

[76] M. Kamal, B. Zhang, J. Cao, X. Zhang, and J. Chang, Comparative Study of Artificial Neural Network and Random Forest Model for Susceptibility Assessment of Landslides Induced by Earthquake in the Western Sichuan Plateau, China. Sustainability, 14, **2022**.

[77] L. Derin, Parameters and methods used in flood susceptibility mapping: a review. Journal of Water and Climate Change. 14, **2023.**

[78] J. Malczewski, GIS and Multicriteria Decision Analysis. 1999: John Wiley & Sons.

[79] S. Das, Geographic information system and AHP-based flood hazard zonation of Vaitarna basin, Maharashtra, India. Arabian Journal of Geosciences. 11(19): p. 576, **2018.**

[80] H.D. Skilodimou, G.D. Bathrellos, K. Chousianitis, A.M. Youssef, and B. Pradhan, Multi-hazard assessment modeling via multi-criteria analysis and GIS: a case study. Environmental Earth Sciences. 78(2): p. 47, **2019.**

[81] A. Wubalem, G. Tesfaw, Z. Dawit, B. Getahun, T. Mekuria, and M. Jothimani, Comparison of statistical and analytical hierarchy process methods on flood susceptibility mapping: In a case study of the Lake Tana sub-basin in northwestern Ethiopia. Open Geosciences. 13(1): p. 1668-1688, **2021.**

[82] S. Bera, A. Das, and T. Mazumder, Evaluation of machine learning, information theory and multi-criteria decision analysis methods for flood susceptibility mapping under varying spatial scale of analyses. Remote Sensing Applications: Society and Environment. 25: p. 100686, **2022.**

[83] U.L. Dano, A.L. Balogun, A.N. Matori, K. Wan Yusouf, I.R. Abubakar, M.A. Said Mohamed, Y.A. Aina, and B. Pradhan, Flood Susceptibility Mapping Using GIS-Based Analytic Network Process: A Case Study of Perlis, Malaysia. Water. 11(3): p. 615, **2019.**

[84] P. Yariyan, M. Avand, R.A. Abbaspour, A. Torabi Haghighi, R. Costache, O. Ghorbanzadeh, S. Janizadeh and T. Blaschke, Flood susceptibility mapping using an improved analytic network process with statistical models. Geomatics, Natural Hazards and Risk. 11(1): p. 2282-2314, **2020.**

[85] Z. Tang, S. Yi, C. Wang, and Y. Xiao, Incorporating probabilistic approach into local multi-criteria decision analysis for flood susceptibility assessment. Stochastic Environmental Research and Risk Assessment. 32(3): p. 701-714, **2018.**

[86] S. Stavropoulos, G.N. Zaimes, E. Filippidis, D.C. Diaconu, D. Emmanouloudis, Mitigating Flash Floods With The Use Of New Technologies: A Multi-Criteria Decision Analysis To Map Flood Susceptibility For Zakynthos Island, Greece. Journal of Urban and Regional Analysis. 12, **2020.**

[87] D. Chaulagain, P.R. Rimal, S.N. Ngando, B.E.K. Nsafon, D. Suh, J.S. Huh, Flood susceptibility mapping of Kathmandu metropolitan city using GIS-based multi-criteria decision analysis. Ecological Indicators. 154: p. 110653, **2023.**

[88] Y. Wang, H. Hong, W. Chen,S. Li, D. Pamučar, L. Gigović, S. Drobnjak, D.Tien Bui, H. Duan, A Hybrid GIS Multi-Criteria Decision-Making Method for Flood Susceptibility Mapping at Shangyou, China. Remote Sensing. 11(1): p. 62, **2019.**

[89] K.C. Swain, C. Singha, and L. Nayak, Flood Susceptibility Mapping through the GIS-AHP Technique Using the Cloud. ISPRS International Journal of Geo-Information. 9(12): p. 720, **2020.**

[90] S.V. Razavi Termeh, A. Kornejady, H.R. Pourghasemi, and S. Keesstra, Flood susceptibility mapping using novel ensembles of adaptive neuro fuzzy inference system and metaheuristic algorithms. Science of The Total Environment. 615: p. 438-451, **2018.**

[91] M. Sahana, and P.P. Patel, A comparison of frequency ratio and fuzzy logic models for flood susceptibility assessment of the lower Kosi River Basin in India. Environmental Earth Sciences. 78(10): p. 289, **2019.**

[92] M. Sepehri, H. Malekinezhad, F. Jahanbakhshi, A.R. Ildoromi, J. Chezgi, O. Ghorbanzadeh and E. Naghipour, Integration of interval rough AHP and fuzzy logic for assessment of flood prone areas at the regional scale. Acta geophysica. 68: p. 477-493, **2020.**

[93] M.S. Tehrany, B. Pradhan, and M.N. Jebur, Spatial prediction of flood susceptible areas using rule based decision tree (DT) and a novel ensemble bivariate and multivariate statistical models in GIS. Journal of hydrology. 504: p. 69-79, **2013.**

[94] K. Khosravi, B.T. Pham, K. Chapi, A. Shirzadi, H. Shahabi, I. Revhaug, I. Prakash, and D. Tien Bui, A comparative assessment of decision trees algorithms for flash flood susceptibility modeling at Haraz watershed, northern Iran. Science of The Total Environment. 627: p. 744-755, **2018.**

[95] M.S. Tehrany, M.J. Lee, B. Pradhan, M.N. Jebur, and S. Lee, Flood susceptibility mapping using integrated bivariate and multivariate statistical models. Environmental earth sciences. 72: p. 4001-4015, **2014.**

[96] K. Chapi, V.P. Singh, A. Shirzadi, H. Shahabi, D.T. Bui, B.T. Pham, K. Khosravi, A novel hybrid artificial intelligence approach for flood susceptibility assessment. Environmental modelling & software. 95: p. 229-245, **2017.**

[97] K. Ullah, and J. Zhang, GIS-based flood hazard mapping using relative frequency ratio method: A case study of Panjkora River Basin, eastern Hindu Kush, Pakistan. PLOS ONE. 15: p. e0229153, **2020.**

[98] S. Lee, J.C. Kim, H.S. Jung, M.J. Lee, and S. Lee, Spatial prediction of flood susceptibility using random-forest and boosted-tree models in Seoul metropolitan city, Korea. Geomatics, Natural Hazards and Risk. 8(2): p. 1185-1203, **2017**.

[99] W. Chen, Y. Li, W. Xue, H. Shahabi, S. Li, H. Hong, X. Wang, H. Bian, S. Zhang, B. Pradhan, B.B. Ahmad, Modeling flood susceptibility using data-driven approaches of naïve Bayes tree, alternating decision tree, and random forest methods. Science of The Total Environment. 701, **2019.**

[100] Tien Bui, D., K. Khosravi, S. Li, H. Shahabi, M. Panahi, V.P. Singh, K. Chapi, A. Shirzadi, S. Panahi, W. Chen, B.B. Ahmad, New Hybrids of ANFIS with Several Optimization Algorithms for Flood Susceptibility Modeling. Water. 10(9): p. 1210, **2018.**

[101] H. Hong, , P. Tsangaratos, I. Ilia, J. Liu, A.X. Zhu, and W. Chen, Application of fuzzy weight of evidence and data mining techniques in construction of flood susceptibility map of Poyang County, China. Science of the total environment. 625: p. 575-588, **2018.**

[102] B. Sozer, S. Kocaman, H.A. Nefeslioglu, O. Firat, and C. Gokceoglu, Preliminary Investigations On Flood Susceptibility Mapping In Ankara (Turkey) Using Modified Analytical Hierarchy Process (M-AHP). Int. Arch. Photogramm. Remote Sens. Spatial Inf. Sci. XLII-5: p. 361-365, **2018.**

[103] T. Yanar, S. Kocaman, and C. Gokceoglu, Use of Mamdani Fuzzy Algorithm for Multi-Hazard Susceptibility Assessment in a Developing Urban Settlement (Mamak, Ankara, Turkey). ISPRS International Journal of Geo-Information. 9(2), **2020.**

[104] M. Alpyürür, and M.A. Lav, An assessment of probabilistic seismic hazard for the cities in Southwest Turkey using historical and instrumental earthquake catalogs. Natural Hazards. 114(1): p. 335-365, **2022.**

[105] C.A. Cornell, Engineering Seismic Risk Analysis. Bulletin of the Seismological Society of America. 58: p. 1583-1606, **1968.**

[106] M. Erdik, Y. A. Biro, T. Onur, K. Sesetyan, and G. Birgoren, Assessment of earthquake hazard in Turkey and neighboring, **1999.**

[107] G.Ç. İnce, and M.U. Yılmazoğlu, Probabilistic seismic hazard assessment of Muğla, Turkey. Natural Hazards. 107(2): p. 1311-1340, **2021.**

[108] K. Gupta, and N. Satyam, Estimation of Arias intensity and peak ground acceleration (PGA) using probabilistic seismic hazard assessment of Uttarakhand state (India). Arabian Journal of Geosciences. 15(5): p. 437, **2022.**

[109] A. Mukhopadhyay, S. Hazra, D. Mitra, C. Hutton, A. Chanda and S. Mukherjee, Characterizing the multi-risk with respect to plausible natural hazards in the Balasore coast, Odisha, India: a multi-criteria analysis (MCA) appraisal. Natural Hazards. 80(3): p. 1495-1513, **2016.**

[110] S.K. Aksha, L.M. Resler, L. Juran, and L.W. Carstensen, A geospatial analysis of multi-hazard risk in Dharan, Nepal. Geomatics, Natural Hazards and Risk. 11(1): p. 88-111, **2020.**

[111] Khatakho, R., D. Gautam, K.R. Aryal, V.P. Pandey, R. Rupakhety, S. Lamichhane, Y.C. Liu, K. Abdouli, R. Talchabhadel, B.R. Thapa, and R. Adhikari, Multi-Hazard Risk Assessment of Kathmandu Valley, Nepal. Sustainability. 13(10): p. 5369, **2021.**

[112] A. Rehman, J. Song, F. Haq, S. Mahmood, M.I. Ahamad, M. Basharat, M. Sajid, M.S. Mehmood, Multi-Hazard Susceptibility Assessment Using the Analytical Hierarchy Process and Frequency Ratio Techniques in the Northwest Himalayas, Pakistan. Remote Sensing. 14, **2022.**

[113] K. Liu, M. Wang, Y. Cao, W. Zhu, and G. Yang, Susceptibility of existing and planned Chinese railway system subjected to rainfall-induced multi-hazards. Transportation Research Part A: Policy and Practice. 117: p. 214-226, **2018**.

[114] H.R. Pourghasemi, N. Kariminejad, M. Amiri, M. Edalat, M. Zarafshar, T. Blaschke and A. Cerda, Assessing and mapping multi-hazard risk susceptibility using a machine learning technique. Scientific Reports. 10(1): p. 3203, **2020.**

[115] S. Yousefi, H.R. Pourghasemi, S.N. Emami, S. Pouyan, S. Eskandari and J.P. Tiefenbacher, A machine learning framework for multi-hazards modeling and mapping in a mountainous area. Scientific Reports. 10(1): p. 12144, **2020.**

[116] J N. Javidan, A. Kavian, H.R. Pourghasemi, C. Conoscenti, Z. Jafarian and J. Rodrigo-Comino, Evaluation of multi-hazard map produced using MaxEnt machine learning technique. Scientific Reports. 11(1): p. 6496, **2021.**

[117] S. Pouyan, H.R. Pourghasemi, M. Bordbar, S. Rahmanian and J.J. Clague, A multi-hazard map-based flooding, gully erosion, forest fires, and earthquakes in Iran. Scientific Reports. 11(1): p. 14889, **2021.**

[118] A.M. Youssef, A.M. Mahdi, M.M. Al-Katheri, S. Pouyan, H.R. Pourghasemi, Multi-hazards (landslides, floods, and gully erosion) modeling and mapping using machine learning algorithms. Journal of African Earth Sciences. 197: p. 104788, **2023.**

[119] H.R. Pourghasemi, A. Gayen, M. Panahi, F. Rezaie and T. Blaschke, Multi-hazard probability assessment and mapping in Iran. Science of The Total Environment. 692: p. 556-571, **2019.**

[120] K. Ullah, Y. Wang, Z. Fang, L. Wang, and M. Rahman, Multi-hazard susceptibility mapping based on Convolutional Neural Networks. Geoscience Frontiers,13(5), **2022.**

[121] CLMS (Copernicus Land Monitoring Service), https://land.copernicus.eu. Last Access: 3 Janunary 2023.

[122] MGM (Meteoroloji Genel Müdürlüğü / Turkish State Meteorological Service). 2022. Official statistics. https://mgm.gov.tr/veridegerlendirme/il-ve-ilceler-istatistik.aspx. Last Access: 15 October 2023

[123] Worldwide land cover mapping: VITO NV.2021, https://esa-worldcover.org/en., Last Access: 24 April 2024.

[124] G. Karakas, S. Kocaman, and C. Gokceoglu, A Hybrid Multi-Hazard Susceptibility Assessment Model for a Basin in Elazig Province, Türkiye. International Journal of Disaster Risk Science. 14(2): p. 326-341, **2023.**

[125] A.Vedat, and M. Sunkar, The relationship of landslides with lithological units and fault lines occurring on the East Anatolian Fault Zone, between Palu (Elazığ) and Bingöl, Turkey. Bulletin of the Mineral Research and Exploration. 157(157): p. 23-38, **2018.**

[126] AFAD, Report on the 24 January 2020 Sivrice (Elazig) Earthquake, p. 47, **2020.**

[127] METU, Elazig-Sivrice earthquake site observations of seismic and structural damage (24 January 2020 Mw 6.8) (24 Ocak 2020 Mw 6.8 Elazığ-Sivrice Depremi Sismik ve Yapısal Hasara İlişkin Saha Gözlemleri. Rapor No: ODTÜ/DMAM 2020-01). **2020**.

[128] E. Herece, 1/100.000 scale Turkish geological maps, K-42 Quadrangle. Publication of General Directorate of Mineral Research and Exploration, No:234, **2016**.

[129] M. Sümengen, 1/100.000 scale Turkish geological maps, K-43 Quadrangle. Publication of General Directorate of Mineral Research and Exploration, No:1*72*, **2011**.

[130] B. Akbaş et. al., 1/100.000 scale Turkish geological maps, L-41 Quadrangle. Publication of General Directorate of Mineral Research and Exploration, No:169,**2016**.

[131] İ. Keskin, 1/100.000 scale Turkish geological maps L-42 Quadrangle. Publication of General Directorate of Mineral Research and Exploration, No:170, **2011**.

[132] İ. Keskin, 1/100.000 scale Turkish geological maps L-43 Quadrangle. Publication of General Directorate of Mineral Research and Exploration No:171, **2011**.

[133] MTA, 24 Ocak 2020 Sivrice (Elazığ) Depremi (Mw=6,8) Saha Gözlemleri Ve Değerlendirme Raporu, p. 48, **2020**.

[134] C.Gokceoglu, M.T. Yurur, S. Kocaman, H.A. Nefeslioglu, M. Durmaz, B. Tavus, G. Karakas, M. Buyukdemircioglu, K. Atasoy, R. Can, and I. Yalcin, Investigation of Elazig Sivrice Earthquake (24 January 2020, Mw=6.8) Employing Radar Interferometry and Stereo Airphoto Photogrammetry. Hacettepe University, Engineering Faculty, Geomatics and Geological Engineering Departments, 51p, **2020.**

[135] Inundated Area_1, https://www.youtube.com/watch?v=PO_b1yNHXPc, Last Access: 01 June 2024.

[136] Inundated Area_2, https://www.youtube.com/watch?v=owZA3FYf668, Last Access: 01 June 2024.

[137] Inundated Area_3, https://www.youtube.com/watch?v=aEwMqSlZ95E, Last Access: 01 June 2024.

[138] Inundated Area_4, https://www.sondakika23.com/elazig-da-yagmur-ve-dolu-hayati-felc-etti/101988/, Last Access: 01 June 2024.

[139] Inundated Area_5, https://www.youtube.com/watch?v=t-02c0AyJuw, Last Access: 01 June 2024.

[140] Inundated Area_6_7, https://www.sondakika.com/haber/haber-elazig-da-saganak-yagis-etkili-oldu-yollar-nehre-15012491/, Last Access: 01 June 2024.

[141] Inundated Area_8, https://www.youtube.com/watch?v=NbHZCSIzSkc, Last Access: 01 June 2024.

[142] Inundated Area_9, https://www.youtube.com/watch?v=j_wpJScuE0o, Last Access: 01 June 2024.

[143] Inundated Area_10, https://www.trthaber.com/haber/guncel/elazigda-saganak-etkili-oldu-818532.html, Last Access: 01 June 2024.

[144] C.J. van Westen, E. Castellanos, and S.L. Kuriakose, Spatial data for landslide susceptibility, hazard, and vulnerability assessment: An overview. Engineering Geology. 102(3): p. 112-131, **2008.**

[145] D. Cruden, and D.J. Varnes, Landslide Types and Processes. In: Turner, A.K., Schuster, R.L. (Eds.), Landslides: investigation and mitigation. National Academy Press, Washington, D.C. 247: p. 36–75, **1996.**

[146] M.E. Popescu, A suggested method for reporting landslide causes. Bulletin of the International Association of Engineering Geology - Bulletin de l'Association Internationale de Géologie de l'Ingénieur. 50(1): p. 71-74, **1994.**

[147] Inventory, U.W.P.O.W.L., A suggested method for describing the activity of a landslide. Bulletin of the International Association of Engineering Geology - Bulletin de l'Association Internationale de Géologie de l'Ingénieur. 47(1): p. 53-57, **1993.**

[148] T. Çan, T. Duman, Ş. Olgun, Ş. Çörekçioğlu, F. Gülmez Karakaya, H. Elmacı, S. Hamzaçebi, Ö. Emre, Türkiye Heyelan Veri Tabani. **2013.**

[149] D.J. Varnes, Slope Movement Types And Processes. Transportation Research Board Special Report: p. 11-33, **1978.**

[150] Ultracam Eagle Camera, Vexcel Imaging, https://www.vexcel-imaging.com/products/, Last Access: 10 May 2024.

[151] M. Çoban and H. Dalkılıç, 1/100.000 scale Turkish geological maps M-39 Quadrangle, Publication of General Directorate of Mineral Research and Exploration, No:262, **2018.**

[152] D. Usta et al., 1/100.000 scale Turkish geological maps M-40 Quadrangle, Publication of General Directorate of Mineral Research and Exploration, No:263. **2018**.

[153] Inundated Area_11, https://www.youtube.com/watch?v=alGuICQURBQ Last Access: 01 June 2024.

[154] Inundated Area_12, https://www.youtube.com/watch?app=desktop&v=43j9sI-6WDE, Last Access: 01 June 2024.

[155] Inundated Area_13, https://artigercek.com/guncel/adiyaman-ve-urfada-saganak-yagis-etkili-ev-is-yerleri-ve-cadirlar-su-icinde-kaldi-246007h, Last Access: 01 June 2024.

[156] HGM Küre Platform, https://kure.harita.gov.tr/, Last Access: 10 May 2024.

[157] S. Kocaman, S. Cetinkaya, N. Tunar Ozcan, G. Karakas, V.E. Karakas, C. Gokceoglu, Evaluation of co-seismic landslides with aerial photogrammetry triggered by 6 February 2023 Kahramanmaras Earthquakes (Türkiye). Landslides, Under Consideration.

[158] Google Earth Pro, https://www.google.com/intl/tr/earth/about/, Last Access: 10 May 2024.

[159] B. Kalantar, B. Pradhan, S.A. Naghibi, A. Motevalli, and S. Mansor, Assessment of the effects of training data selection on the landslide susceptibility mapping: a comparison between support vector machine (SVM), logistic regression (LR) and artificial neural networks (ANN). Geomatics, Natural Hazards and Risk. 9(1): p. 49-69, **2018.**

[160] I.D. Moore, R. Grayson, and A. Ladson, Digital terrain modelling: a review of hydrological, geomorphological, and biological applications. Hydrological processes. 5(1): p. 3-30, **1991.**

[161] O. Conrad, B. Bechtel, M. Bock, H. Dietrich, E. Fischer, L. Gerlitz, J. Wehberg, V. Wichmann, and J. Böhner, System for automated geoscientific analyses (SAGA) v. 2.1. 4. Geoscientific model development. 8(7): p. 1991-2007, **2015.**

[162] Esri ArcGIS, https://www.esri.com/en-us/arcgis/about-arcgis/overview, Last Access: 10 May 2023.

[163] C.F. Dormann, J. Elith, S. Bacher, C. Buchmann, G. Carl, G. Carré, J.R. G. Marquéz, B. Gruber, B. Lafourcade, P.J. Leitão, T. Münkemüller, C. McClean, P.E. Osborne, B. Reineking, B. Schröder, A.K. Skidmore, D. Zurell, S.L. Collinearity, A review of methods to deal with it and a simulation study evaluating their performance. Ecography. 36: p. 27-46, **2013.**

[164] G.D. Booth, M.J. Niccolucci, and E.G. Schuster, Identifying proxy sets in multiple linear regression: an aid to better coefficient interpretation. 1994, U.S. Dept. of Agriculture, Forest Service, Intermountain Research Station: Ogden, UT.

[165] D.A. Belsley, A Guide to using the collinearity diagnostics. Computer Science in Economics and Management. 4(1): p. 33-50, **1991.**

[166] J.R. Schuerman, Principal Components Analysis, in Multivariate Analysis in the Human Services, J.R. Schuerman, Editor. 1983, Springer Netherlands: Dordrecht. p. 93-119.

[167] J.F. Hair, B.J. Babin, W.C. Black, and R.E. Anderson, Multivariate Data Analysis. 2019: Cengage.

[168] D. Liao, and R. Valliant, Variance inflation factors in the analysis of complex survey data. Survey Methodology. 38: p. 53-62, **2012.**

[169] I. Kononenko, Estimating attributes: Analysis and extensions of RELIEF. in Machine Learning: ECML-94. 1994. Berlin, Heidelberg: Springer Berlin Heidelberg.

[170] D. Dubois, and H. Prade, Rough Fuzzy Sets And Fuzzy Rough Sets*. International Journal of General Systems. 17(2-3): p. 191-209, **1990.**

[171] B. Hunt, J. Marin, and P.J. Stone, Experiments in Induction. 1966: Academic Press.

[172] S.L. Salzberg, C4.5: Programs for Machine Learning by J. Ross Quinlan. Morgan Kaufmann Publishers, Inc., 1993. Machine Learning. 16(3): p. 235-240, **1994.**

[173] L. Breiman, Random forests. Machine learning. 45: p. 5-32, **2001.**

[174] H.B. Kibria, and A. Matin, The severity prediction of the binary and multi-class cardiovascular disease − A machine learning-based fusion approach. Computational Biology and Chemistry. 98: p. 107672, **2022.**

[175] Scikit-learn Pythonlibrary, https://scikitlearn.org/stable/modules/generated/sklearn.model_selection.RandomizedSearchCV.html, Last Access: 29 Dec 2023.

[176] J. Bergstra, and Y. Bengio, Random search for hyper-parameter optimization. J. Mach. Learn. Res. 13(null): p. 281–305, **2012.**

[177] S. Lundberg, S.I. Lee, A Unified Approach to Interpreting Model Predictions, **2017**. https://arxiv.org/abs/1705.07874v2.

[178] T.Y. Miao, and M. Wang. Susceptibility Analysis of Earthquake-Induced Landslide Using Random Forest Method. in Proceedings of the International Conference on Computer Information Systems and Industrial Applications. 2015. Atlantis Press.

[179] L.Tang, X. Yu, W. Jiang, J. Zhou, Comparative study on landslide susceptibility mapping based on unbalanced sample ratio. Scientific Reports. 13(1): p. 5823, **2023.**

[180] S.R. Kotha, F. Cotton, and D. Bindi, A new approach to site classification: Mixed-effects Ground Motion Prediction Equation with spectral clustering of site amplification functions. Soil Dynamics and Earthquake Engineering. 110: p. 318-329, **2018.**

[181] R.D. Borcherdt, and G. Glassmoyer, On the characteristics of local geology and their influence on ground motions generated by the Loma Prieta earthquake in the San Francisco Bay region, California. Bulletin of the Seismological Society of America. 82(2): p. 603-641, **1992.**

[182] S.Castellaro, F. Mulargia, and P.L. Rossi, VS30: Proxy for seismic amplification? seismological research letters. 79(4): p. 540-543, **2008.**

[183] K. Chousianitis, V.D. Gaudio, P. Pierri, G.A. Tselentis, Regional ground-motion prediction equations for amplitude-, frequency response-, and duration-based parameters for Greece. Earthquake Engineering & Structural Dynamics. 47(11): p. 2252-2274, **2018.**

[184] V. Del Gaudio, P. Pierri, and K. Chousianitis, Influence of site response and focal mechanism on the performance of peak ground motion prediction equations for the Greek region. Soil Dynamics and Earthquake Engineering. 125: p. 105745, **2019.**

[185] K.W. Campbell, and Y. Bozorgnia, A Ground Motion Prediction Equation for the Horizontal Component of Cumulative Absolute Velocity (CAV) Based on the PEER-NGA Strong Motion Database. Earthquake Spectra. 26(3): p. 635-650, **2010.**

[186] R.E. Kayen, and J.K. Mitchell, Assessment of liquefaction potential during earthquakes by Arias intensity. Journal of Geotechnical and Geoenvironmental Engineering. 123(12): p. 1162-1174, **1997.**

[187] A. Arias, A measure of earthquake intensity. Seismic design for nuclear plants: p. 438-483, **1970.**

[188] D.K. Keefer, Landslides caused by earthquakes. Geological Society of America Bulletin. 95(4): p. 406-421, **1984.**

[189] H. Wang, K. Sassa, and W. Xu, Analysis of a spatial distribution of landslides triggered by the 2004 Chuetsu earthquakes of Niigata Prefecture, Japan. Natural Hazards. 41: p. 43-60, **2007.**

[190] M. Karpouza, K. Chousianitis, G.D. Bathrellos, H.D. Skilodimou, G. Kaviris and A. Antonarakou, Hazard zonation mapping of earthquake-induced secondary effects using spatial multi-criteria analysis. Natural Hazards. 109: p. 637-669, **2021.**

[191] R. Foulser-Piggott, and K. Goda, Ground-motion prediction models for Arias intensity and cumulative absolute velocity for Japanese earthquakes considering single-station sigma and within-event spatial correlation. Bulletin of the Seismological Society of America. 105(4): p. 1903-1918, **2015.**

[192] Turkish Accelerometric Database and Analysis System, https://tadas.afad.gov.tr/login, Last Access: 11 May 2023.

[193] S.A. Kalogirou, Chapter eleven - Designing and Modeling Solar Energy Systems, in Solar Energy Engineering, S.A. Kalogirou, Editor. 2009, Academic Press: Boston. p. 553-664.

[194] E.H. Mamdani, and S. Assilian, An experiment in linguistic synthesis with a fuzzy logic controller. International journal of man-machine studies. 7(1): p. 1-13, **1975.**

[195] C. Gokceoglu, and K. Zorlu, A fuzzy model to predict the uniaxial compressive strength and the modulus of elasticity of a problematic rock. Engineering Applications of Artificial Intelligence. 17(1): p. 61-72, **2004.**

[196] A. Akgun, E.A. Sezer, H.A. Nefeslioglu, C. Gokceoglu and B. Pradhan, An easy-to-use MATLAB program (MamLand) for the assessment of landslide susceptibility using a Mamdani fuzzy algorithm. Computers & Geosciences. 38(1): p. 23-34, **2012**.

[197] T. Osna, E.A. Sezer, and A. Akgun, GeoFIS: an integrated tool for the assessment of landslide susceptibility. Computers & Geosciences. 66: p. 20-30, **2014.**

[198] MATLAB, User's Guide Version 9.4, R2018a. 2018, MathWorks Co., USA.

[199] S. Piramuthu, Input data for decision trees. Expert Systems with applications. 34(2): p. 1220-1226, **2008.**

[200] Natural breaks classification, https://doc.arcgis.com/en/microsoft-365/latest/get-started/classification-methods.htm#:~:text=The%20natural%20breaks%20classification%20method,a%20national%20forest%E2%80%94are%20identified, Last access: 10 May 2024.

[201] D.K. Keefer, and R. Wilson, Predicting earthquake-induced landslides, with emphasis on arid and semi-arid environments. Landslides in a semi-arid environment. 2(PART 1): p. 118-149, **1989.**

[202] G. Karakas, S. Kocaman, and C. Gokceoglu, On The Effect Of Dem Quality For Landslide Susceptibility Mapping. ISPRS Ann. Photogramm. Remote Sens. Spatial Inf. Sci. V-3-2022: p. 525-531, **2022.**

[203] T. Görüm, H. Tanyas, F. Karabacak, A. Yılmaz, S. Girgin, K.E. Allstadt, M. L. Süzen and P. Burgi, Preliminary documentation of coseismic ground failure triggered by the February 6, 2023 Türkiye earthquake sequence. Engineering Geology. 327: p. 107315, **2023.**

[204] M.S.G. Adnan, M.S. Rahman, N. Ahmed, B. Ahmed, M.F. Rabbi,and R.M. Rahman, Improving spatial agreement in machine learning-based landslide susceptibility mapping. Remote Sensing. 12(20): p. 3347, **2020.**

[205] H. Aktas, and B.T. San, Landslide susceptibility mapping using an automatic sampling algorithm based on two level random sampling. Computers & Geosciences. 133: p. 104329, **2019.**

[206] K. He, L. Lombardo, L. Chang, N. Sadhasivam et al., Investigating earthquake legacy effect on hillslope deformation using InSAR-derived time series. Earth Surface Processes and Landforms, 1-11, **2023.**

[207] B. Sozer, et al., Preliminary investigations on flood susceptibility mapping in Ankara (Turkey) using modified analytical hierarchy process (M-AHP). The International Archives of the Photogrammetry, Remote Sensing and Spatial Information Sciences. 42: p. 361-365, **2018.**

[208] A. Costanzo, Shaking Maps Based on Cumulative Absolute Velocity and Arias Intensity: The Cases of the Two Strongest Earthquakes of the 2016–2017 Central Italy Seismic Sequence. ISPRS International Journal of Geo-Information. 7(7): p. 244, **2018.**

[209] H.R. Pourghasemi, and N. Kerle, Random forests and evidential belief function-based landslide susceptibility assessment in Western Mazandaran Province, Iran. Environmental earth sciences. 75: p. 1-17, **2016.**

[210] G. Marin, M. Modica, S. Paleari, R. Zoboli, Assessing disaster risk by integrating natural and socio-economic dimensions: A decision-support tool. Socio-Economic Planning Sciences. 77: p. 101032, **2021.**

APPENDIX

Table A.1 Parameter weights used in M-AHP for producing the FSMs.

Parameters			
Land Use Land Cover Class		Weight	
Tree cover		4	
Shrubland		4	
Grassland		4	
Cropland		4	
Built-up		12	
Bare/sparse vegetation		10	
Permanent water bodies		12	
Lithology Class		Weight	
Elazig site	Adiyaman Site		
Undifferentiated Alluvial	Undifferentiated Alluvial	4	4
Terrigenous clastics	Non-graded terrigenous clastics	8	6
Sheeted dyke complex	Basalt	11	11
Volcanites and sedimentary rocks	Volcanites and sedimentary	11	11
Granitoids	rocks	12	
Basalt	Terrigenous clastics	11	6
Clastics and carbonates	Ophiolitic melange	8	12
Marble	Clastics and carbonates	12	8
Undifferentiated basic - ultrabasic rocks	Pelagic limestone	11	8
Gabbro	Neritic limestone	12	8
Serpentinite	Undifferentiated basic-	4	11
Ophiolitic melange	ultrabasic rocks	12	
Diorite, tonalite, monzonite, gabbro etc.	Peridotite	12	12
Pelagic limestone, clastics, radiolarite, chert etc.	Marble, schist in places	8	12
Neritic limestone		8	
Schist		12	
Quartzite, quartzschist		6	
Amphibolite		11	
Gneiss, schist		12	
TWI Class		Weight	
<5		2	
5 – 10		4	
10 – 15		6	
15 – 20		10	

>20	12
Slope Class	 Weight
<3 3 – 5 5 – 7 7 – 9 9 – 11 11 – 13 >13	7 6 5 4 3 2 1
Altitude Class	 Weight
<1000 1000 – 1200 1200 – 1400 1400 – 1600 1600 – 1800 1800 – 2000 >2000	6 5 4 3 2 1 1
Distance to Permanent Rivers Class	 Weight
<20 20 – 40 40 – 60 60 – 80 80 – 100 >100	6 5 4 3 2 1
Distance to Dry Rivers Class	 Weight
<20 20 – 40 40 – 60 60 – 80 80 – 100 >100	6 5 4 3 2 1

EK 1 - Tezden Türetilmiş Yayınlar

Karakas, G., Kocaman, S., & Gokceoglu, C. (2022). Comprehensive performance assessment of landslide susceptibility mapping with MLP and random forest: a case study after Elazig earthquake (24 Jan 2020, Mw 6.8), Turkey. Environmental Earth Sciences, 81(5), 144. https://doi.org/10.1007/s12665-022-10225-y

Karakas, G., Kocaman, S., & Gokceoglu, C. (2023). A hybrid multi-hazard susceptibility assessment model for a basin in Elazig Province, Türkiye. International Journal of Disaster Risk Science, 14(2), 326-341. https://doi.org/10.1007/s13753-023-00477-y

EK 2 - Tezden Türetilmiş Bildiriler

Karakas, G., Kocaman, S., and Gokceoglu, C. (2021). Aerial Photogrammetry and Machine Learning Based Regional Landslide Susceptibility Assessment for an Earthquake Prone Area in Turkey. Int. Arch. Photogramm. Remote Sens. Spatial Inf. Sci., XLIII-B3-2021, 713–720. https://doi.org/10.5194/isprs-archives-XLIII-B3-2021-713-202

Karakas, G., Kocaman, S., and Gokceoglu, C. (2022). On the Effect of DEM Quality for Landslıde Susceptibility Mapping. ISPRS Ann. Photogramm. Remote Sens. Spatial Inf. Sci., V-3-2022, 525–531. https://doi.org/10.5194/isprs-annals-V-3-2022-525-2022.

Karakas, G., Kocaman, S., and Gokceoglu, C. (2023). Multi-Hazard Susceptibility Assessment with Hybrid Machine Learnıng Methods for Tut Region (Adıyaman, Turkiye). Int. Arch. Photogramm. Remote Sens. Spatial Inf. Sci., XLVIII-M-1-2023, 529–536, https://doi.org/10.5194/isprs-archives-XLVIII-M-1-2023-529-2023.